Exhumed mantle at ultra-slow spreading ridges and magma-poor rifted margins : what can we learn from marine magnetic anomalies ?

Adrien Bronner

UNIVERSITÉ DE STRASBOURG

ÉCOLE DOCTORALE DES SCIENCES DE LA TERRE DE L'UNIVERS ET DE L'ENVIRONNEMENT

Institut de Physique du Globe de Strasbourg (UMR 7516)

THÈSE

présentée par :

Adrien BRONNER

soutenue publiquement le **19 juin 2013**

pour obtenir le grade de : **Docteur de l'Université de Strasbourg**

Discipline/ Spécialité : Géologie - Géophysique

Étude des anomalies magnétiques dans les domaines de manteau exhumé. Apport sur les processus de l'océanisation.

THÈSE dirigée par :

Daniel SAUTER	Chargé de recherche, Université de Strasbourg
Gianreto MANATSCHAL	Professeur, Université de Strasbourg

RAPPORTEURS :

Tim MINSHULL	University of Southampton
Jean-Yves ROYER	Directeur de recherche, IUEM Brest

EXAMINATEURS :

Marc MUNSCHY	Physicien des observatoires, Université de Strasbourg
Roger SEARLE	University of Durham

UNIVERSITÉ DE STRASBOURG

ÉCOLE DOCTORALE DES SCIENCES DE LA TERRE DE L'UNIVERS ET DE L'ENVIRONNEMENT

Institut de Physique du Globe de Strasbourg (UMR 7516)

THÈSE

présentée par :

Adrien BRONNER

soutenue publiquement le **19 juin 2013**

pour obtenir le grade de : **Docteur de l'Université de Strasbourg**

Discipline/ Spécialité : Géologie - Géophysique

Étude des anomalies magnétiques dans les domaines de manteau exhumé. Apport sur les processus de l'océanisation.

THÈSE dirigée par :

Daniel SAUTER	Chargé de recherche, Université de Strasbourg
Gianreto MANATSCHAL	Professeur, Université de Strasbourg

RAPPORTEURS :

Tim MINSHULL	University of Southampton
Jean-Yves ROYER	Directeur de recherche, IUEM Brest

EXAMINATEURS :

Marc MUNSCHY	Physicien des observatoires, Université de Strasbourg
Roger SEARLE	University of Durham

Remerciements

Voilà que ce travail s'achève, il m'est agréable de remercier les personnes qui ont participé à la concrétisation de ces trois années de labeur.

Mes premiers remerciements vont naturellement à l'équipe qui m'a encadré, je n'aurais pu espérer meilleure ambiance de travail. Merci Daniel sans toi cette thèse ne serait pas, merci de m'avoir encadré, soutenu et impliqué dans ton travail de recherche. Merci pour tes qualités humaines, ce fut (et ça restera) un réel plaisir de travailler avec toi. Merci Gianreto pour ta gentillesse, ta passion et l'énergie que tu investis au service de tes étudiants. Enfin, merci Marc pour ton expertise et ta disponibilité.

Merci Julie et Roger d'avoir accepté de contribuer à ce travail, merci à vous deux de m'avoir apporté votre précieuse aide.

Un grand merci à mes amis sans qui cette thèse n'aurait pas été si agréable. Merci Thiébaud pour les « knack & schneck », Adrien[2] pour ta passion pour l'émission « Tellement vrai », Alexandre pour tes plus beaux « bides », Alexandra R. pour ta disponibilité sur MSN (R.I.P.), Basile pour la pêche au crocodile, JR pour tes meilleures citations (que je ne citerai pas), Cyril pour ton sex appeal, Christian pour ton accent allemand, Paul pour ta clavicule (R.I.P.[2]), Julie M. pour les pauses déjeuner à rallonge, Julie T. pour tes chocolats suisses, Emilie N. pour ne jamais avoir été blasée, Alexandra G., Emilie S., Pauline et Anne So pour m'avoir accepté dans votre bureau, Philiiiiipe parce que tu le vaux bien et Izabella pour avoir amélioré ma géographie des Balkans.

Je remercie le café Milano pour sa proximité indispensable en cas de bonnes ou de mauvaises affaires.

Merci à mon frère et ma sœur pour leur soutien de près ou de plus loin.

Merci à mes parents qui m'ont inculqué la force d'aller au bout de mes projets, je leur dédie cette thèse.

Enfin, merci infiniment Candice, merci pour ton amour, ton énergie, ton optimisme et tes encouragements. Ta présence à mes cotés est un réconfort permanent.

Table des matières

INTRODUCTION

1.LA STRUCTURE CONVENTIONNELLE DE LA CROÛTE OCÉANIQUE 14

2.LES ANOMALIES MAGNÉTIQUES MARINES: RÉSULTAT DE L'ACCRÉTION OCÉANIQUE 15

3.LES DORSALES À TAUX D'ACCRÉTION LENT ET ULTRA-LENT: EXCEPTIONS AU MODÈLE CONVENTIONNEL? 16

4.LA TRANSITION OCÉAN-CONTINENT: UN ANALOGUE DES DORSALES LENTES OU ULTRA-LENTES ? 21

5.LA PROBLÉMATIQUE DES ANOMALIES MAGNÉTIQUES EN DOMAINE DE MANTEAU EXHUMÉ 23

Chapitre 1: Calibration et interprétation de données

magnétiques trois composantes acquises proche du fond

1.INTRODUCTION 31

2.SCALAR CALIBRATION 32

2.1. SOLVING THE NINE ERRORS OF MEASUREMENT 32

2.2. COMPENSATION OF THE MAGNETIC EFFECT OF THE TOW-VEHICLE 34

2.3. CASE STUDY 36

3.THE EQUIVALENT LAYER, PRELIMINARY INTERPRETATION OF THE MAGNETIC SIGNAL 39

3.1. THEORY 39

3.2. APPLICATION 42

3.3. MAGNETIC VECTOR 45

4.CONCLUSION 46

Chapitre 2: Le signal magnétique associé aux domaines de manteau exhumé de la dorsale Sud-Ouest Indienne

1.INTRODUCTION 53

2.GEOLOGICAL BACKGROUND 53

3.ACQUISITION AND PROCESSING OF MAGNETIC DATA 54

4.MAGNETIC SIGNAL OVER VOLCANIC SEAFLOOR A SEAFLOOR SPREADING MODEL. 57

5.MAGNETIC SIGNAL OVER EXHUMED SERPENTINIZED MANTLE. 59

5.1. THE WESTERN CORRIDOR 59

5.2. THE EASTERN CORRIDOR 60

5.3. MAGNETIC STRUCTURE OF THE DIFFERENT TYPES OF SEAFLOOR 61

6.MAGNETIC PROPORTIES OF THE DREDGED SAMPLES 63

7.FORWARD MODELING. 65

7.1. SEAFLOOR SPREADING MODEL 65

7.2. INDUCED MAGNETIZED MODEL 66

8.DEPTH OF THE MAGNETIC SOURCES 66

9.DISCUSSION 68

9.1. SEAFLOOR SPREADING ANOMALIES 68

9.2. WHICH MAGNETIC SIGNATURE FOR WHICH SEAFLOOR? 69

9.2.1. CONTRIBUTION OF MANTLE DERIVED ROCKS 69

9.2.2. CORRUGATED SEAFLOOR AND THE MAGNETIC SIGNAL 70

9.2.3. VOLCANIC SEAFLOOR AND THE MAGNETIC SIGNAL 71

9.2.4. MARINE MAGNETIC ANOMALIES AT OCT 71

10. CONCLUSION 72

Chapitre 3: Quelle est l'origine du signal magnétique associé à la transition océan-continent des marges Ibérie/Terre-Neuve?

1.HOW ROBUST IS THE IDENTIFICATION OF THE M SEQUENCE OF MAGNETIC ANOMALIES AT THE IBERIA – NEWFOUNDLAND CONJUGATED MARGINS? 79

2.THE J ANOMALY: THE MAGNETIC SIGNATURE OF A MAGMATIC EVENT 80

3.FORWARD MODELING OF MAGNETIC ANOMALY PROFILES 81

4.DISCUSSION 83

5.METHODS SUMMARY 85

6.SUPPLEMENTARY INFORMATION 86

6.1. Forward modelling of the magnetic contribution of the underplated gabbroic rocks. 86

6.2. Forward modelling of the magnetic contribution of the serpentinized mantle rocks .. 87

6.3. Forward modelling of the magnetic contribution of basaltic rocks 88

7.CONTROVERSIAL ISSUES 90

7.1. Interpretation of SCEECH line 1 90

7.2. Plate reconstruction 90

7.2.1. Problematic plate reconstruction 91

7.2.2. Reply to 'Problematic plate reconstruction' 93

Synthèse et Perspectives

1.LES MESURES « DEEP-TOW » TROIS COMPOSANTES DU CHAMP MAGNÉTIQUE TERRESTRE, MÉTHODOLOGIE. 98

2.APPLICATION À L'EXPLORATION MAGNÉTIQUE MARINE..... 99

3.LE SIGNAL MAGNÉTIQUE ASSOCIÉ AUX DOMAINES DE MANTEAU EXHUMÉ DE LA DORSALE SUD-OUEST INDIENNE. 99

4.LE SIGNAL MAGNÉTIQUE ASSOCIÉ À LA TRANSITION CONTINENT OCÉAN DES MARGES IBÉRIE/TERRE-NEUVE : UNE ANOMALIE LIÉE À UNE RUPTURE CONTINENTALE MAGMATIQUE ?.....100

5.IMPLICATIONS SUR L'INTERPRÉTATION DES ANOMALIES MAGNÉTIQUES.....101

Bibliographie

INTRODUCTION

La théorie de la tectonique des plaques nous apprend que les plaques continentales sont amenées à se fragmenter en d'autres plaques, plus petites, s'éloignant les unes des autres au niveau de frontières lithosphériques divergentes appelées dorsales océaniques. Ainsi, la lithosphère continentale subit une phase d'étirement et d'amincissement tectonique qui conduit à sa rupture et à la formation d'une dorsale où la totalité de la divergence sera accommodée par formation d'une nouvelle lithosphère océanique. Si l'accrétion océanique est étudiée à l'axe des dorsales médio-océaniques depuis une cinquantaine d'années, les processus qui mènent de la rupture des plaques lithosphériques vers l'accrétion d'une nouvelle lithosphère océanique restent mal compris. Ici, nous nous intéresserons au signal magnétique associé à l'accrétion océanique depuis la dorsale jusqu'à la transition océan-continent. Ceci dans le but de mieux comprendre les phénomènes en jeu lors de la rupture continentale et la naissance d'un océan.

1.LA STRUCTURE CONVENTIONNELLE DE LA CROÛTE OCÉANIQUE

Depuis les années 60 et jusqu'aux années 90, la structure de la croûte océanique a été décrite à partir de l'étude de la propagation des ondes sismiques (Raitt, 1963), l'échantillonnage (forages (Anderson et al., 1982) et dragages) et l'étude des ophiolites (e.g. Penrose Conference on Ophiolites ; Anonymous, 1972). Le modèle conventionnel est un modèle à deux couches (Figure 1) : une couche supérieure constituée de laves et de filons basaltiques reposant sur une couche inférieure formée de gabbros. Dans ce modèle, la géométrie et la composition minéralogique de la croûte océanique résultent du cheminement et de la cristallisation du magma lors de son transit, depuis le manteau asthénosphérique jusqu'à l'espace créé lors de l'écartement des plaques tectoniques, à l'aplomb des dorsales médio-océaniques. Ainsi, la couche supérieure forme le plancher océanique, elle est constituée de laves (« pillow lava») et de filons basaltiques (« dikes »). Les pillows sont le produit d'un refroidissement très rapide du magma au contact de l'eau de mer alors que les dikes sous-jacents résultent d'injections verticales de magma depuis la chambre magmatique. Celle-ci formera la couche inférieure de gabbros lors d'une cristallisation plus lente. Dans ce modèle, l'épaisseur totale moyenne de la croûte océanique est de l'ordre de 5 à 7 km (1 à 2 km pour la couche supérieure et 4 à 5 km pour la couche inférieure), l'ensemble est séparé des roches du manteau, les péridotites, par la discontinuité de Mohorovičić. Ainsi, jusqu'aux années 90, la croûte océanique était vue comme une structure d'épaisseur et de constitution homogène couvrant les deux tiers de la surface du manteau terrestre (Macdonald, 1989).

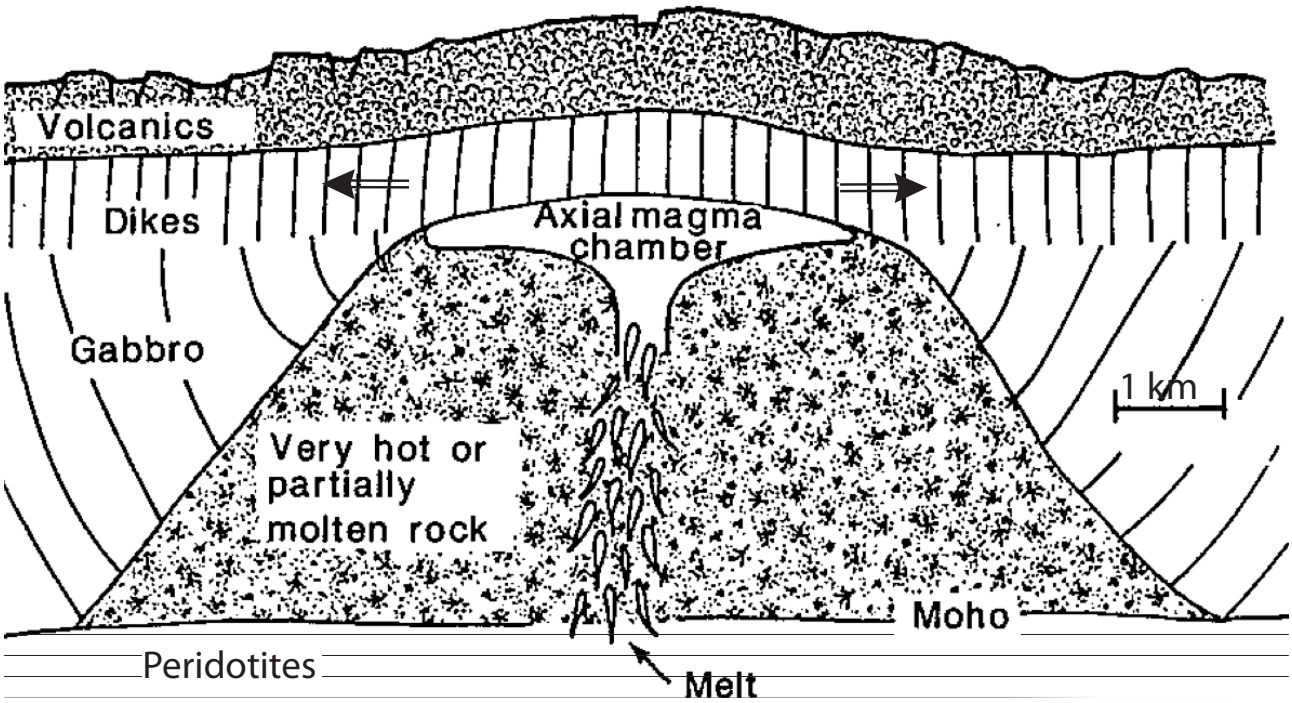

Figure 1 : Schéma illustrant le modèle classique d'accrétion de la croûte océanique. Les pillows forment le plancher océanique, ils surplombent les dikes qui résultent de l'injection verticale de magma depuis la chambre magmatique. La couche inférieure de gabbros est le résultat de la cristallisation plus lente des magmas contenus dans la chambre magmatique. D'après Macdonald (1989).

2.LES ANOMALIES MAGNÉTIQUES MARINES: RÉSULTAT DE L'ACCRÉTION OCÉANIQUE

Parallèlement à ce modèle, il a été démontré que les roches qui composent la croûte océanique ont un comportement ferromagnétique (Bullard and Manson, 1963). De la même façon que la structure de la croûte océanique décrite ci-dessus témoigne du cheminement du magma asthénosphérique venant combler l'espace créé par la séparation des plaques tectoniques, les magmas fossilisent la direction du champ magnétique dans lequel ils se refroidissent. Ainsi, au cours des temps géologiques, lorsque la croûte océanique se forme, elle enregistre les changements successifs de polarité du champ magnétique et présente, en s'éloignant de l'axe de la dorsale, une alternance de blocs d'aimantation normale ou inverse. Les contrastes d'aimentation entre ces blocs entraînent l'apparition d'anomalies magnétiques parallèles à l'axe d'accrétion et isochrones (Vine and Matthews, 1963) dont l'âge peut être déterminé à l'aide d'échelles d'inversions géomagnétiques (Heirtzler et al., 1968; Cande and Kent, 1992, 1995) (Figure 2). L'étude de ces anomalies a été et reste primordiale car elle a permis la confirmation de la théorie de l'expension des fonds océaniques (Dietz, 1962) et permet d'établir les taux d'accrétion et l'âge de la lithosphère océanique à l'échelle du globe (e.g. Müller et al., 2008).

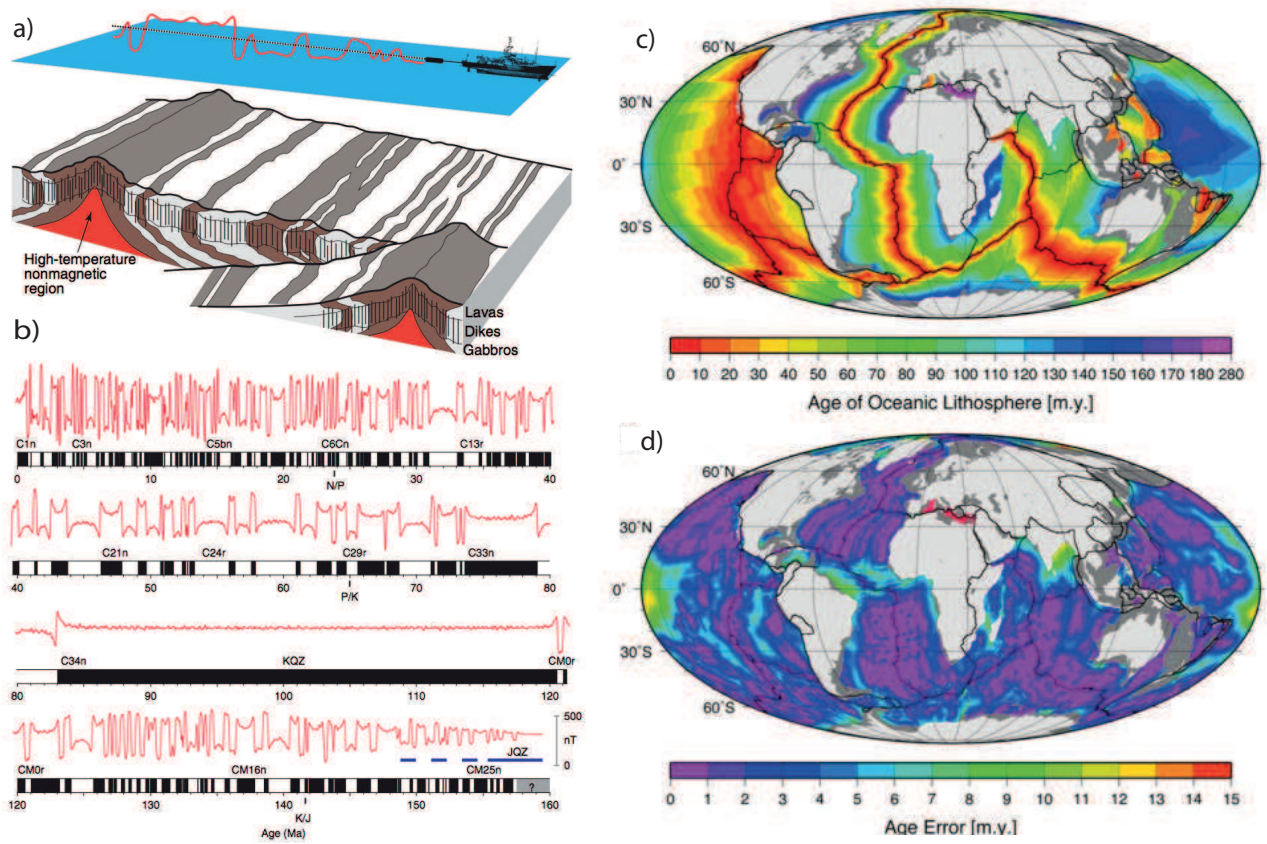

Figure 2 : a. Schéma tridimensionnel illustrant le lien entre les inversions de polarité du champ magnétique et l'accrétion océanique. Les bandes noires représentent la croûte océanique accrétée durant les périodes normales et les bandes blanches durant les périodes inverses. D'après Gee and Kent (2007). b. Echelle d'inversion géomagnétique et profil synthétique d'anomalie magnétique associé. D'après Gee and Kent (2007) c. Age de la croûte océanique déduit de l'étude des anomalies magnétiques. d. L'erreur est calculée à partir de la distance à la plus proche anomalie magnétique identifiée. c. et d. sont d'après Müller et al. (2008).

3.LES DORSALES À TAUX D'ACCRÉTION LENT ET ULTRA-LENT: EXCEPTIONS AU MODÈLE CONVENTIONNEL?

Ces 20 dernières années, les nombreuses campagnes océanographiques menées sur les dorsales à taux d'accrétion lent et ultra-lent ont remis en question le modèle classique d'accrétion océanique décrit précédemment. L'étude des anomalies gravimétriques (Lin et al., 1990) et le dragage de roches mantelliques à certaines extrémités de segments de la dorsale medio-atlantique (Cannat et al., 1995) ont d'abord montré que l'activité magmatique était absente en certains points le long de l'axe d'accrétion, entraînant des variations d'épaisseur de croûte de l'ordre de 50% (Lin et al., 1990). Contrairement au modèle classique décrit précédemment, ces études ont donc d'abord mis en évidence un caractère tridimensionnel des mécanismes d'accrétion océanique à taux lent et ultra-lent (Figure 3).

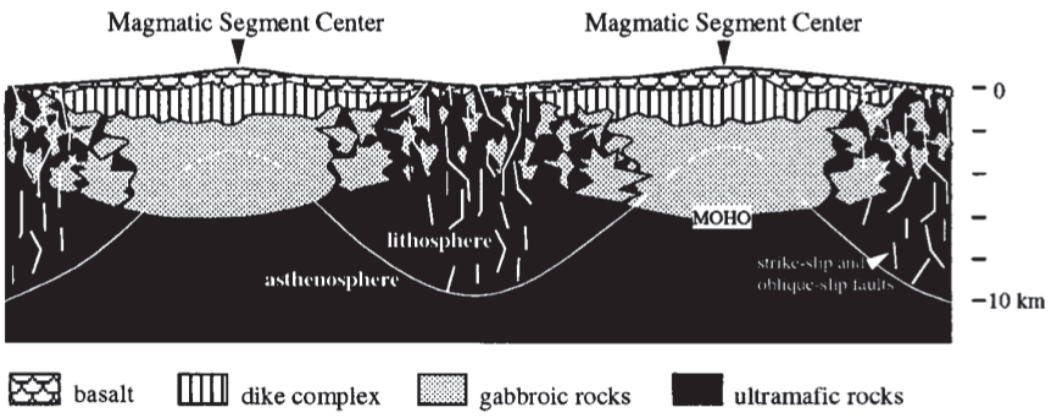

Figure 3 : Schéma illustrant le caractère tridimensionnel de l'accrétion crustale pour les dorsales à taux lent et ultra-lent. La variabilité de l'épaisseur des roches intrusives et extrusives est illustrée le long de l'axe de la dorsale (profil perpendiculaire à celui présenté en Figure 1). L'activité magmatique est focalisée au centre de segment, où la structure thermique de la lithosphère est la plus chaude, permettant une accrétion magmatique « classique » en deux couches. Aux extrémités de segments la transition lithosphère-asthénosphère est plus profonde, le flux magmatique est appauvri et la croûte océanique classique laisse place aux roches mantelliques tectonisées et à quelques intrusions magmatiques. D'après Cannat et al. (1995).

Plus tard, la découverte à l'axe de la dorsale médio-atlantique de roches de la croûte inférieure ou du manteau, exhumées par l'intermédiaire de failles normales à fort rejet ou de failles de détachement (Cann et al., 1997; Cannat et al., 1997), a mis en évidence une importante activité tectonique liée à la divergence des plaques. Ces observations ont montré que la croûte océanique pouvait se former de façon asymétrique, le long de failles de détachement (Cann et al., 1997). Lors de l'écartement des plaques tectoniques, la faille prend racine dans l'axe d'accrétion et dénude progressivement, sur une dizaine de kilomètres, les roches gabbroïques ou mantelliques. A l'inverse, la plaque opposée est accrétée par l'intermédiaire d'un volcanisme « classique ». Les structures résultantes ont été appelées « cores complexes océaniques », ils forment des dômes topographiques constitués de roches plutoniques et mantelliques dont la surface est striée selon la direction d'écartement des plaques tectoniques (Figure 4). Ainsi, il a été proposé que les failles de détachement pouvaient contribuer de 50 à 70% à la séparation des plaques tectoniques sur une durée de l'ordre de 1 à 2 Ma (Buck et al., 2005; Olive et al., 2010), les striations (ou corrugations) étant le résultat de l'interaction entre l'activité magmatique et tectonique durant l'exhumation (Figure 4).

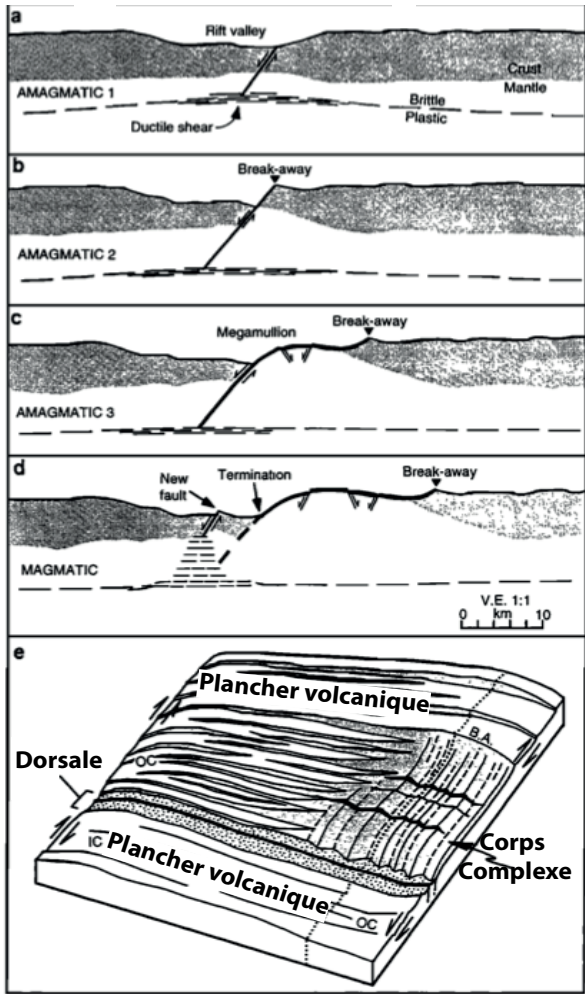

Figure 4 : Schéma illustrant la formation d'un core complexe océanique, résultat de l'exhumation de roches mantelliques par l'intermédiaire de failles de détachement. a. En l'absence de flux magmatique suffisant la faille de détachement prend racine dans l'axe de la dorsale. b-c. Les roches mantelliques sont exhumées jusqu'au plancher océanique, elles forment un dôme topographique strié composé de gabbros et de péridotites serpentinisées. d. La faille cesse de fonctionner suite à un regain d'activité magmatique e. Schéma tridimensionnel d'un core complexe océanique, contrairement au plancher océanique volcanique, sa surface est striée dans la direction perpendiculaire à l'axe d'accrétion. D'après Tucholke et al. (1998).

Finalement, la découverte récente de larges zones de manteau exhumé (~50 km de part et d'autre de la dorsale) dans la partie Est de la dorsale Sud-Ouest Indienne (Cannat et al., 2006; Sauter et al., 2013) complexifie encore plus le modèle d'accrétion océanique. Elle montre que la totalité de la séparation des plaques tectoniques peut se faire par l'intermédiaire de failles de détachement sans ou avec très peu d'apport magmatique, remettant ainsi en cause le modèle classique d'accrétion magmatique présenté précédemment. Sauter et al. (2013) montrent que dans certaines portions de la partie Est de la dorsale Sud-Ouest Indienne ni le plancher volcanique ni les striations associées aux «cores complexes» ne sont observés (Figure 5). A l'inverse, le plancher de ces zones est formé d'une succession de rides dont la topographie lisse est formée, d'après les dragages, de roches d'origine mantellique et altérées de type péridotites serpentinisées. Les auteurs proposent ainsi une accrétion crustale par changement successif de la polarité des failles de détachement, chaque faille venant en recouper une autre d'une plaque divergente à l'autre (Figure 5d et 7c).

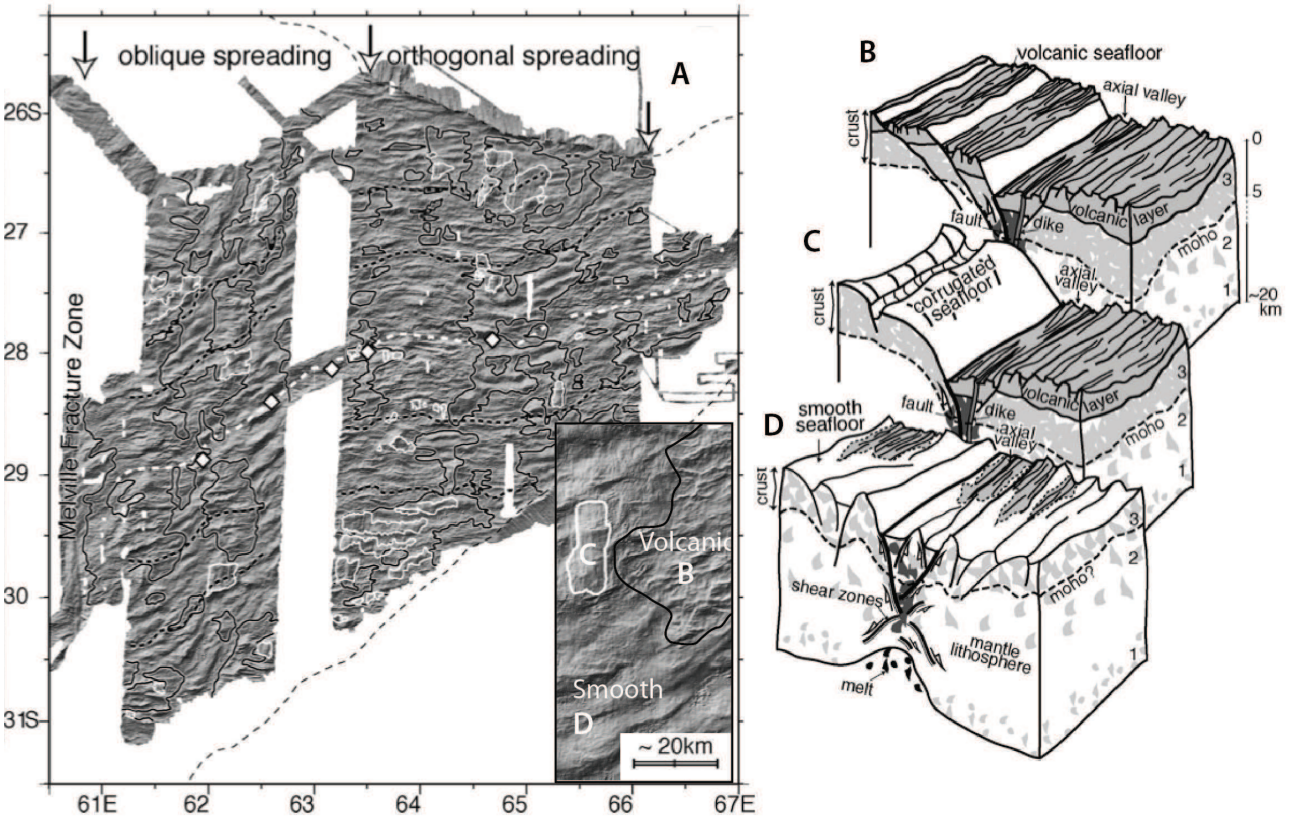

Figure 5 : Différents modes d'accrétions océaniques observés dans la partie Est de la dorsale Sud-Ouest Indienne. A. L'axe d'accretion est représenté par les tirets blancs. Les cores complexes sont délimités par les lignes blanches, leur surface est striée car ils se forment en regard d'un plancher océanique volcanique (voir C), les stries s'étendent sur une dizaine de kilomètres et les dragages montrent qu'ils sont composés de roches grabbroïques et mantelliques de type péridotites serpentinisées. Le « smoothseafloor » est délimité par les lignes noires, sa surface est lisse car il se forme en quasi absence de magmatisme par une inversion de polarité successive des failles de détachement (voir Figure 7c). Les dragages confirment la présence quasi exclusive de péridotites serpentinisées. Les surfaces exhumées peuvent atteindre une cinquantaine de kilomètres de part et d'autre de la vallée axiale. Le reste de la zone est formé d'un plancher océanique de type classique mais d'épaisseur variable. D'après Cannat et al. (2006).

Il existe des modèles reliant le taux d'accrétion à l'axe de la dorsale et la structure de la lithosphère. Ils prédisent un épaississement significatif de la lithosphère pour des taux d'accrétion lents et ultra-lents et la présence d'une lentille magmatique stable associée à une injection magmatique continue uniquement pour des dorsales à taux rapides (Phipps Morgan and Chen, 1993). L'épaisseur prédite de la lithosphère pour les taux lents et ultra-lents est déduite de la profondeur maximale des séismes et la présence d'une lentille magmatique à des taux d'accrétion supérieurs à 6 cm/a est validée par la sismique réflexion (Figure 6).

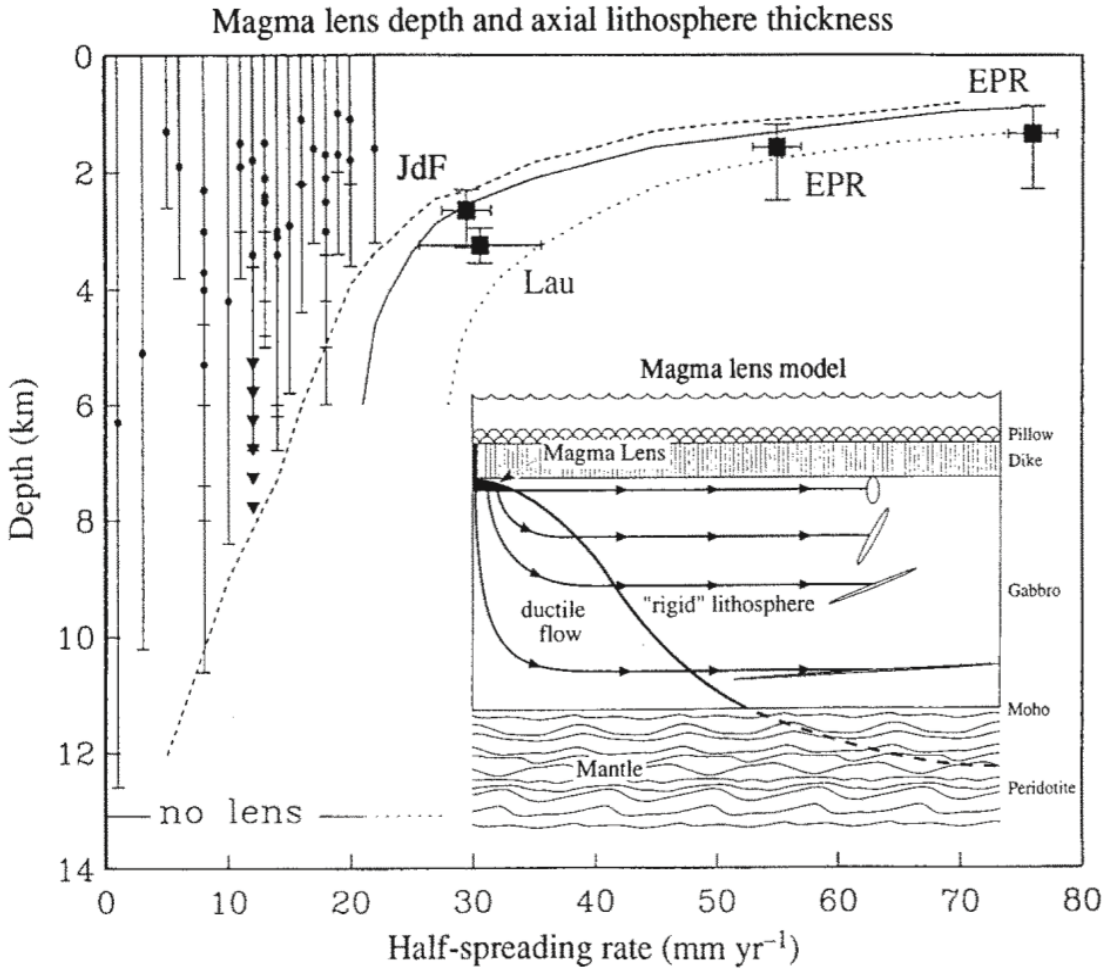

Figure 6 : Profondeur de la lentille magmatique en fonction du demi taux d'accrétion. Ce modèle prédit l'équilibre entre l'apport de chaleur et le refroidissement par circulation hydrothermale en fonction du taux d'accrétion. La présence continue d'une lentille magmatique n'est prédite que pour les vitesses supérieures à 6 cm/a (taux complet) elle est confirmée par la sismique réflexion (carrés noirs ; JdF : Juan de Fuca, EPR : East Pacific Rise). L'isotherme 750° est représenté pour les taux inferieurs à 3 cm/a (demi taux), il correspond à la limite ductile-cassant et corrèle avec la profondeur des séismes observés (points noirs). D'après Phipps Morgan and Chen (1993).

Aucun modèle de fusion (e.g. Bown and White, 1994; Reid and Jackson, 1981) ne permet d'expliquer la large variabilité de l'épaisseur crustale, c'est-à-dire la large variabilité de flux magmatique associée aux différents modes d'accrétion océanique observés aux dorsales lentes et ultra-lentes (Figure 5 et 6). Ces récentes études montrent à l'inverse que le modèle d'accrétion classique n'est valable que dans le cas d'un flux magmatique stable grâce auquel la quasi totalité de l'espace créé par la séparation des plaques tectoniques est comblé. Il s'applique donc relativement aisément aux dorsales à taux d'accrétion rapides et intermédiaires (taux supérieur à 5 cm/a ;e.g. dorsales du Pacifique) et à quelques exceptions de dorsales lentes sous l'influence de points chauds (e.g. Reykjanes, 2 cm/a ; Bell and Buck, 1992), pour lesquelles la structure thermique permet la présence d'une accrétion crustale homogène (Figure 7). Mais à l'heure actuelle, les modèles d'accrétion ne permettent pas d'expliquer pleinement la formation de «cores complexes» océaniques, les variations de flux magmatique observées le long des dorsales lentes ou ultra-lentes et le passage d'un régime d'accrétion magmatique vers un régime a-magmatique.

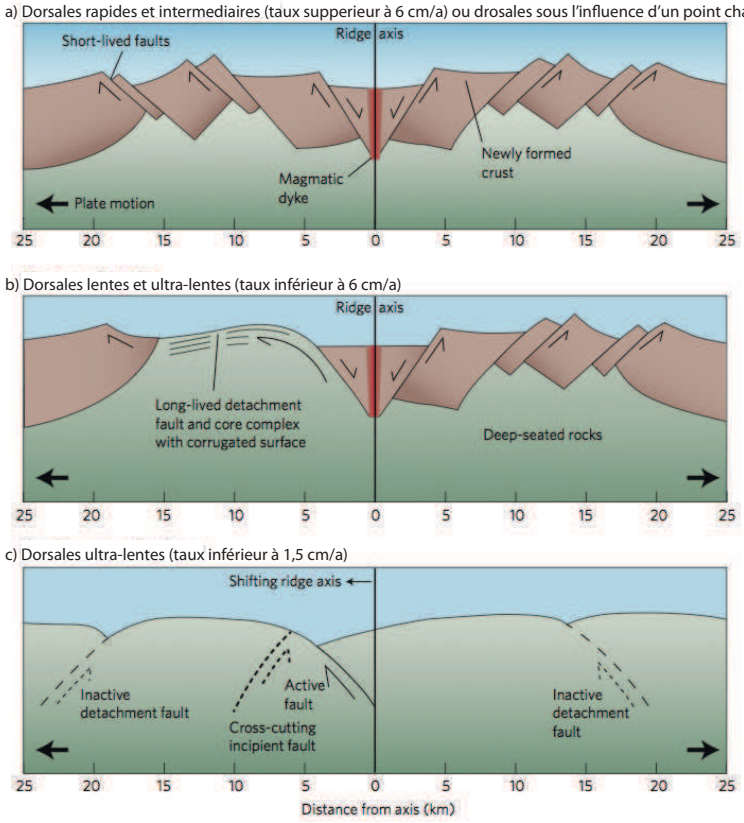

Figure 7 : Modes d'accrétion observés en fonction de la vitesse de divergence des plaques a. Dorsales rapides et intermédiaires, le mode d'accrétion est principalement magmatique, la part de la tectonique dans l'accommodation de la divergence des plaques ne dépasse pas 10%. b. Dorsales lentes et ultra-lentes, l'accrétion peut se faire de façon asymétrique par l'intermédiaire d'une faille de détachement et en regard d'un plancher océanique de type magmatique; 50 à 70% de la divergence est accommodée par la tectonique entraînant la formation de cores complexes océaniques. c. Dorsales ultra-lentes, l'accrétion peut être a-magmatique, les failles de détachements coupent successivement l'une ou l'autre des plaques divergentes. D'après Smith (2013)

4.LA TRANSITION OCÉAN-CONTINENT: UN ANALOGUE DES DORSALES LENTES OU ULTRA-LENTES ?

Dans les modèles classiques de la tectonique des plaques, la rupture continentale est représentée par un contact direct entre la croûte océanique et la croûte continentale (McKenzie, 1978). Néanmoins, de la même façon que les mécanismes d'accrétion au niveau des dorsales médio-océaniques lentes et ultra-lentes se sont révélés d'une complexité insoupçonnée, la découverte de marges dites « appauvries en magma » a remis en question ce point de vue. Les données sismiques et les forages révèlent une large zone de transition (~100 km, Boillot et al., 1980; Whitmarsh et al., 2001) entre l'océan et le continent (TOC) caractérisée par un changement progressif depuis la croûte continentale étirée vers des roches mantelliques exhumées de type péridotites serpentinisées jusqu'aux premières roches éruptives marquant l'apparition de ce qui semble correspondre aux prémisses de l'accrétion océanique (Jagoutz et al., 2007). La principale question que pose la présence d'une telle zone de transition est donc celle de l'endroit où se forme la première lithosphère océanique. Les forages effectués sur les marges Ibérie/Terre-Neuve montrent que la TOC est formée de roches mantelliques héritées de la lithosphère continentale (Muntener and Manatschal, 2006). De plus, ils montrent qu'une large portion de ces roches subit un magmatisme de type alcalin complexe et polyphasé alors que le

magmatisme de type MORB (Mid Oceanic Ridge Basalt), caractéristique des dorsales océaniques, n'est présent que dans la partie la plus distale de la TOC. Il s'exprime par des veines intrusives et des coulées basaltiques de faible épaisseur (~40 m, Jagoutz et al., 2007) Figure 8) recouvrant le socle péridotitique. De plus, certains modèles proposent un mécanisme d'exhumation des roches mantelliques dans la TOC similaire à celui observé aux dorsales ultra-lentes, avec de nombreuses failles d'exhumation dont la polarité change de manière répétée (Reston and McDermott, 2011). En revanche d'autres modèles ne propose qu'un seul système de failles de détachement (Péron-Pinvidic and Manatschal, 2008).

La question réside donc dans la localisation, à l'extrémité de la TOC, de la lithosphère océanique correspondant à la mise en place d'un régime de type dorsale, en état d'équilibre thermique entre apport de chaleur et refroidissement et où la déformation se focalise et se traduit par la formation d'une nouvelle lithosphère océanique. C'est à cette limite que nous nous intéresserons dans ce travail.

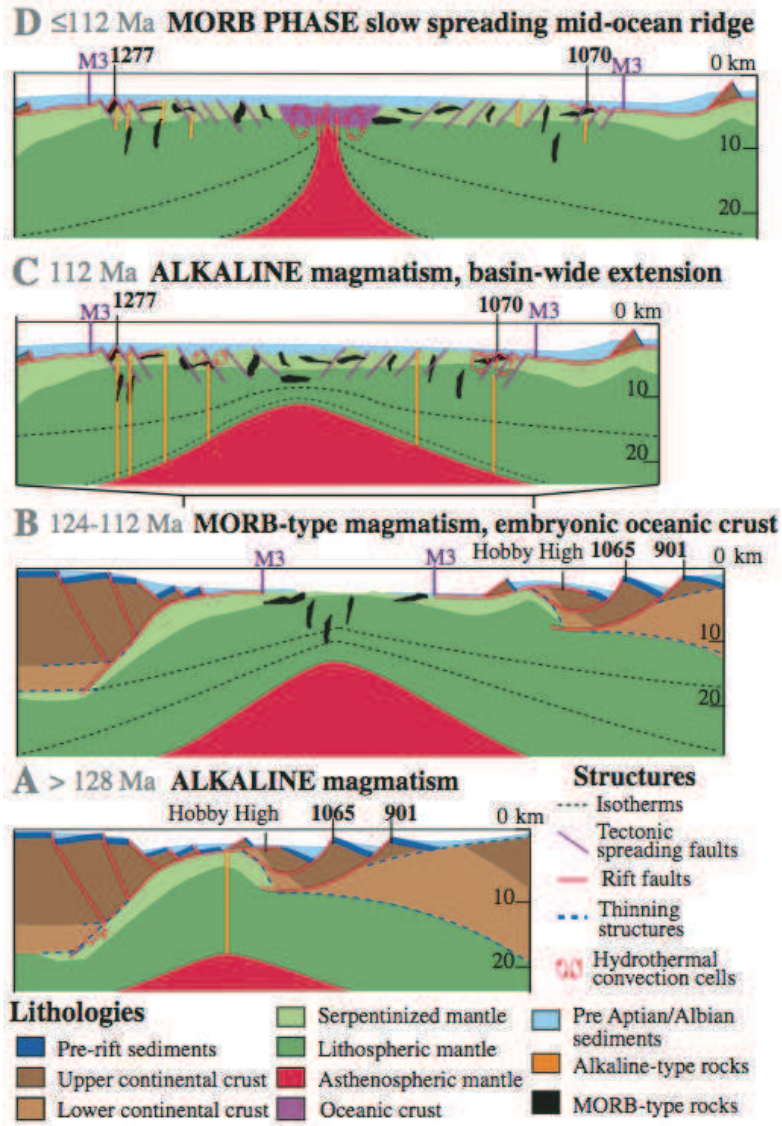

Figure 8 : Schéma illustrant les différentes phases tectoniques et magmatiques durant la séparation de l'Ibérie et de Terre-Neuve. Les forages localisés au plus loin vers l'océan (1277 et 1070) révèlent le premier magmatisme de type MORB. D'après Jagoutz et al. (2007).

5.LA PROBLÉMATIQUE DES ANOMALIES MAGNÉTIQUES EN DOMAINE DE MANTEAU EXHUMÉ

Les linéations magnétiques en domaines océaniques sont utilisées depuis une cinquantaine d'années pour contraindre la cinématique des plaques et calculer les taux d'accrétion des dorsales médio-océaniques. De nombreux forages et dragages ont d'abord permis de montrer que les basaltes extrusifs formant le plancher océanique avaient un comportement ferromagnétique et étaient porteurs d'une aimantation rémanente (NRM) stable et intense. Ils sont donc considérés comme la source principale des anomalies magnétiques océaniques avec des valeurs moyennes d'aimantation de l'ordre de 5 à 20 A/m (Harrison, 1987; Gee and Kent, 2007).

Le complexe filonien situé jusqu'à 1000 m sous les coulées basaltiques a rarement été atteints par les forages et ses propriétés magnétiques sont moins bien contraintes. L'étude du forage ODP 504B au large du Costa-Rica (~1 km à travers une croûte océanique supérieure formée à un taux de 7,2 cm/a) montre que les filons basaltiques ont une aimantation relativement stable mais en moyenne deux fois inférieure à celle des laves (NRM moyenne de 2,1 A/m; Pariso et al., 1995; Figure 9).

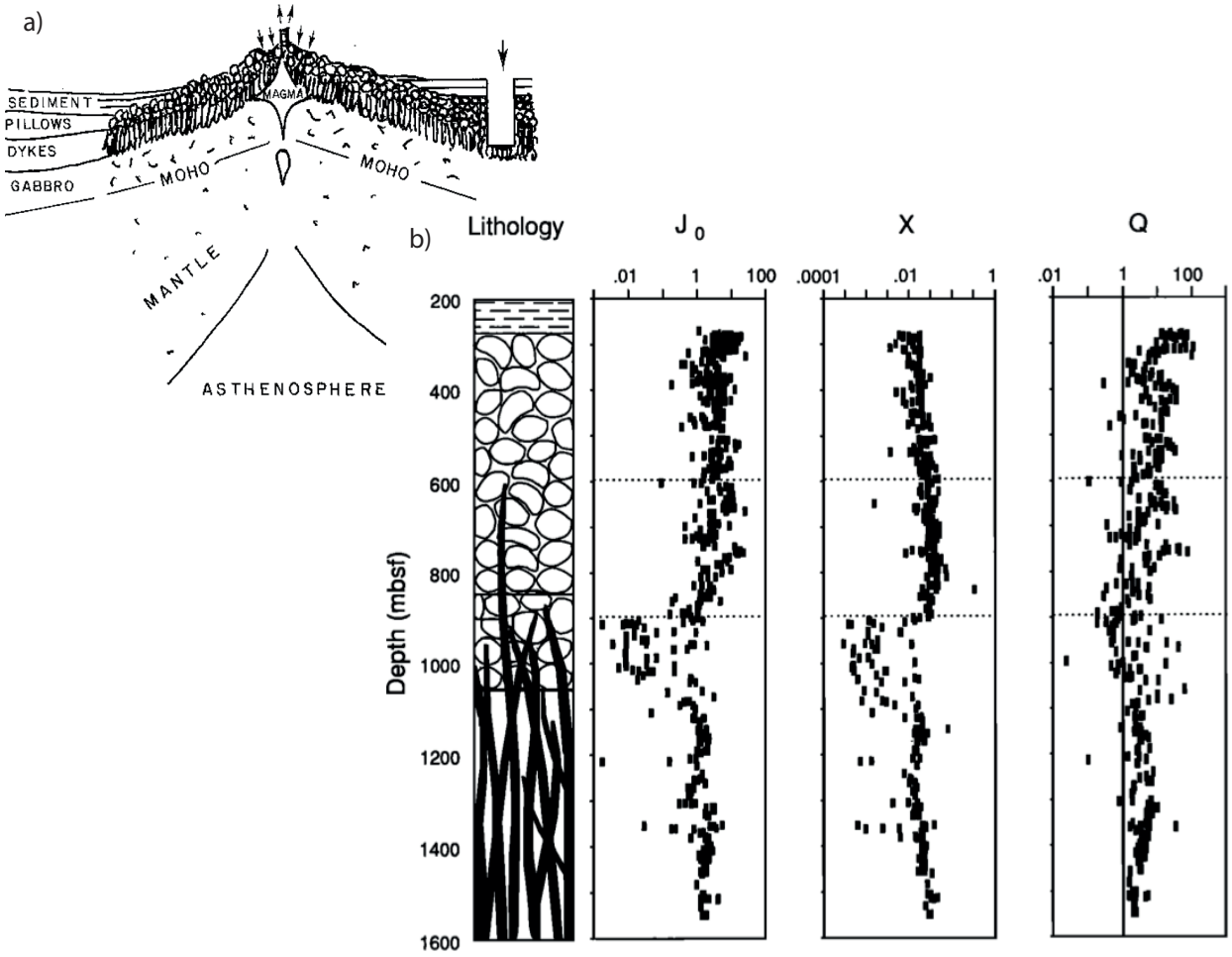

Figure 9 : a. Section schématique de la dorsale des Galápagos illustrant la localisation du forage 504B au large du Costa-Rica. D'après Anderson et al. (1982). b. Interprétation géologique et propriétés magnétiques de la croûte océanique supérieure issues de la compilation des données de forage au trou ODP 504B. La profondeur est indiquée en mètre sous le plancher océanique. J0 représente la NRM, X la susceptibilité magnétique et Q le coefficient de Koenigsberger (ratio NRM sur aimantation induite). D'après Pariso and Johnson (1991).

De la même façon, très peu de forages ont atteint la couche inférieure de gabbros et les mesures de NRM sur échantillons semblent contradictoires. Elles montrent que les gabbros ont une aimantation rémanente d'amplitude plus faible que les basaltes (par exemple, la NRM moyenne est de 2 A/m pour le site ODP 735B ; Pariso and Johnson, 1993) et les NRM mesurées semblent plus variables que celles des basaltes. De plus, la contribution des gabbros aux anomalies magnétiques n'est pas pleinement comprise car la distribution de l'aimantation rémanente dans ces roches dépend du moment où elle est acquise. Le refroidissement des gabbros étant plus lent que celui des basaltes de la croûte supérieure, il n'est pas évident que la polarité de l'aimantation soit la même dans ces deux types de roches.

Le comportement ferromagnétique des péridotites diffère de celui des roches extrusives et intrusives car elles peuvent acquérir une aimantation rémanente lors du processus serpentinisation à leur entrée en contact avec l'eau de mer (Cann, 1979; Toft et al., 1990). L'interaction entre les fluides et les minéraux ferromagnétiques tels que l'olivine ou le pyroxène forme la magnétite, porteuse de l'aimantation. Il a été démontré qu'un taux de serpentinisation supérieur à 75% est nécessaire pour produire une susceptibilité magnétique similaire à celle des basaltes (Oufi et al., 2002). Ce taux de serpentinisation semble atteint dans les deux premiers kilomètres des zones de manteau exhumé aux dorsales ultra-lentes et aux TOC (Chian et al., 1999; Dean et al., 2008; Minshull et al., 1998). Néanmoins, les échantillons de forages ODP montrent une forte variabilité d'aimantation rémanente d'un site à l'autre et même le long d'une seule et même carotte (Oufi et al., 2002). Ils montrent également une susceptibilité magnétique plus importante que celle généralement observée sur les basaltes océaniques. En raison de ces propriétés et du mode d'accrétion de ces roches, leur contribution aux anomalies magnétiques océaniques est donc, à l'heure actuelle, la moins bien comprise.

En règle générale, une couche uniformément magnétisée, drapée sur la topographie, d'épaisseur constante et formée d'une succession de blocs d'aimantation opposée aux limites verticales suffit à la modélisation et à l'identification des anomalies magnétiques océaniques (e.g. Gee and Kent, 2007). Les modèles classiques de la tectonique des plaques représentent la limite entre domaines continental et océanique par un contact direct entre ces deux types de lithosphères et cette limite est généralement définie par l'apparition de la première anomalie magnétique océanique. Toutefois, dans les TOC des marges appauvries en magma, le signal magnétique est de faible amplitude et de faible continuité spatiale. La complexité insoupçonnée des processus d'accrétion et la variété des roches formant le plancher océanique rendent l'interprétation difficile et leur source est controversée (Whitmarsh and Miles, 1995; Russell and Whitmarsh, 2003; Sibuet et al., 2007).

Le but de ce travail est donc d'étudier le signal magnétique associé à l'exhumation de roches mantelliques à proximité de la dorsale océanique ultra-lente et à la transition océan-continent afin d'en déduire (1) si l'exhumation de roches mantelliques aux dorsales océaniques est compatible avec l'enregistrement d'inversions de polarité du champ magnétique terrestre, (2) quels processus sont associés aux anomalies magnétiques observées à l'aplomb des zones de transitions océan-continent et (3) quelles sont les conséquences de ces processus sur les mécanismes de rupture continentale.

Parce que les données magnétiques déjà publiées et acquises à l'aplomb de zones de manteau exhumé des dorsales ultra-lentes (Sauter et al., 2008) et des marges appauvries en magma (Miles et al., 1996 ; Srivastava et al., 2000; Russell and Whitmarsh, 2003; Sibuet et al., 2007) révèlent un signal magnétique complexe de faible amplitude et de faible continuité spatiale, il nous faudra travailler avec des données de qualité et de résolution maximale. Ainsi, dans une première partie, nous développerons les méthodes de traitement et d'interprétation nécessaires à la calibration et l'interprétation des anomalies magnétiques acquises à l'aide de magnétomètres trois composantes tractés proche du fond (« deep-tow magnetic data»). Dans une deuxième partie, nous nous focaliserons sur l'étude du signal magnétique associé aux domaines de manteau exhumé de la dorsale Sud-Ouest Indienne. A l'aide de données haute résolution acquises à proximité du fond et des méthodes développées dans la première partie, nous tenterons de mieux contraindre la contribution de chaque type de plancher océanique aux anomalies magnétiques. Nous tenterons de comprendre si l'exhumation de roches mantelliques est compatible avec la formation de linéations magnétiques telles que présentées dans le modèle classique d'accrétion océanique. Finalement, dans une dernière partie, nous nous concentrerons sur le signal magnétique associé à la transition océan-continent des marges Ibérie/Terre-Neuve. Nous tenterons de comprendre quels processus et quelles sources contribuent à ce signal. Ceci dans le but d'y contraindre la localisation de la rupture continentale, c'est-à-dire l'endroit où se localise la déformation et débute la formation de la nouvelle lithosphère océanique.

Chapitre 1: Calibration et interprétation de données magnétiques trois composantes acquises proche du fond

La première partie de cette thèse est consacrée au développement de méthodes de traitement et d'analyse de données magnétiques acquises en domaine océanique. Nous présentons dans ce mémoire un certain nombre de profils dit « de fond de mer ». Ils ont été acquis à l'aide d'un magnétomètre trois composantes monté sur un sonar latéral lui même remorqué par un navire océanographique. Cet instrument permet l'acquisition de données magnétiques haute résolution en raison de sa proximité avec le plancher océanique. Néanmoins, il est soumis à certaines contraintes techniques liées à l'environnement marin et les mesures réalisées nécessitent de nombreux traitements avant interprétation.

Le levé de profils magnétiques de fond de mer pose deux principaux problèmes : le premier est lié à l'interférence magnétique de la structure du véhicule remorqué dans lequel est intégré le magnétomètre et le second est lié aux variations d'altitude du véhicule pendant la plongée. Les anomalies magnétiques respectivement engendrées par l'aimantation du véhicule et les variations de distance à la source aimantée masquent le signal magnétique associé aux contrastes géologiques.

Nous appliquons ici une méthode de calibration issue de la magnétométrie satellitaire pour traiter les mesures magnétiques de fond de mer. Nous montrons que contrairement aux méthodes communément utilisées en géophysique marine, l'interférence magnétique du véhicule peut-être confortablement corrigée sans connaissance préalable de l'orientation spatiale du magnétomètre.

Nous développons ensuite une méthode d'inversion des profils d'anomalies magnétiques. Nous montrons que malgré les variations d'altitude du véhicule durant l'acquisition du champ magnétique, il est possible, par l'intermédiaire d'une unique inversion linéaire, d'estimer l'aimantation de la croûte océanique. En s'affranchissant de la topographie du fond marin et en ramenant les mesures à altitude constante cette méthode permet une analyse plus fine de la lithologie magnétique crustale.

Ce chapitre a été publié dans la revue « Geophysics » sous la référence (la version publié est disponible en annexe) suivante :

Bronner, A., Munschy, M., Sauter, D., Carlut, J., Searle, R., and Maineult, A., 2013, Deep-tow 3C magnetic measurement: Solutions for calibration and interpretation: Geophysics, 78, J15-J23.

Deep-tow three component magnetic measurement: Solutions for calibration and interpretation.

Adrien Bronner[1], Marc Munschy[1], Daniel Sauter[1], Julie Carlut[2], Roger Searle[3], Alexis Maineult[2]

[1]Institut de Physique du Globe de Strasbourg, IPGS UMR CNRS 7516, Université de Strasbourg, 1 rue Blessig 67084, Strasbourg cedex France

[2]Institut de Physique du Globe de Paris, IPGP, Sorbonne Paris Cité Univ Paris Diderot, UMR CNRS 7154, F-75005 Paris, France

[3]Department of Earth Sciences, Durham University, Durham, DH1 3LE, United Kingdom

ABSTRACT

Two main problems are encountered in deep-tow three component magnetic surveys. The first is related to the instrumental error due to the manufacturing of the sensor, its integration in the tow-fish structure and the magnetization of the vehicle carrying the magnetometer; the second is related to the variation in altitude of the instruments during the dive. In this paper, we introduce a new type of calibration approach for deep-tow fluxgate magnetometers. We show that the magnetometer can be calibrated with no recourse to the vehicle attitude (pitch, roll and heading, as it is usually achieved) but only using the three components recorded by the magnetometer and an approximation of the scalar intensity of the Earth's magnetic field. This method, called scalar calibration, allows us to eliminate the intrinsic instrumental errors as well as the magnetization effect of the tow-vehicle. Thus, despite the low maneuverability of the tow-fish during the calibration experiment we provide a significant improvement in obtaining accurate magnetic anomaly profiles. As only the total field anomaly and not the magnetic vector is suitable for this method, we investigate the possibility of calculating the three components via an equivalent source approach. Therefore, assuming a 2D topographic equivalent layer, we provide a stable and a meaningful magnetization of the oceanic crust. We show that although magnetic data are acquired along uneven tracks, this model based on one single linear inversion is sufficient to provide a first order depth and magnetization intensity of the crust and also to carry out upward continuation of the total anomalous field as well as its associated vector.

1.INTRODUCTION

As they are compact and low cost, three-component magnetometers are commonly used for deep-tow work (Isezaki, 1986). Unlike proton precession magnetometers, they provide not only a measurement of the total intensity of the Earth's magnetic field but also of its vector components. However, the manufacturing of the sensor as well as the magnetic effect of the vehicle (up to thousands of nanoteslas) carrying it lead to measurement artifacts and non-absolute values that require compensation and calibration prior to any data processing or interpretation. Once the magnetometer is calibrated a second problem occurs: magnetic data are acquired at uneven altitudes and the amplitude of measured magnetic anomalies depends not only on the magnetization of the seafloor but also on the distance between the magnetometer and the magnetized sources.

The method proposed by Isezaki (1986) and Korenaga (1995) is commonly used for the instrumental correction. This method is based on a vector calibration and requires both intensity and orientation of the Earth's magnetic field in the sensors' coordinate system. To achieve this, accurate vehicle-fixed gyroscopes are required but such devices are costly and most of them provide only an approximation of the vehicle's attitude. Korenaga (1995) has shown that a measurement error of 0.1° in the vehicle's attitude within an ambient field of 25000 nT results in a 40 nT error in the magnetic profile. Then, inaccurate estimation of the vehicle motion and logging both attitude and magnetic data simultaneously results in noise generation. Such limitations explain why, since the first marine vector magnetometer was deployed (Isezaki, 1986), only a few cruises have used this instrument (Seama et al., 1993; Korenaga, 1995; Tivey et al., 2003; Yamamoto et al., 2005; Kato et al., 2007; Sato et al., 2009; Searle et al., 2010).

The aim of this paper is to provide new solutions that overcome the limitations described above. These solutions are developed for the calibration aspect as well as for data processing and preliminary interpretation of magnetic anomalies. In the following sections we propose a calibration approach called scalar calibration. This method was already successful for satellite magnetic measurements (Merayo et al., 2000; Olsen et al., 2001) and has been used for laboratory calibration of surface towed three-component magnetometers (Gee and Cande, 2002; Engels et al., 2008). However, it has never been applied to highly magnetized tow vehicles. We show that this method allows significant improvement in obtaining accurate magnetic anomaly profiles. We also investigate the possibility of using the equivalent source technique (Dampney, 1969) to provide an accurate model of the seafloor magnetization that can be used to compute the total anomalous magnetic field as well as its corresponding vector at any point outside the source. All the methods presented in this paper are implemented via Matlab and scripts are available upon request.

2.SCALAR CALIBRATION

2.1. SOLVING THE NINE ERRORS OF MEASUREMENT

The first issue inherent to deep-tow magnetic measurements is related to the calibration of the three-component magnetometer. It has been shown that the fluxgate magnetometer suffers from nine errors relative to the manufacturing of the sensor (Munschy et al., 2007). First, due to technical difficulties, the three fluxgate sensors cannot be mounted with a perfect orthogonality to each other and are skewed by about 1° (Figure 1). According to Isezaki (1986) the orthogonality of the three sensors is adjusted for a minimum accuracy of 100 nT in the measurement of the total geomagnetic field. Moreover, each of the three sensors suffers both an error of offset and an error of sensitivity. Usually, since the upper part of the oceanic crust has a substantial intensity of magnetization (Vine and Matthews, 1963), an accuracy of 100 nT is sufficient for magnetization analysis of the seafloor. Nevertheless, this limitation remains highly problematic in areas of weak and ill-defined magnetic signal. Indeed, the recent discovery at slow spreading ridges (Cannat et al., 2006) and ocean-continent transitions (Whitmarsh et al., 2001) of new types of seafloor, mainly formed with ultramafic rocks and associated with no or very little volcanic activity, shows an unexpected weakness and complexity of the associated magnetic signal (Sauter et al., 2008; Bronner et al., 2011).

The error of sensitivity for each of the three sensors, denoted S_x, S_y and S_z can be written as a diagonal matrix **S** in the non-orthogonal (X", Y", Z") sensor's coordinate system (Figure 1).

$$\mathbf{S} = \begin{bmatrix} S_x & 0 & 0 \\ 0 & S_y & 0 \\ 0 & 0 & S_z \end{bmatrix} \tag{1}$$

The offset errors, b_x , b_y and , b_z or "errors of zero", are equivalent to the output of the three sensors when no magnetic field is applied to the magnetometer,

$$\mathbf{b} = \begin{bmatrix} b_x \\ b_y \\ b_z \end{bmatrix} \tag{2}$$

and assuming (X',Y',Z') an orthogonal coordinate system associated to the magnetometer (with X'=X"; Figure 1).

The non-orthogonality is written as a 3x3 lower triangular matrix, **P**, which transforms the ambient magnetic vector to the non-orthogonal sensor's system i.e. from (X',Y',Z') to (X'',Y'',Z'')

$$\mathbf{P} = \begin{bmatrix} 1 & 0 & 0 \\ -\sin(u_1) & \cos(u_1) & 0 \\ \sin(u_2) & \sin(u_3) & \sqrt{1-\sin^2(u_2)-\sin^2(u_3)} \end{bmatrix} \tag{3}$$

where **u** is defined in Figure 1. Assuming **f'** is the unprocessed output of the sensor and **f** the ambient magnetic field applied to the magnetometer, in the sensors' skewed coordinate system (X'',Y'',Z'') the expression of the output of the magnetometer relative to the ambient magnetic vector is written as (Olsen et al., 2001)

$$\mathbf{f'} = \mathbf{S}\cdot\mathbf{P}\cdot\mathbf{f} + \mathbf{b} = \begin{bmatrix} S_1 & 0 & 0 \\ -\sin(u_1) & S_2\cos(u_1) & 0 \\ \sin(u_2) & \sin(u_3) & S_3\sqrt{1-\sin^2(u_2)-\sin^2(u_3)} \end{bmatrix} \begin{bmatrix} f_x \\ f_y \\ f_z \end{bmatrix} + \begin{bmatrix} b_x \\ b_y \\ b_z \end{bmatrix}, \tag{4}$$

whereas in the corrected orthogonal sensors' coordinate system (X',Y',Z'), the expression for the ambient magnetic vector relative to the output of the magnetometer is,

$$\mathbf{f} = \mathbf{P}^{-1}\cdot\mathbf{S}^{-1}\cdot(\mathbf{f'}-\mathbf{b}) = \begin{bmatrix} \frac{1}{S_1} & 0 & 0 \\ \frac{\sin(u_1)}{\cos(u_1)} & \frac{1}{S_2\cos(u_1)} & 0 \\ -\frac{\sin(u_1)\sin(u_3)+\cos(u_1)\sin(u_2)}{\cos(u_1)\sqrt{1-\sin^2(u_2)\sin^2(u_3)}} & -\frac{\sin(u_3)}{\cos(u_1)\sqrt{1-\sin^2(u_2)\sin^2(u_3)}} & \frac{1}{S_3\sqrt{1-\sin^2(u_2)\sin^2(u_3)}} \end{bmatrix} \left(\begin{bmatrix} f'_x \\ f'_y \\ f'_z \end{bmatrix} - \begin{bmatrix} b_x \\ b_y \\ b_z \end{bmatrix} \right) \tag{5}$$

Hence, the scalar intensity of the corrected ambient magnetic field is,

$$|\mathbf{f}| = \sqrt{\mathbf{f}^{\mathrm{T}}\cdot\mathbf{f}} = \sqrt{[\mathbf{P}^{-1}\cdot\mathbf{S}^{-1}\cdot(\mathbf{f'}-\mathbf{b})]^{\mathrm{T}}\cdot\mathbf{P}^{-1}\cdot\mathbf{S}^{-1}\cdot(\mathbf{f'}-\mathbf{b})} \tag{6}$$

The problem is non-linear for the nine parameters above but can be solved by minimizing the χ^2-misfit as (Olsen et al., 2001) proposed:

$$\chi^2 = \sum \frac{|\mathbf{f}| - F_0}{\sigma_B} \tag{7}$$

Where σ_b is the data error and $|\mathbf{f}|$ is the corrected scalar intensity of the measured magnetic field (**f'**) using equation 6 and $\mathbf{F_0}$ the estimated intensity of the Earth's magnetic field, which can be approximated by a model of the Earth's field (e.g., the IGRF), provided by another absolute magnetometer or supposed to be constant depending on the context of the calibration experiment.

Mathematically, as the vector calibration not only uses the intensity of the magnetic vector but also its orientation to resolve the calibration parameters, it is more effective than a scalar calibration. However, most of the deep-tow instruments host low-resolution tiltmeters and gyrocompasses that do not provide sufficiently precise orientations for calibration. In contrast to a vector calibration, our approach is called scalar calibration because, during the calibration experiment, only the intensity of the magnetic field has to be known ($\mathbf{F_0}$) and not the three components (which require vehicle attitude

to be expressed in the sensors' coordinate system). Therefore, most of the instrumental errors due to the vehicle motion are avoided and the accuracy of the magnetometer is significantly improved.

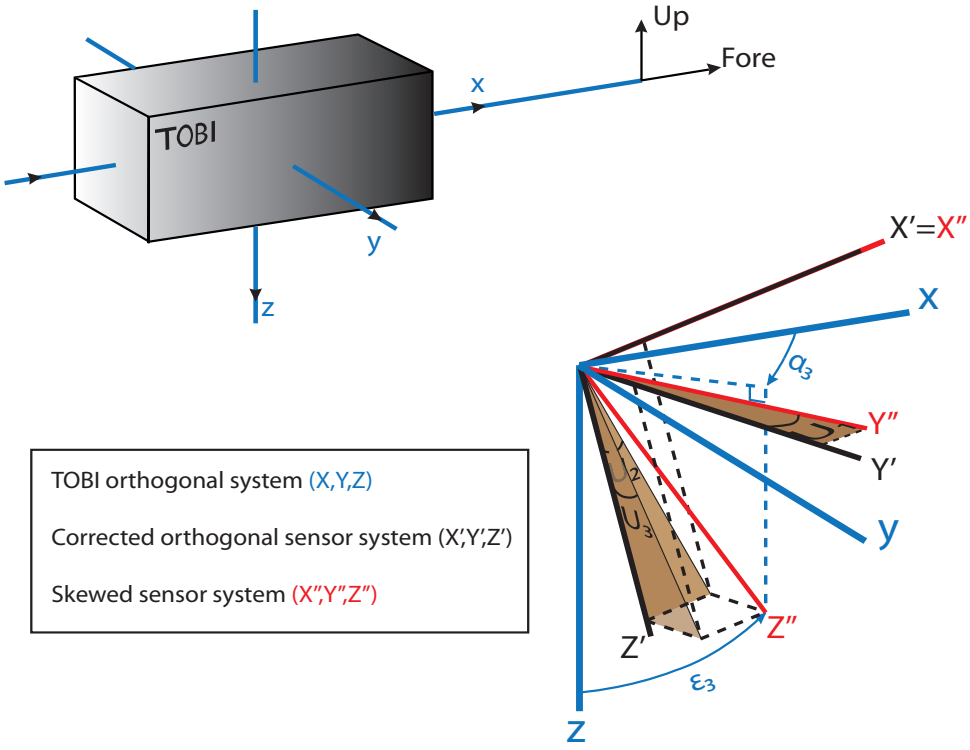

Figure 1 : Representation of the three skewed sensors coordinate system (X", Y", Z"), the orthogonal corrected coordinate system associated with the magnetometer (X', Y', Z') and the vehicle's coordinate system (X, Y, Z). The angles **u** represent the errors of orthogonality whereas angles **α** and **ε** represent the orientation of the three sensors in the TOBI reference frame. The (X', Y', Z') coordinate system is used for a scalar calibration and the (X, Y, Z) system is used for a vector calibration.

2.2. COMPENSATION OF THE MAGNETIC EFFECT OF THE TOW-VEHICLE

The second issue in deep-tow magnetic measurement is related to the magnetic effect generated by the ferro/paramagnetic structure of the tow-fish. This effect leads to up to thousands of nanoteslas artifact in the measured signal and has to be corrected. The measured vector field near the tow-vehicle (**f'**) is assumed to be the sum of the ambient geomagnetic field, the magnetic field produced by the induced magnetic moment of the vehicle and the magnetic field produced by the permanent magnetic moment of the vehicle (Leliak, 1961). The induced effect of the vehicle itself is assumed to be proportional to each component of the Earth's magnetic field (Leliak, 1961). Thus, the output vector of the magnetometer (**f'**) in the vehicle's coordinate system (X, Y, Z) can be written as Isezaki (1986) and Korenaga (1995) popose,

$$\mathbf{f}' = \mathbf{R}^{t}\mathbf{f} + \mathbf{G}\mathbf{R}^{t}\mathbf{f} + \mathbf{b}_{r} \tag{8}$$

where $\mathbf{b}_r$ represents the permanent effect of the vehicle, **G** is a matrix that depends on the distribution of the magnetic susceptibility of the vehicle and **R** the matrix of rotation from the vehicle coordinate system to the geographic coordinate system.

Nevertheless, equation 8 is only true for the condition that the sensors are rigidly fixed to the vehicle and mounted perpendicularly to each other, but such a condition is practically never satisfied. It is clear that the error of orthogonality as well as the integration of the sensor within the vehicle's structure (Figure 1) lead to errors of orientation.

The direction of each sensor (axis X", Y" and Z") within the gyroscopes' system (Figure 1) is represented by two angles ε_1 (respectively, ε_2 , ε_3), which corresponds to the angle between the X" axis (respectively, Y", Z") and the X axis (respectively, Y, Z) and α_1 (respectively, α_2 , α_3), which corresponds to the angle between the projection of the X" axis (respectively, Y", Z") direction on to the plane (Y, Z) (respectively, (Z, X), (X, Z)) and the Y axis (respectively, Z, X) .

The matrix **C** which represents the orientation of the three skewed sensors (X", Y", Z") within the vehicle reference frame is then

$$\mathbf{C} = \begin{pmatrix} \cos\varepsilon_1 & \sin\varepsilon_2 \sin\alpha_2 & \sin\varepsilon_3 \cos\alpha_3 \\ \sin\varepsilon_1 \cos\alpha_1 & \cos\varepsilon_2 & \sin\varepsilon_3 \sin\alpha_3 \\ \sin\varepsilon_1 \sin\alpha_1 & \sin\varepsilon_2 \cos\alpha_2 & \cos\varepsilon_3 \end{pmatrix} \tag{9}$$

The true expression for equation 8 of the unprocessed output of the magnetometer at the skewed sensors' coordinate system (X", Y", Z") becomes then,

$$\mathbf{f}' = \mathbf{C}^{-1}(\mathbf{R}^t\mathbf{f} + \mathbf{G}\mathbf{R}^t\mathbf{f} + \mathbf{b}_r) \tag{10}$$

The 12 parameters of the matrices $\mathbf{C^{-1}G}$ and $\mathbf{b_r}$ represent not only the magnetic distribution of the vehicle, as Isezaki (1986) and Korenaga (1995) propose, but also the orientation of the sensors within the vehicle reference frame. In contrast to a vector calibration, the originality of the scalar approach is that the calibration is performed on the intensity of the field and not its vector, i.e. the matrices **C** and **R**, which represent the spatial orientation of the sensors, do not have to be considered. The problem is then written as

$$\mathbf{f}' = \mathbf{G}\mathbf{f} + \mathbf{b}_r \tag{11}$$

Leliak (1961) has shown that the susceptibility matrix **G** is expressed as a matrix containing six unknowns like $\mathbf{S}\cdot\mathbf{P}$ in equations 1 and 3 while the permanent effect of the vehicle $\mathbf{b_r}$ is included in the offset errors of the sensor. This means that the scalar calibration and the magnetic compensation of the effect of the vehicle use the same equations. Consequently, the scalar calibration includes the instrumental correction as well as the magnetic compensation and since the sensors are fixed to a relatively strong magnetized body (up to thousands of nanoteslas), the estimation of the nine "intrinsic" parameters is not separated from the magnetized effect of the vehicle. In other words, each parameter is a combination between the instrumental errors and the magnetic effect of the vehicle (Figure 2).

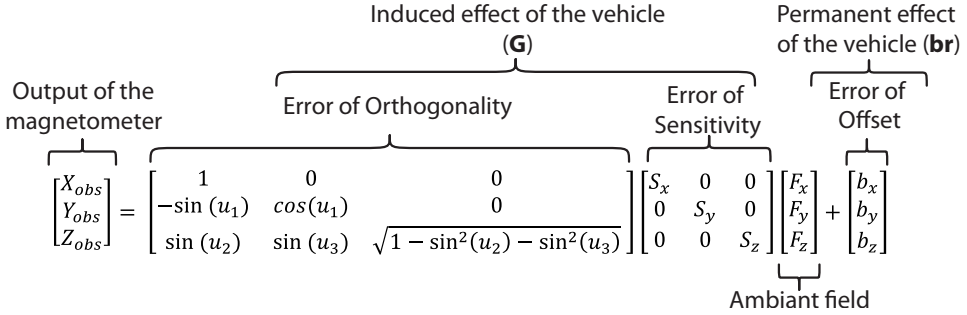

Figure 2 : Equations representing the effect of the intrinsic errors of measurement of the magnetometer and the magnetic effect of the vehicle on the output of the magnetometer. This Figure shows that the magnetic compensation and the scalar calibration use the same equations.

2.3. CASE STUDY

Calibration and compensation of the magnetometer are usually achieved using data acquired during a calibration experiment. In order to constrain as much as possible the calibration parameters, the magnetic field is recorded in a region where it is either known or constant and with the most variable attitude of the vehicle. Therefore, the tow-fish is maneuvered in a loop with heading variations of at least 360° whereas variations of pitch and roll are obtained by successively hauling in and paying out the wire.

Figures 3a to 3e show the result of the scalar calibration performed on the three-component magnetometer of the Towed Ocean Bottom Instrument (TOBI) (Flewellen et al., 1993) during the Smoothseafloor cruise of the R/V Marion Dufresne (Fall 2010). The TOBI was towed in a 360° turn (Figure 3c) within an area of the Southwest Indian Ridge where the geomagnetic field was assumed to be constant. During the turn, variations of pitch and heading clearly affect the magnetic signal with an effect of up to 3000 nT (blue curve Figure 3a) relative to the theoretical regional field (IGRF). After calibration and without filtering the data, the standard deviation of the corrected signal was only 4.11 nT (for a standard deviation of the IGRF of about 3.53 nT; Figure 3a and 3e). This means that even with a low maneuverability during the turn (only 1° of roll and a maximum of 10° of pitch), the magnetic effect of the tow vehicle is well estimated using the scalar calibration. This was confirmed by two other calibration loops achieved during the same cruise and leading to a standard deviation of the corrected field of 4.58 nT and 3.11 nT. As a comparison, for the same calibration experiments, the standard deviation of the magnetic field after using a vector calibration approach was about 100 nT. Hence, we provide here a significant improvement in obtaining valuable marine magnetic anomaly profiles with an accuracy of the corrected signal similar to that of proton precession magnetometers.

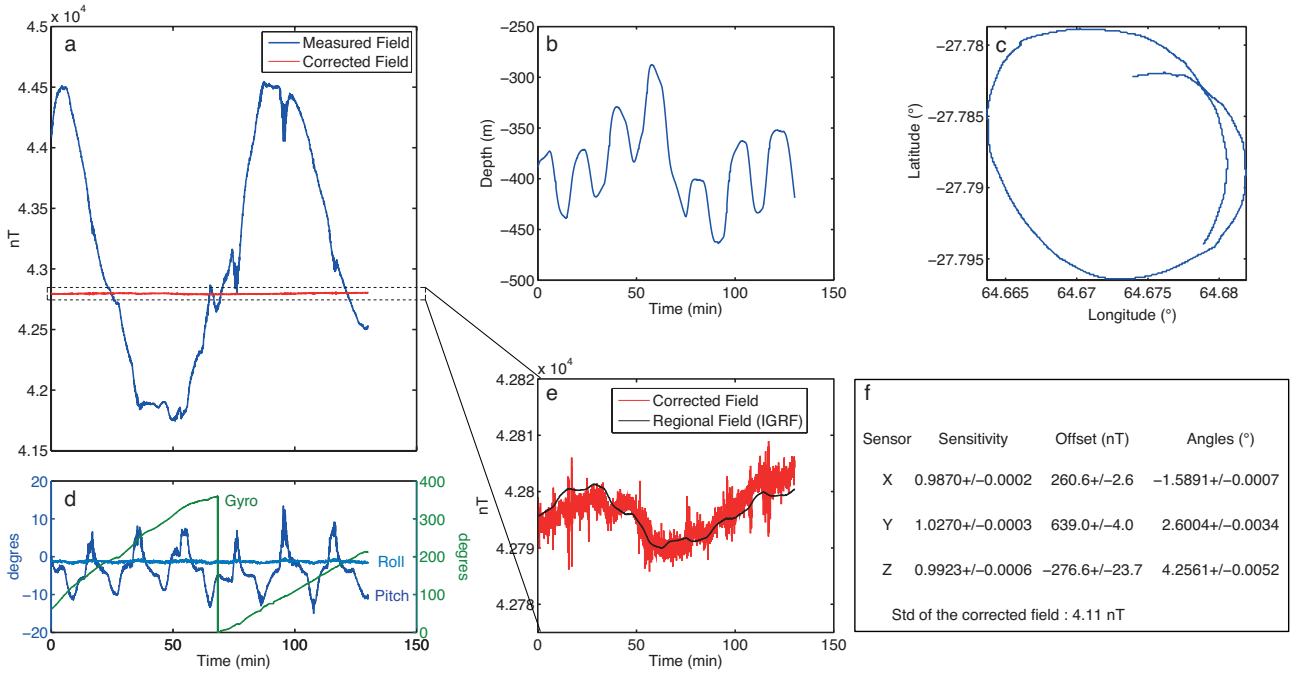

Figure 3 : Scalar calibration of the deep-tow fluxgate magnetometer. a, the blue line indicates the measured field during the calibration experiment and the red line indicates the corrected field. b, depth of the tow-vehicle during the calibration experiment. c, route of the vehicle. d, attitude of the vehicle during the experiment. e, regional field (IGRF) versus corrected field. f, the nine calibration parameters and their associated errors estimated by the scalar approach.

In our case, the attitude of TOBI was given by two inclinometers and a gyrocompass that record respectively pitch, roll and heading. The range of TOBI's SSY0091P dual axis inclinometer was ±20°, with an accuracy of ±0.06° at 10° and ±0.6° at 20° (Flewellen et al., 1993), whereas the Octan 6000 gyrocompass provided the heading within a resolution of 0.01° and an accuracy of 0.1°. Korenaga (1995) demonstrated that for a vector calibration approach, measurement errors in the vehicle attitude result in errors of estimation in the vehicle magnetization. This is well illustrated on Figure 4. This Figure shows a magnetic profile across the eastern part of the Southwest Indian Ridge. During the acquisition of the magnetic field, TOBI was towed at low speed (about 2 kt or 1 $m.s^{-1}$) along a South-North straight line. In order to maintain the tow-fish as close as possible to the magnetic source, the wire was successively hauled in and payed out. Although, the TOBI was designed to be stable to roll (buoyancy high up on the frame), the tow system makes it susceptible to pitch. Variation in roll and heading were thus very low (about 1°) whereas pitch varied within a range of ±10° as vehicle tends to pitch up (respectively down) while being hauled in (respectively payed out). The magnetic effect of the vehicle is thus well illustrated by the clear correlation between variations in pitch (blue curve Figure 4b) and variations in the measured magnetic signal (black curve Figure 4a). Although these high frequency magnetic anomalies related to variations in the vehicle motion were attenuated using a vector calibration approach (blue curve Figure 4a), they were completely removed using the scalar calibration (red curve Figure 4a). This was also well demonstrated for a land survey by Munschy et al. (2007) who showed that after scalar calibration the remaining signal was very close to the Gaussian noise generated by the sensor and the analog-digital converter itself. We stress that the data were not filtered, the scalar or vector calibration being the only processing applied to the raw data (Figure 4).

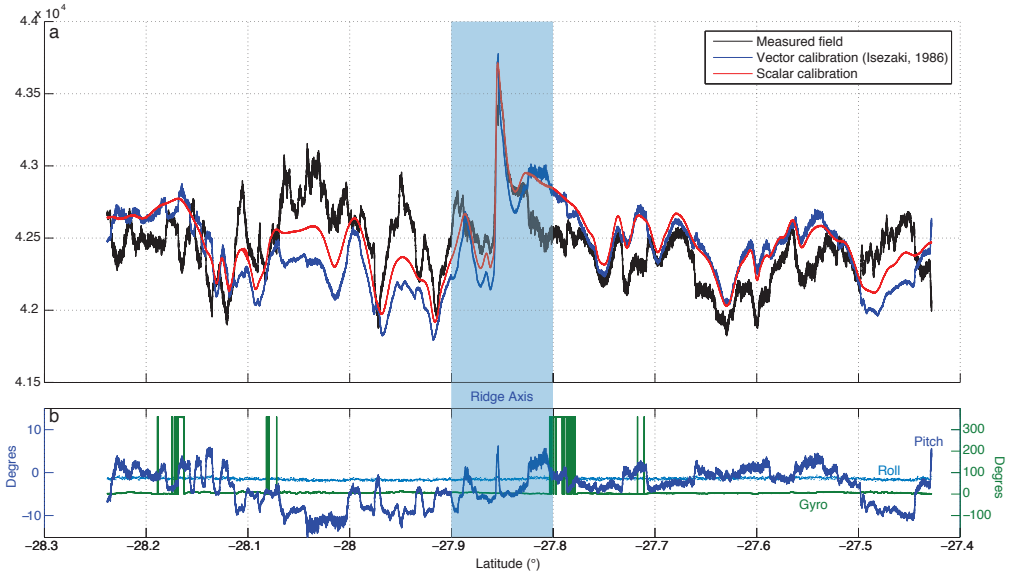

Figure 4 : North-south line acquired across the Southwest Indian Ridge at 64°E. a, comparison between measured data, data after vector calibration and data after scalar calibration. b, attitude of the tow-fish along the line.

Laboratory calibration of towed surface vector magnetometers has demonstrated a significant instrumental drift mainly related to the temperature-dependency of the calibration parameters (Gee and Cande, 2002; Engels et al., 2008). Nevertheless, for such a highly magnetized vehicle as sidescan sonar, intrinsic errors are negligible compared to the tow-instrument's magnetic interference. Therefore, it is neither technically possible to determine the vehicle signal separately from the intrinsic parameters, nor possible to draw conclusions about their temperature-dependency. Moreover, during the calibration turn (Figure 3) the mean water temperature was about 12.3°C for a standard deviation of 0.4°C whereas during near-bottom data acquisition (line presented Figure 4) the mean water temperature was about 2°C for a standard deviation of 0.8°C. Thus, despite the 10°C difference between the calibration experiment and the near-bottom survey, the calibration parameters look stable during data collection. All the short wavelengths associated with the vehicle movements are well corrected (Figure 4). This illustrates that our estimation of the calibration parameters (i.e. intrinsic errors and vehicle magnetization) is valuable all along the 100 km profile with no significant instrumental drift.

Similarly, moving the vehicle structure through an inhomogeneous magnetic field may have induced eddy-currents, but it is not clear in the literature whether this effect has a significant influence during data acquisition; most of the papers that deal with marine magnetic data overlooked this problem. In our case, the comparison between upward continued data and data from a sea surface proton magnetometer (Figure 5b) is the only indication we have to suggest that this effect has little if any impact on the calibrated data.

Note also that the scalar approach gives only the corrected components at the sensor's orthogonal coordinate system ([X', Y', Z']; Figure 1) for which the spatial orientation remains unknown. Consequently, only the total field anomaly is suitable using this method.

3. THE EQUIVALENT LAYER, PRELIMINARY INTERPRETATION OF THE MAGNETIC SIGNAL

After calibration the corrected signal corresponds to the magnetic field acquired along the vehicle path. This signal includes two components that must be removed before it is useful for the analysis of seafloor tectonics: one related to the variations in altitude of the tow-vehicle and the other to the seafloor topography. Here we develop an approach based on the equivalent layer technique proposed by Dampney (1969) in order to establish the magnetization distribution within the oceanic crust which can be further used for upward continuation and vector computation.

3.1. THEORY

Dampney (1969) has shown that a potential field measured on an even or uneven surface (z) can be explained by a source located on another surface (z') for which geometry and location are not necessary representative of the true causative sources. In other words, multitude of equivalent sources can explain one single measured field. This means that whatever the distance between z and z', there always exists a unique correspondence between the given potential field and a given distribution of magnetic dipoles.

The potential field V at the point $\mathbf{x}(x_i, y_i, z_i)$ due to a magnetized dipole $\mathbf{m}(m_x, m_y, m_z)$ located at the point $\mathbf{y}(x_j, y_j, z_j)$ can be written as

$$V(x_i, y_i, z_i) = \frac{m_x(x_j - x_i) + m_y(y_j - y_i) + m_z(z_j - z_i)}{\left[(x_j - x_i)^2 + (y_j - y_i)^2 + (z_j - z_i)^2\right]^{\frac{3}{2}}} = \mathbf{m} \cdot \frac{(\mathbf{y} - \mathbf{x})}{|\mathbf{y} - \mathbf{x}|^3} \tag{12}$$

Then, the magnetic field due to the dipole is defined as

$$\mathbf{f}(x_i, y_i, z_i) = -\nabla V(x_i, y_i, z_i) \tag{13}$$

Thus,

$$\mathbf{f}(x_i, y_i, z_i) = \begin{bmatrix} \dfrac{m_x\left[2(x_j - x_i)^2 - (y_j - y_i)^2 - (z_j - z_i)^2\right] + 3m_y(x_j - x_i)(y_j - y_i) + 3m_z(x_j - x_i)(z_j - z_i)}{\left[(x_j - x_i)^2 + (y_j - y_i)^2 + (z_j - z_i)^2\right]^{\frac{5}{2}}} \\ \dfrac{3m_x(x_j - x_i)(y_j - y_i) + m_y\left[-(x_j - x_i)^2 + 2(y_j - y_i)^2 - (z_j - z_i)^2\right] + 3m_z(y_j - y_i)(z_j - z_i)}{\left[(x_j - x_i)^2 + (y_j - y_i)^2 + (z_j - z_i)^2\right]^{\frac{5}{2}}} \\ \dfrac{3m_x(x_j - x_i)(z_j - z_i) + 3m_y(y_j - y_i)(z_j - z_i) + m_z\left[-(x_j - x_i)^2 - (y_j - y_i)^2 + 2(z_j - z_i)^2\right]}{\left[(x_j - x_i)^2 + (y_j - y_i)^2 + (z_j - z_i)^2\right]^{\frac{5}{2}}} \end{bmatrix} \tag{14}$$

We introduce $x_{ij}= x_j - x_i$, $y_{ij}= y_j - y_i$, $z_{ij}= z_j - z_i$, where the indices i correspond to the points where the magnetic field is measured and j the indices of the dipoles. The magnetic field at the point i corresponds then to the sum of the magnetic effect of all dipoles as

$$\begin{aligned} f_{x_i} &= \sum_j \frac{m_{jx}\left(2{x_{ij}}^2 - {y_{ij}}^2 - {z_{ij}}^2\right) + 3m_{jy}x_{ij}\,y_{ij} + 3m_{jz}x_{ij}z_{ij}}{\left[{x_{ij}}^2 + {y_{ij}}^2 + {z_{ij}}^2\right]^{\frac{5}{2}}} \\ f_{y_i} &= \sum_j \frac{3m_{jx}x_{ij}\,y_{ij} + m_{jy}\left(-{x_{ij}}^2 + 2\,{y_{ij}}^2 - {z_{ij}}^2\right) + 3m_{jz}\,y_{ij}z_{ij}}{\left[{x_{ij}}^2 + {y_{ij}}^2 + {z_{ij}}^2\right]^{\frac{5}{2}}} \\ f_{z_i} &= \sum_j \frac{3m_{jx}x_{ij}z_{ij} + 3m_{jy}\,y_{ij}z_{ij} + m_{jz}\left(-{x_{ij}}^2 - {y_{ij}}^2 + 2{z_{ij}}^2\right)}{\left[{x_{ij}}^2 + {y_{ij}}^2 + {z_{ij}}^2\right]^{\frac{5}{2}}} \end{aligned} \tag{15}$$

Because we work with marine magnetic profiles, we assume the structures to be parallel to the spreading ridge, with x normal to the ridge axis, y parallel to the axis and z vertically down. In other words, we assume that the anomalous magnetic field is due to an equivalent layer that extends infinitively and perpendicularly to the profile. After integration of equation 15 from -∞ to +∞ in the y-direction, the components become

$$\begin{aligned} f_{x_i} &= 2\sum_j \frac{m_{jx}\left({x_{ij}}^2 - {z_{ij}}^2\right) + 2m_{jz}x_{ij}z_{ij}}{\left[{x_{ij}}^2 + {z_{ij}}^2\right]^2} \\ f_{y_i} &= 0 \\ f_{z_i} &= 2\sum_j \frac{2m_{jx}x_{ij}z_{ij} - m_{jz}\left({x_{ij}}^2 - {z_{ij}}^2\right)}{\left[{x_{ij}}^2 + {z_{ij}}^2\right]^2} \end{aligned} \tag{16}$$

The anomalous magnetic field (A) due to the layer is the projection of the three components in the direction of the Earth's magnetic field itself,

$$A_i = f_{z_i}\sin I + f_{x_i}\cos\,(D - \alpha)\cos I \tag{17}$$

where D, I and α are respectively the declination and inclination of the Earth's magnetic field and the azimuth of the profile. We also introduce the magnetization of the dipole as a function of its inclination and declination (i and d):

$$\begin{aligned} m_x &= |\mathbf{m}_j|\cos d\cos i \\ m_y &= |\mathbf{m}_j|\sin d\cos i \\ m_z &= |\mathbf{m}_j|\sin i \end{aligned} \tag{18}$$

The anomalous field at the point i is then written as

$$A_i = \left(\sum_j \frac{2|\mathbf{m}_j| \text{cosdcosix}_{ij} z_{ij} - |\mathbf{m}_j| \text{sini}\left(x_{ij}^2 - z_{ij}^2\right)}{\left[x_{ij}^2 + z_{ij}^2\right]^2} \right) \text{sinI}$$
$$+2 \left(\sum_j \frac{|\mathbf{m}_j| \text{cosdcosi}\left(x_{ij}^2 - z_{ij}^2\right) + 2|\mathbf{m}_j| \text{sinix}_{ij} z_{ij}}{\left[x_{ij}^2 + z_{ij}^2\right]^2} \right) \cos(D - \alpha)\, \text{cosI} \tag{19}$$

Introducing:

$$\begin{aligned} a &= \text{cosicosdsinI} + \text{sinicos}(D - \alpha)\text{cosI} \\ b &= \text{cosicosdcos}(D - \alpha)\text{cosI} - \text{sinisinI}, \end{aligned} \tag{20}$$

we have

$$A_i = 2 \sum_j |\mathbf{m}_j| \left[\frac{2x_{ij} z_{ij} a + \left(x_{ij}^2 - z_{ij}^2\right) b}{\left[x_{ij}^2 + z_{ij}^2\right]^2} \right] \tag{21}$$

Assuming the magnetic direction of both the Earth's magnetic field and the equivalent source is known (equation 17 and 18), equation 21 is linear in and the magnetization strength can be solved by a linear least-square approach:

$$m = (\mathbf{X}'\mathbf{X})^{-1}\mathbf{X}'A \tag{22}$$

where **X** is the NxM matrix,

$$\mathbf{X} = 2 \left[\frac{2x_{ij} z_{ij} a + \left(x_{ij}^2 - z_{ij}^2\right) b}{\left[x_{ij}^2 + z_{ij}^2\right]^2} \right] \tag{23}$$

A represents the N samples of the measured magnetic field and m is the magnetization distribution along the M points of the equivalent layer.

Once the equivalent layer is computed, the magnetic field (equation 21) as well as its components (equation 16) can be calculated at any location outside the source. In contrast to a frequency domain reduction (Guspi, 1987), the field can be calculated at constant or variable altitude with no recourse to an iterative resolution and using all the information available in the measured field.

Because there are an infinity of equivalent source configurations that could explain the measured anomalous field, the spatial distribution of the discrete magnetized equivalent points has no particular significance to carry out vertical continuation. Nevertheless, besides the projection and interpolation of a known field at any other points in space, we investigate the possibility of using the equivalence layer method to estimate (1) the depth of the magnetic sources, (2) the magnetization intensity of the oceanic crust, (3) the location of the magnetic boundaries (i.e. the location of the reversals of the Earth magnetic field) and (4) the value of the anomalous vector. To do so, as usually assumed for oceanic crust generated at mid oceanic spreading centers, we consider that a 2D source layer draped on the bathymetry with successive polarity inversions is responsible for the observed magnetic anomalies. The magnetization vector orientation is chosen to be constant and homogeneous along the layer (equations 17 and 18) and its orientation collinear to the Earth's magnetic field. Dampney (1969) showed that the distance between the surface where the field is measured and the location of the equivalent layer should satisfy a lower and upper bounds for avoiding respectively aliasing effect in the computed field and ill-conditioned matrix A (equation 17). In our case, because the data spacing (~10 m) is clearly inferior to the altitude of the TOBI from the seafloor, the upper bound can be constrained by the top of the seafloor rather than the aliasing frequency. On the other hand, an equivalent source located too far below the measurement surface makes the matrix X ill defined and the associated solution unreliable (Dampney, 1969). In marine geophysics the sources responsible for the magnetic anomalies are supposed to be located in the upper part of the oceanic crust and within a layer of constant thickness. Therefore, the lower bound (i.e. depth where the matrix X becomes ill-defined) provides a first guess on the maximum depth of the "true" causative sources. This can be empirically estimated by iteratively increasing the depth of the source until both losses of high frequencies content in the computed field and first appearance of oscillations in the magnetization solution.

3.2. APPLICATION

We use the same data set acquired on the Southwest Indian Ridge at 64°E. Figure 5 shows the results from the equivalent layer technique applied on the same deep-tow magnetic profile that was presented in Figure 4. Figure 5c shows the difference between measured field along the TOBI path and that calculated from the chosen equivalent sources, while Figure 5d shows the magnetization intensity of this equivalent layer. Assuming that a homogeneous 500 m layer accounts for the observed magnetic anomalies (a classical model for marine magnetic anomaly), inferred magnetization values (equation 18) were divided by the dipole spacing and layer thickness values in order to be expressed in units of ampere per meter. The aim was to find the best combination of the minimized difference between measured and calculated field and a stable magnetized distribution of the layer by varying the depth and spacing of the equivalent dipoles. The whole frequency content of the measured filed

was retrieved (Figure 5a) for dipoles spaced 800 m apart and 500 m below the seafloor; whereas solution became unreliable for deepest sources. The mean value of the residual (Figure 5c) was 6 nT and its standard deviation 25 nT. Only a few high frequency magnetic anomalies, related to the very close proximity between the tow instrument and the ocean floor (Figure 5e), were not explained by the equivalent layer.

The validity of the method was tested through a comparison with classical inversions (Hussenoeder et al., 1995) using the same data spacing, layer thickness and with no data filtering (black dashed curve; Figure 5d). Both methods provided similar results, but the equivalent source technique presented here only requires one linear inversion to be computed (equation 22) with no recourse to an equivalent source geometry (Hussenoeder et al., 1995; Pilkington and Urquhart, 1990) or to a frequency domain reduction (Guspi, 1987; Hussenoeder et al., 1995). Therefore, within the assumptions made above, the equivalent layer allows us to draw conclusions about the magnetization intensity of the oceanic crust as well as a first guess regarding the depth of the magnetic sources. As shown in Figure 5e, the magnetization of the layer is also a first order aid constraining the spreading rate and the location of the magnetic polarity boundaries. The magnetic block corresponding to chron C1 is clearly identifiable on the magnetization profile, although it is more difficult to recognize older blocks. This may result from contamination between small adjacent magnetic polarity blocks due to the ultra-slow spreading rate in this part of the SWIR.

Moreover, once the equivalent layer is computed, the synthetized field can be easily calculated at any altitude (i.e. recalculation of the anomalous field from the inferred equivalent source using the appropriate depth in equation 21). This is well illustrated on Figure 5b where the sea-surface proton magnetometer profile is compared with the deep-tow upward continued profile. The good correlation between the two curves validates the effectiveness of the scalar calibration procedure. However, the calculated profile shows a higher amplitude than the measured profile. The maximum offset (~50 nT) between the two curves is obtained for the central anomaly. Two explanations may account for this difference as the presence of fresh and highly magnetized basalts at the ridge axis. Indeed, it has been suggested that the magnetization of the oceanic crust decreases rapidly with respect to the distance from the volcanic ridge (i.e. degree of rock alteration; Gee and Kent, 2007). The deep-towed magnetic data may have thus been more sensitive to this high and superficial magnetization of the ridge axis than the sea-surface magnetometer. Alternatively, a non-perfect two-dimensional geometry of the magnetic sources could be responsible for this data offset. More investigations have to be done to constrain these points.

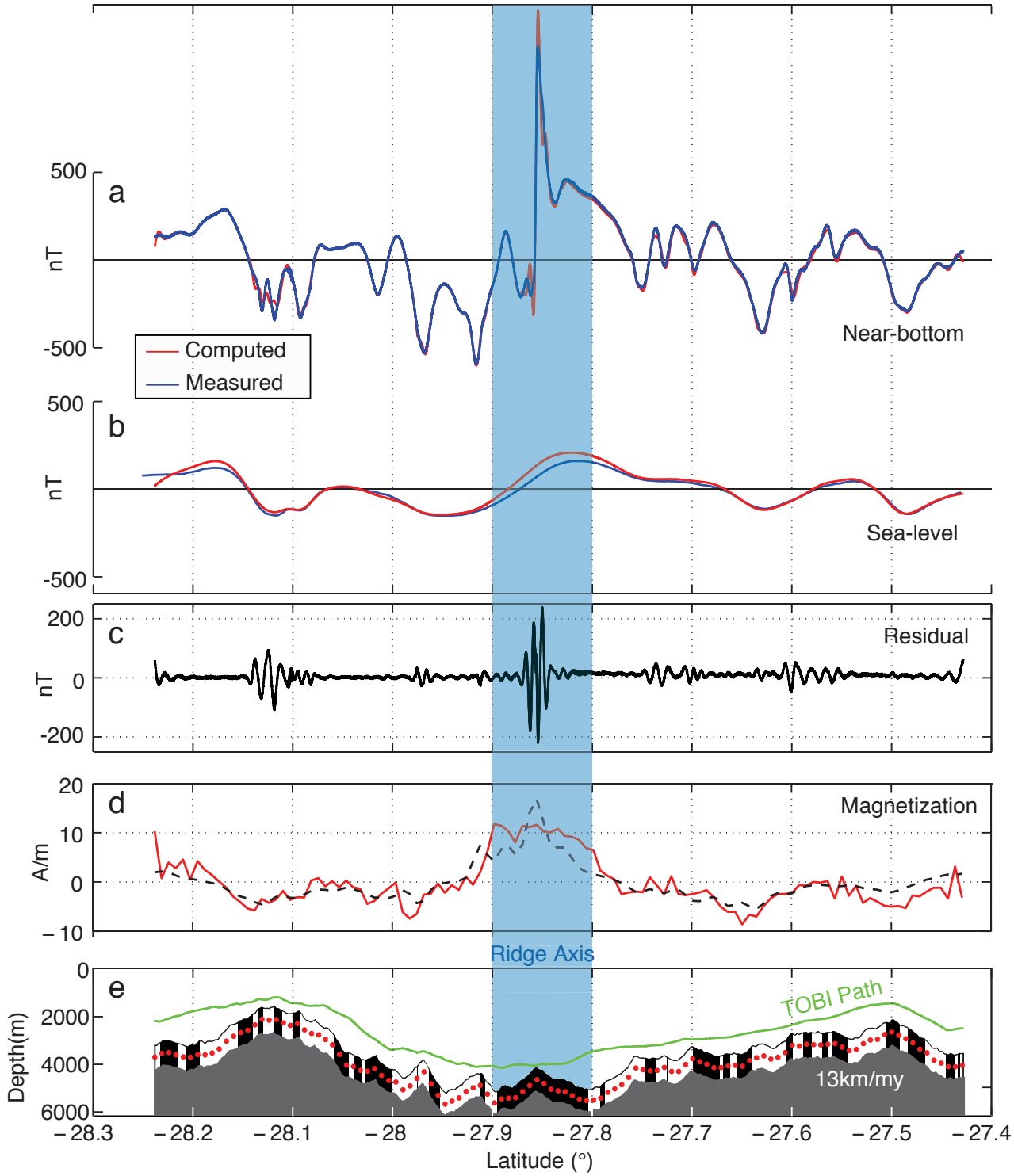

Figure 5 : North-south line acquired at 64°E on Southwest Indian ridge. a, the measured field is compared to the field calculated along the TOBI path for the inferred equivalent sources. b, The sea level upward continued anomalous field (red) is compared to the field measured by the sea-surface proton magnetometer (blue). c difference between measured and calculated fields (of panel a) along the TOBI path. The mean value of this residual was 6 nT and its standard deviation 25 nT. d, the magnetization of the equivalent layer (red curve) is compared with the one obtain by direct inversion from Hussenoeder et al. (1995) (black dotted line) . e, the magnetic reversal pattern is based on a 13 km/m.y. constant spreading rate and is superimposed on the sea-bottom bathymetry. The red dots indicate the locations of the equivalent sources (500 m below the sea-floor) and the green curve indicate the uneven TOBI track.

3.3. MAGNETIC VECTOR

The combination of the scalar calibration and the equivalent source technique is a powerful tool for providing a valuable model of magnetization intensity of the oceanic crust. Nevertheless, both calibration and equivalent layer methods have two main limitations: (1) the calibration provides only the corrected intensity of the magnetic field and not the corrected components, (2) the equivalent layer assumes a 2D geometry of the magnetic sources and does not allow conclusions about local crustal heterogeneities. Thus, the main remaining question concerns what information may have been included in the measured components and what may have been lost due to both the calibration procedure and the 2D assumptions. In order to quantify this error we decided to compare the measured components obtained by vector calibration (Isezaki, 1986; Korenaga, 1995) with the components calculated from the equivalent layer. Figure 6 shows the comparison of the calculated and measured components for the magnetic profile acquired across the Southwest Indian Ridge at 64°E. The noise on the measured vertical is the lowest of the three components (Figure 6a). This is well explained by the orientation of the magnetic field in this area (declination: ~ -29°; inclination ~ -61°). Indeed, due to signal to noise ratio, as the vector calibration uses the components to resolve the magnetic effect of the vehicle, the best resolution is obtained for the strongest geomagnetic component (i.e., the vertical component with up to ~36000 nT in this area) whereas the lowest resolution is obtained for the weakest components, (i.e North and East with respectively ~17000 nT and ~10000 nT).

A good fit between calculated and measured data is observed for the vertical component, where the overall measured magnetic anomalies are present in the synthesized signal. In contrast, there is a poor fit between the calculated and the measured north components. This is well explained by the inaccuracy of the vector calibration procedure combined with the large field inclination, E-W strike of the ridge axis, and vehicle motion mainly represented by pitch, making the north component the most affected by the tow-fish movement. This is well illustrated in Figure 6b where a clear correlation between pitch and north-measured component is observed. Note also that despite up to 500 nT of noise in the east-measured component, the apparent absence of magnetic anomalies seems to confirm the East-West strike of the magnetic boundaries.

Figure 6 shows that the accuracy of the vector-calibrated components is no more valuable than the components computed from the scalar-calibrated total field anomaly. We conclude that a well-calibrated measurement of the total intensity of the magnetic field as well as a 2D assumption regarding the geometry of the sources is sufficient to provide, via an equivalent source method, a model that is valuable to carry out upward continuation of the anomalous magnetic vector as well as to provide the depth and magnetization intensity of the magnetic sources within the oceanic crust.

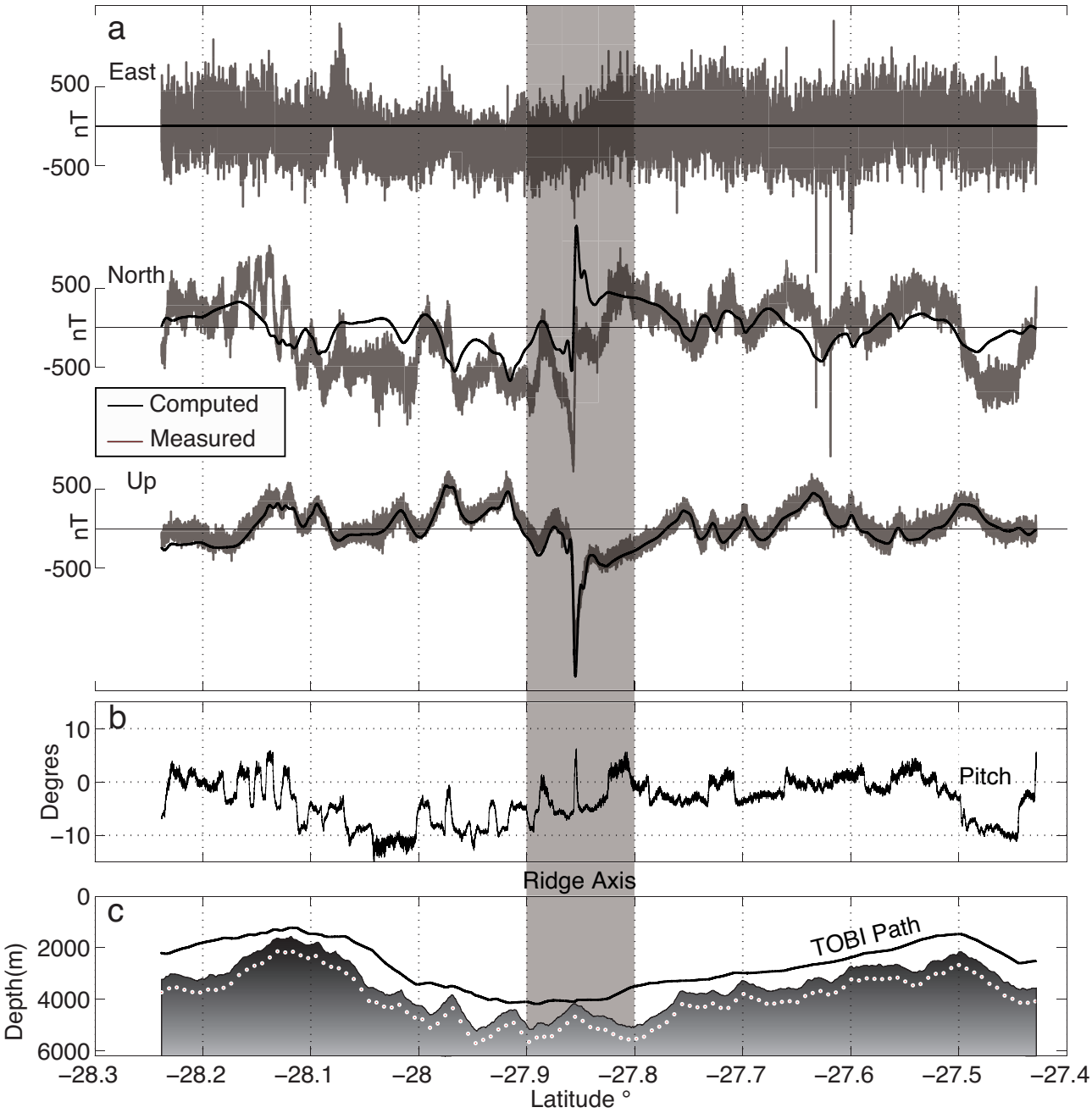

Figure 6 : North-south line acquired at 64°E across the Southwest Indian Ridge. a, Comparison between calculated and measured anomalous vector. Calculated components are obtained using the same equivalent sources as Figure 5 and measured components are corrected using a vector calibration. b, pitch of the vehicle during the survey. c, same as Figure 5e.

4.CONCLUSION

We have presented an analysis of the main problems encountered using deep-tow three-component magnetometers. We show that these magnetometers are affected by three types of intrinsic errors (offset, sensitivity and orthogonality) mainly due to manufacturing and technical difficulties in the orientations of the three sensors. We also demonstrate that vector magnetometry requires a very good knowledge of the spatial orientation of the three sensors in order to reconstruct the geographic components. Due to technical difficulties and gyroscopes' inaccuracy, such a condition is practically never satisfied. Therefore, we propose a new calibration approach. We show that this method allows

one to correct the magnetic data for errors arising from the intrinsic parameters of the magnetometer as well as from the magnetic effects of the structure of the bearing vehicle. We also demonstrate that, in contrast to vector calibration, this method does not require the vehicle's attitude and thus eliminates most of the instrumental noise related to the low accuracy of gyroscopes and inclinometers. The estimation of the vehicle magnetic interference is then significantly improved and the corrected signal seems to be only affected by the noise generated by the magnetometer and its analog-digital converter, providing an accuracy of a few nanoteslas.

As only the total field anomaly is suitable for scalar calibration, we developed a method based on the equivalent layer technique in order to compute the vector components. We show that this method, based on a topographic equivalent layer, is sufficient to carry out vertical continuation of the total field as well as its associated vector, and also to provide a first order magnetization of the oceanic crust and estimation of the depth of the sources. We compare the measured components obtained by a vector calibration and the computed components from the inferred equivalent layer and show that the computed vector preserved all the information recorded by the tow-instrument. This means that through a two-dimensional assumption regarding the geometry of the equivalent layer, it is possible to predict the marine magnetic vector anomalies from the measured total field.

Chapitre 2: Le signal magnétique associé aux domaines de manteau exhumé de la dorsale Sud-Ouest Indienne.

La dorsale Sud-Ouest Indienne est caractéristique d'une dorsale de type ultra-lente car les plaques tectoniques s'y séparent à une vitesse d'environ 14 km par million d'années. A cet endroit du globe, le mode d'accrétion océanique diffère du schéma conventionnel car il se produit de façon magmatique mais aussi a-magmatique, comme en témoigne les large zones récemment découvertes formées quasi exclusivement de roches mantelliques exhumées.

Dans ce deuxième chapitre, nous étudions les données acquises lors de la campagne en mer MD183 "Smootheafloor" (Octobre 2010), à la terminaison Est de la dorsale Sud-Ouest Indienne. Nous mettons en parallèle les données magnétiques haute résolution acquises proche du fond, les interprétations géologiques des images sonar (proposées par Sauter et al. (2013)) ainsi que les résultats pétrologiques des dragages. Nous montrons que les fortes variabilités d'aimantation mesurées en laboratoire, sur les échantillons dragués, se retrouvent à l'échelle des zones de manteau exhumé, le long des profils d'anomalie acquis proche du fond. En effet, le signal magnétique associé à la présence de roches mantelliques exhumées apparait plus faible et hétérogène que celui des roches de type basaltique. Nous montrons également, via une modélisation directe des profils d'anomalie magnétique que ni une aimantation induite ni un modèle d'accrétion océanique ne permettent d'expliquer le signal magnétique associé à l'exhumation des roches mantelliques. Finalement, l'absence d'anomalie axiale et l'hétérogénéité magnétique du signal à une échelle de quelques kilomètres nous permet de conclure que l'aimantation rémanente des péridotites serpentinisées n'est pas suffisamment stable pour que celles-ci puissent porter des anomalies magnétiques d'accrétion océanique.

Le texte présenté dans ce chapitre fait l'objet d'un article à soumettre à la revue: "Geochemistry, Geophysics, Geosystems" (G^3) ou "Solid Earth" (SE) et fait suite à la publication de Sauter et al. (2013):

Sauter, D., Cannat, M., Roumejon, S., Andreani, M., Birot, D., Bronner, A., Brunelli, D., Carlut, J., Delacour, A., Guyader, V., MacLeod, C. J., Manatschal, G., Mendel, V., Menez, B., Pasini, V., Ruellan, E., and Searle, R., 2013, Continuous exhumation of mantle-derived rocks at the Southwest Indian Ridge for 11 million years: Nature Geoscience, 6, 314-320.

Magnetic signature of large exhumed mantle domains of the Southwest Indian Ridge: results from a deep-tow geophysical survey over 0 to 11 Ma old seafloor.

Adrien Bronner[1], Daniel Sauter[1], Marc Munschy[1], Julie Carlut[2], Roger Searle[3], Mathilde Cannat[2], Gianreto Manatschal[1]

[1] Institut de Physique du Globe de Strasbourg, IPGS, Strasbourg

[2] Institut de Physique du Globe de Paris, IPGP, Paris

[3] Durham University, Durham, United Kingdom

ABSTRACT

We investigate the magnetic signature of an ultramafic seafloor along the eastern part of the Southwest Indian Ridge (SWIR) where large areas of exhumed mantle formed by successive detachment faulting are observed. They occur in the form of broad ridges associated with smooth, rounded non-volcanic topography and have been suggested to be formed by 11 Myr of continuous exhumation faulting. We present high-resolution data combining deep-tow magnetics, side-scan images and results from dredged samples collected within two exhumed mantle domains. We show that, despite an ultraslow spreading rate, areas where the volcanic upper part of the oceanic crust is clearly established are characterized by well defined seafloor spreading anomalies. However, the exhumed mantle domains where only a few thin volcanic patches are occasionally observed reveal a weak and highly variable magnetic pattern that neither a spreading model nor an induced magnetization can plainly explain. The analysis of the magnetic proprieties of the dredged samples and careful comparison between the nature of the seafloor, the deep-tow magnetic anomalies and the seafloor magnetization suggest that the serpentinized peridotites do not carry a sufficiently stable remanent magnetization to produce seafloor spreading magnetic anomalies in exhumed mantle domains.

1.INTRODUCTION

The eastern part of the ultraslow-spreading Southwest Indian Ridge (SWIR) is among the deepest mid oceanic ridges and represents a melt-poor end-member for this system (Cannat et al., 1999; Cannat et al., 2008). In this region, crustal accretion differs from the conventional seafloor spreading scheme as it occurs at about a 14 mm/a full spreading rate (Patriat et al., 1997) in the form of magmatic but also non-magmatic processes (Cannat et al., 2006). In the past two decades, numerous papers have revealed the presence of exhumed mantle-derived rocks in the oceanic domain (Karson et al., 1987; Cannat et al., 1992; Cannat et al., 1995) but mechanisms leading to the formation of such a peculiar seafloor remain poorly understood. Although it has been proposed that long-lived detachment faults could often accommodate 50% to 70% (Buck et al., 2005) of the plate separation over ~3 Myr, the eastern part of the SWIR is currently the only known oceanic area where continuous mantle exhumation over 11 Myr has been observed (Sauter et al., 2013). Detachment faulting associated with no or very little volcanic activity seems to be the only process producing the oceanic lithosphere. The resulting seafloor, called "smooth seafloor" (Cannat et al., 2006), is thought to be formed by alternating "flip flop" exhumation faulting (Sauter et al., 2013), a mechanism that has also been proposed to explain the formation of the "zone of exhumed continental mantle" (Reston and McDermott, 2011) observed along the ocean continent transition (OCT) in the Western Iberia margin.

In this paper, we investigate the magnetic signal over large exhumed mantle domains in the easternmost part of the SWIR. We present results from a deep-tow geological-geophysical survey over two areas between 62 and 65°E combining magnetic data, geological mapping from sidescan sonar images (from Sauter et al., (2013), see appendix) and dredge sampling. We examine the magnetic signature over a 0 to 11 Ma old smooth seafloor. The aim is to better understand the complexity of the marine magnetic anomalies observed above the serpentinized mantle rocks exhumed at both mid oceanic ridges (Sauter et al., 2008) and OCTs of magma-poor rifted margins (Russell and Whitmarsh, 2003; Sibuet et al., 2007 ;Bronner et al., 2011).

2.GEOLOGICAL BACKGROUND

A significant change in the SWIR's plate motion occured between anomaly C8 and C6 (~24 Ma ago) resulting in a 50% decrease in full spreading rate from slow (24 mm/a) to ultra-slow (14 mm/a) (Patriat et al., 2008). This ultra slow spreading rate varies only slightly along the 7700 km ridge axis. However, compilations of geophysical and geochemical data along the SWIR reveal a large-scale variation of the density and thermal structure of the axial region (e.g. Cannat et al., 1999; Georgen et al., 2001; Cannat et al., 2008). Unusually cold mantle temperatures and relatively thin crust at the eastern SWIR, in particular, east of the Melville transform fault (60°45'E), are supported by evidence on axis (Cannat et al., 2008) as well as off-axis (Sauter et al., 2011). An eastward decreasing crustal

thickness and/or mantle temperature is inferred from gravity data along the SWIR axis (Cannat et al., 1999). It is further supported by geochemical proxies for the degree of partial melting in the mantle (e.g. average of the composition of the sodium content of axial basalts derived from the axial zone) suggesting a progressive eastward decrease of the ridge melt supply (Meyzen et al., 2003; Seyler et al., 2003; Cannat et al., 2008). Thin crust in the easternmost part of the SWIR (3.7 km average crustal thickness) is also confirmed by seismic data (Minshull et al., 2006).

The easternmost part of the SWIR axial valley displays a ridge segmentation that significantly differs from what is observed at faster spreading ridges such as the Mid-Atlantic Ridge (MAR). High-relief ridge segments (>3000 m high) are linked by >100 km long, deep axial sections with almost no volcanic activity (Sauter et al., 2004). The ridge flanks display the widest known areas of seafloor with no evidence of a volcanic upper crustal layer (Cannat et al., 2006). This non-volcanic ocean floor has no equivalent at faster spreading ridges. Cannat et al. (2006) called this seafloor "smooth seafloor" because it occurs in the form of broad ridges with a smooth, rounded topography and lacks the telltale hummocky morphologies of submarine volcanism (Cannat et al., 2006). This non-volcanic seafloor also lacks the corrugations identified on oceanic core complexes at slow spreading ridges. A few dredges in the axial valley from earlier cruises suggested that the smooth seafloor is associated with outcrops of serpentinized mantle-derived peridotites (Cannat et al., 2006). Off-axis dredges and sidescan sonar imagery confirmed that this smooth seafloor is almost entirely composed of seawater-altered mantle rocks resulting in serpentinized peridotites that were brought to the surface by large detachment faults on both sides of the ridge axis (Sauter et al., 2013). The detachment faults have repeatedly flipped polarity and have accommodated nearly 100 % of the plate divergence for the last 10 Myr.

3. ACQUISITION AND PROCESSING OF MAGNETIC DATA

Data presented in this paper were collected during R/V Marion Dufresne cruise MD183 in October 2010 using a 30 kHz sidescan sonar and a three component (3C) magnetometer carried by the Towed Ocean Bottom Instrument (TOBI; Flewellen et al., 1993). The survey was divided into two corridors, a western corridor from 62 to 63°E and an eastern corridor from 64 to 65°E. Seven profiles were acquired in the western corridor, all above exhumed mantle, and four profiles were acquired in the eastern corridor, one above volcanic seafloor and three above exhumed mantle rocks (Figure 1). TOBI was operated at altitudes of 250-700 m above the seafloor at a tow speed of about 2 knots.

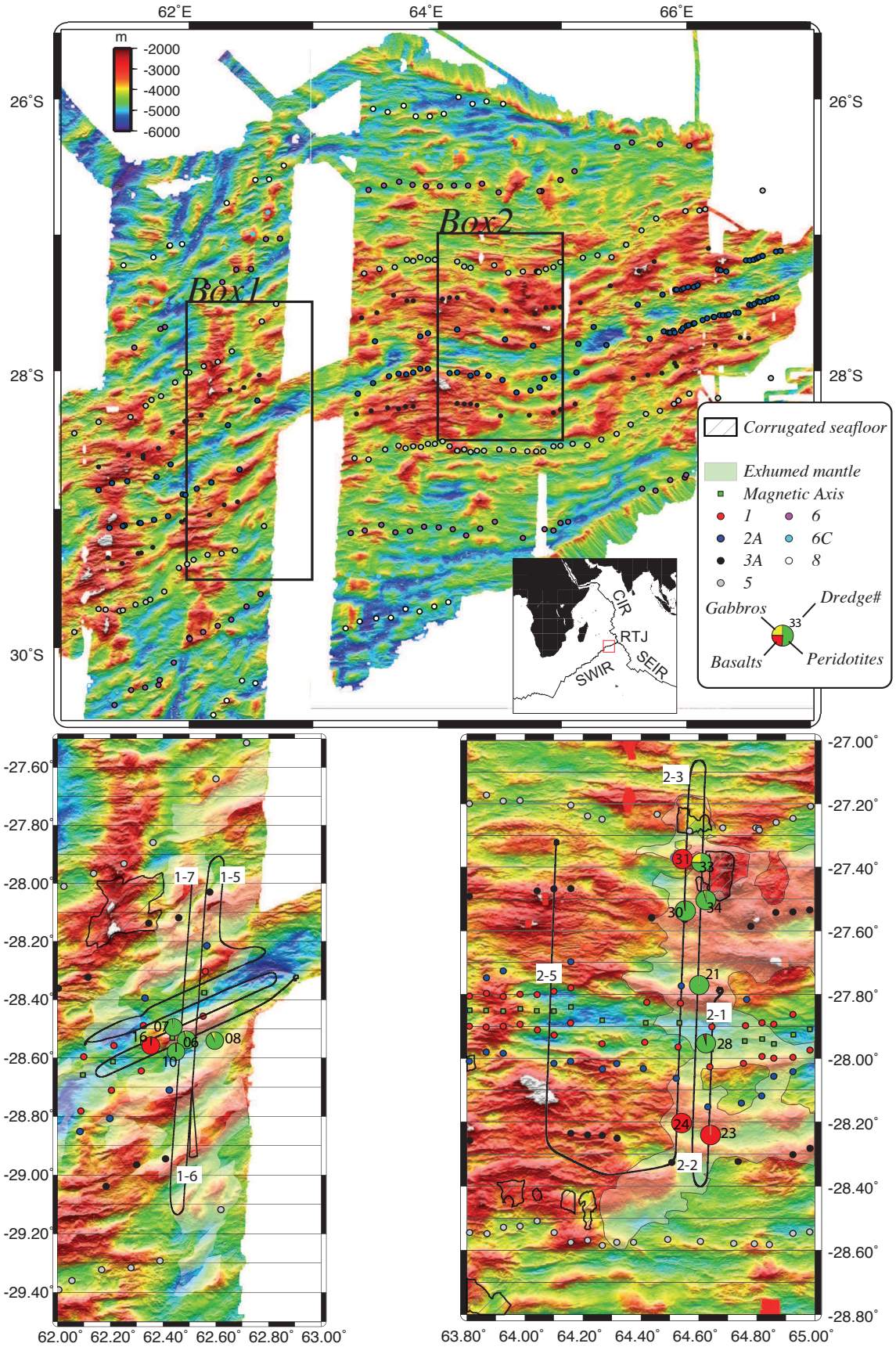

Figure 1 : Location of the two survey areas. Magnetic anomaly picks are from Sauter et al. (2008). The nature of the seafloor was deduced either from the side-scan images when available (as Sauter et al. (2013) propose; see appendix) or from the multibeam bathymetric data (as Cannat et al. (2006) propose). The dredges numbers and the proportion of rocks by weight represented by pie charts are from Sauter et al. (2013). We have only represented the dredges for which we have measured the magnetic properties (see table 1 and Figure 3 and 5)

The three component magnetic data were corrected for the magnetization of the TOBI vehicle using a scalar calibration procedure (Bronner et al., 2013). The magnetic effect of the vehicle was removed with no recourse to its attitude (pitch, roll or heading) as it is commonly done (Isezaki, 1986; Korenaga, 1995), but only using the output of the magnetometer and a model of the scalar intensity of the geomagnetic field (e.g. IGRF). Calibration parameters were thus free from orientation bias (i.e. reduced in number from 12 to 9); moreover, the estimation of both instrumental mis-calibration and removal of the vehicle effect were performed simultaneously. In order to constrain the calibration parameters as much as possible, the geomagnetic field was recorded in a 360° calibration loop in a region of the SWIR where the field was expected to be constant, and with the most variable possible attitude of the vehicle. Indeed, better results would have been expected using the output of the proton sea-surface magnetometer as a reference during the turn but, due to maneuverability issues, it was not possible to have both proton and TOBI magnetometers in the water. Variations of pitch and roll were obtained by successively hauling in and paying out the wire. The magnetic signal of the vehicle was found to be about 3500 nT and reduced to less than 10 nT after calibration. Magnetic data presented in this paper were only corrected via these calibration parameters; no filtering was applied and the validity of the processing was confirmed through a comparison between upward continued data and data from a sea-surface proton magnetometer (Bronner et al., 2013).

As magnetic data were acquired along uneven altitudes, we used an equivalent source approach (Dampney, 1969) to invert the magnetic profiles and to perform an upward continuation to a constant observation level. We assume that the measured magnetic anomalies are due to uniformly magnetized dipoles that extend infinitely perpendicular to the spreading and profile direction. The so-called "equivalent layer" is draped on the bathymetry 500 m below the seafloor and magnetization directions are assumed to be parallel to the Earth magnetic field (-60° inclination and -30° declination in this area of the SWIR). Magnetization of the dipoles is then computed in the spatial domain as a single linear inversion to the distances between dipoles and observation points (Bronner et al., 2013). Once the magnetization is obtained, upward continuation is performed by computing the magnetic field due to the equivalent sources at the desired observation level (Figure 2). Over the volcanic seafloor we assume that a standard homogeneous 500 m layer accounts for the observed magnetic anomalies (Gee and Kent, 2007). The inferred magnetization values are thus divided by the assumed dipole spacing and layer thickness to yield units of ampere per meter. Magnetizations above exhumed mantle areas are calculated in the same way, although we have little knowledge about the source layer thickness there. These magnetizations have thus to be taken with care and are only presented as a comparison to the volcanic seafloor. Variations of inverted magnetizations over exhumed mantle domains could either result from changes of intrinsic magnetization or from variability in the source thickness.

To be consistent, all deep-tow magnetic anomaly profiles displayed in figure 2 are upward continued to a constant level of 1200 m below sea level (shallowest depth of the TOBI during the whole survey). 2D magnetic anomaly profiles are represented above seafloor topography in which geological interpretations from side scan images (from Sauter et al., 2013) are superimposed (Figure 2). As the profiles are about 6 km apart (the TOBI side-scan swath width) we do not perform 3D inversion or magnetic mapping; instead, we calculate magnetizations along profiles and display them as colored strips of arbitrary width (Figure 3) superimposed on the bathymetry. Identification of magnetic anomalies are based on Sauter et al. (2008) and Searle and Bralee (2007).

The TOBI 30 kHz side-scan sonar provides 3 m resolution acoustic images of the seafloor. Interpretation of the reflectivity combined with results from dredges leads to the distinction between three types of seafloor (see Sauter et al. (2013) in the appendix): (1) volcanic seafloor, corresponding to highly reflective surfaces composed of volcanic cones (<200 m across) and sinuous scarps characteristic of the presence of pillow lava flows, (2) smooth seafloor, corresponding to smooth and homogeneous topography associated with low and uniform reflectivity and, (3) corrugated seafloor (Cannat et al., 2006) associated with striations comparable to the slip surfaces that are commonly observed at oceanic core complexes of the MAR (Cann et al., 1997). As the sedimentary cover is limited to small patches in this region, the nature of the seafloor below is extrapolated from the surrounding exposed rocks.

4.MAGNETIC SIGNAL OVER VOLCANIC SEAFLOOR: A SEAFLOOR SPREADING MODEL

Profile 2-5 was acquired between anomalies 3A above exclusively volcanic seafloor associated with relatively thick crust suggested by low Residual Mantle Bouguer Anomalies (RMBA < 20mGal; Cannat et al., 2006). We use it as a reference to calibrate the spreading rate and identify the main polarity reversals. The inverted magnetization values reach around 10 A/m at the axis (resulting in a ~500 nT amplitude for the central anomaly) and 5 A/m off-axis. These values are in agreement with previous observations in this area (Searle and Bralee, 2007) and in another section of the SWIR near 58ºE (Hosford et al., 2003). Despite the ultra-slow spreading rate, the main polarity blocks are quite well resolved (Figure 2 and 3) and associated with relatively strong magnetic contacts.

Seafloor spreading anomalies are modeled using MODMAG (Mendel et al., 2005). A 14 mm/a uniform full spreading rate associated with a 500 m thick source layer draped over the topography and a 10 A/m magnetization on-axis decreasing to 5 A/m off-axis are sufficient to reproduce the main magnetic anomalies observed over the volcanic crust at profile 2-5 (Figure 2). A 0.7 contamination coefficient (Tisseau and Patriat, 1981) is used as a good compromise to both account for contamination between adjacent magnetic polarity blocks and preserve the small wavelength anomalies such as anomaly C2 (Figure 2; profile 2-5). There is a reasonable fit between the observed magnetic anomaly

profile and this forward model regarding the central Brunhes anomaly while southern C2A and northern C3A are in agreement with previous identifications on sea surface magnetic anomaly profiles (Sauter et al., 2008). Anomaly C2A is not clearly identified on the northern flank. This is consistent with observations from Searle and Bralee (2007) who showed that this polarity reversal was either smaller than predicted or missing in the northern flank in this area. We also suggest that C2 could account for the two small wavelength events observed on both sides of the central anomaly.

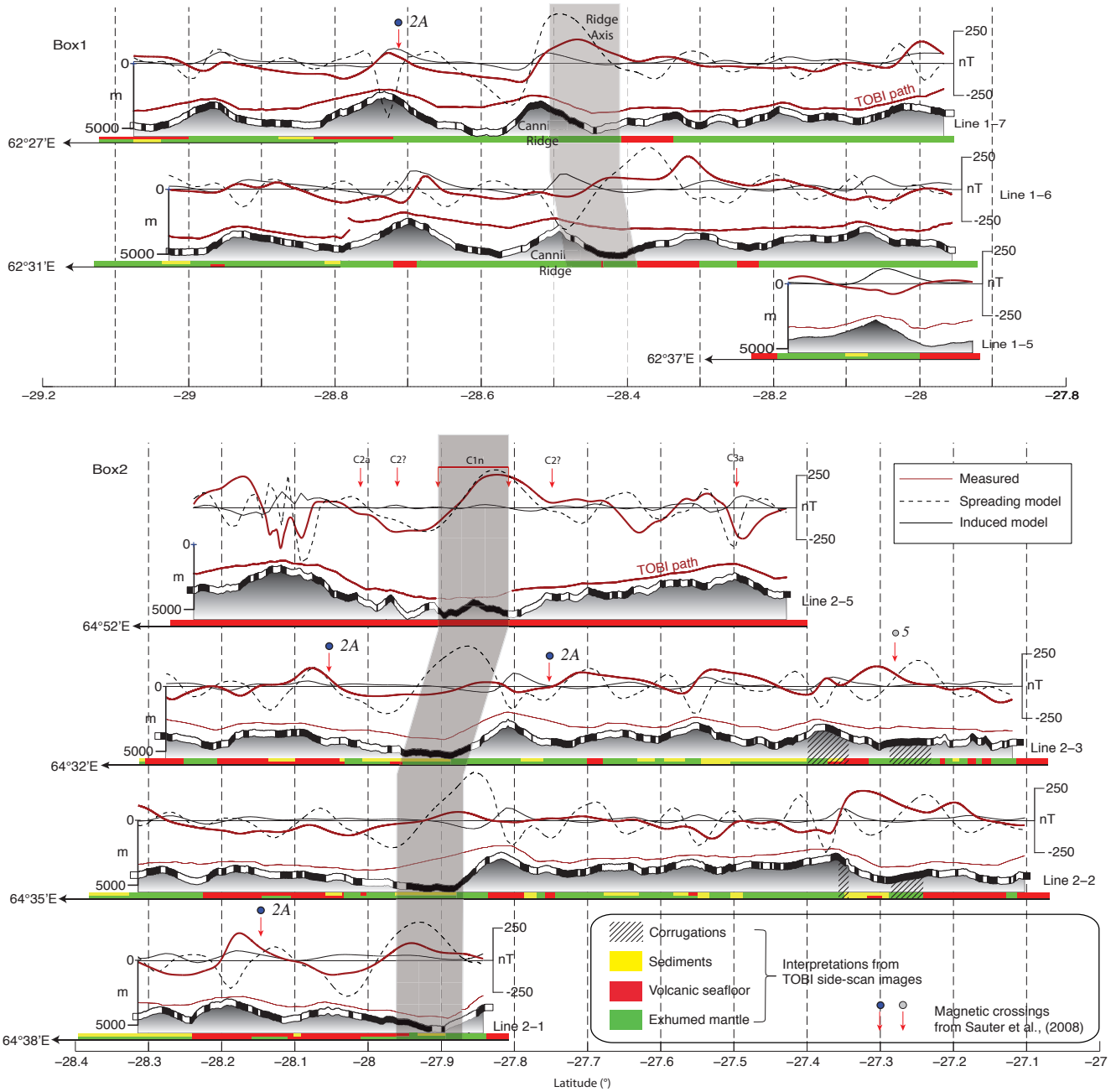

Figure 2 : 2D magnetic profiles recorded within the two survey areas. Magnetic data (continuous red lines) have been upward continued to an altitude of 1200 m below the sea level. Broken lines represent the anomaly predicted by a 14 mm/a. seafloor spreading model calibrated on the volcanic seafloor (Profile 2-5). Black solid lines represent a model based on a 2 km thick source layer for which a solely induced and uniform magnetization is applied (1.5 A/m). Interpretations from the side-scan images are represented below the bathymetry profiles (from Sauter et al., 2013).

5.MAGNETIC SIGNAL OVER EXHUMED SERPENTINIZED MANTLE.

5.1. THE WESTERN CORRIDOR

The western corridor extends between magnetic anomalies C3A (Cannat et al., 2006), and includes two ~100 km long north-south magnetic profiles 6 km apart (Profiles 1-6 and 1-7) and one short (~30 km) profile that does not cross the axis (Profile 1-5; Figure 1). The magnetic data of the east-west profiles are not presented in this paper because the 2D assumption used for the upward continuation and the computation of the magnetization is unreliable in that case. Therefore, we only use the side scan images from these east-west lines to constrain the nature of the seafloor. Careful analysis of bathymetry, side scan images and dredge samples suggest that the seafloor in this corridor is exclusively made of wide serpentinized peridotite ridges topped by thin (<100-200 m thick) volcanic patches (Sauter et al., 2013) (Figures 2 and 3). The axial valley is marked by an unconventional morphology comprising a 2000 m high peridotite ridge, called "Cannibal Ridge" that emerges from the axial domain.

The axial magnetic anomaly is almost missing on profile 1-6 (Figure 2) whereas a higher (~300 nT) amplitude anomaly is observed on profile 1-7 at the top of the Cannibal Ridge. Similarly, few kilometers north of the ridge axis, a ~150 nT amplitude magnetic anomaly that was recorded on profile 1-6 is absent from profile 1-7. Only one anomaly previously picked as C2A (Sauter et al., 2008) and located on top of the first ridge south of the axis is continuous between the two profiles. On the inverted magnetization profiles (Figures 3 and 4), a local magnetic high (up to 10 A/m) located on the north flank of the Cannibal Ridge appears as the axial magnetic block (profile 1-7), whereas just to the east, on profile 1-6, the same feature is shifted northward to the deeper part of the axial valley. Off-axis, the magnetization is quite weak and associated with smooth magnetic contacts.

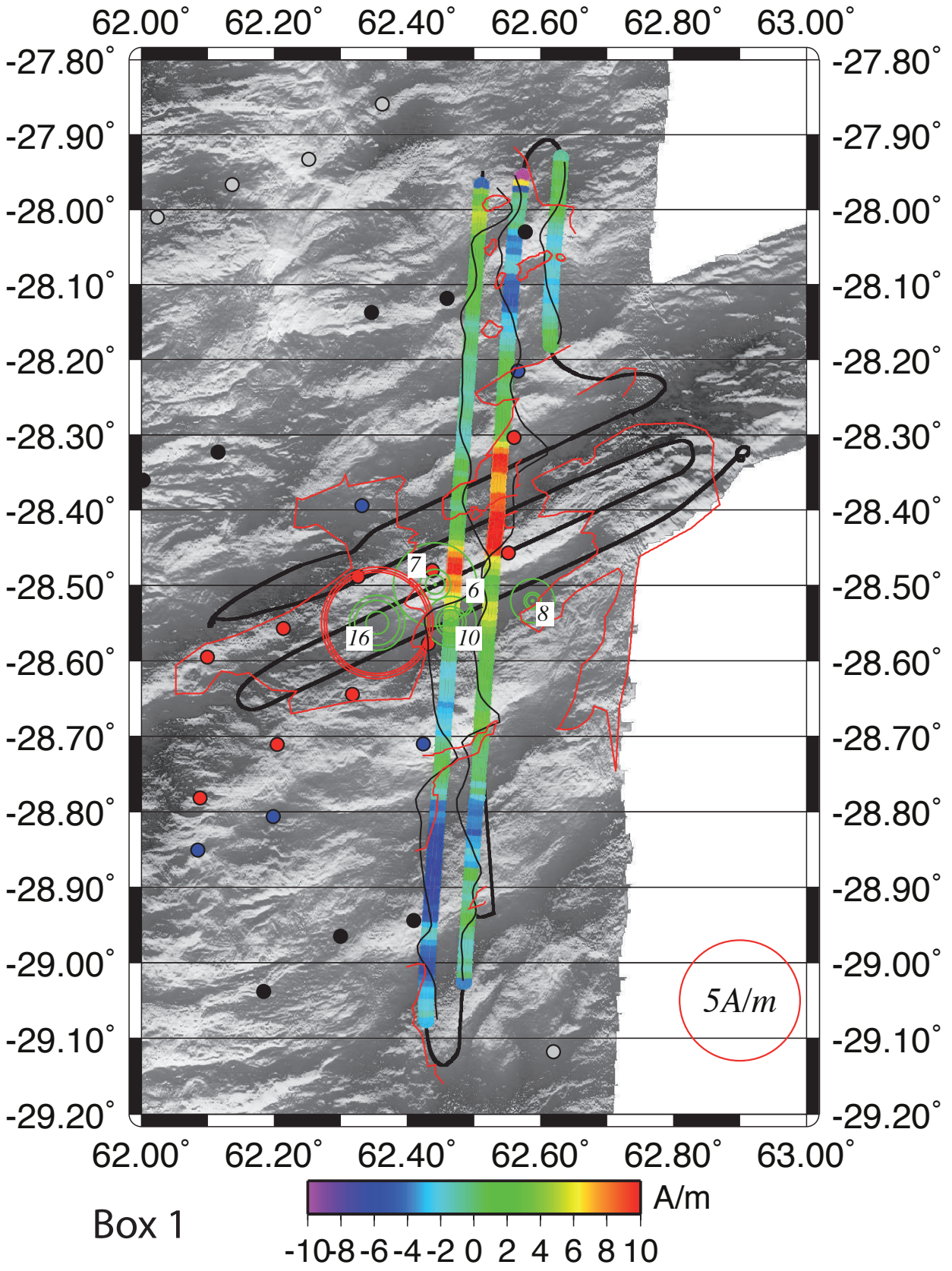

Figure 3 : Box 1, Inverted magnetization represented by colored strips on which the magnetic anomaly profile is superimposed. The multibeam bathymetry is represented as a shaded gray scale background. Red circles represent relative NRM values of dredged basalts whereas green circles represent NRM of dredged peridotites. The red lines representing the edges of the volcanic seafloor, are from Sauter et al. (2013). Picking of magnetic anomalies is the same as Figure 1.

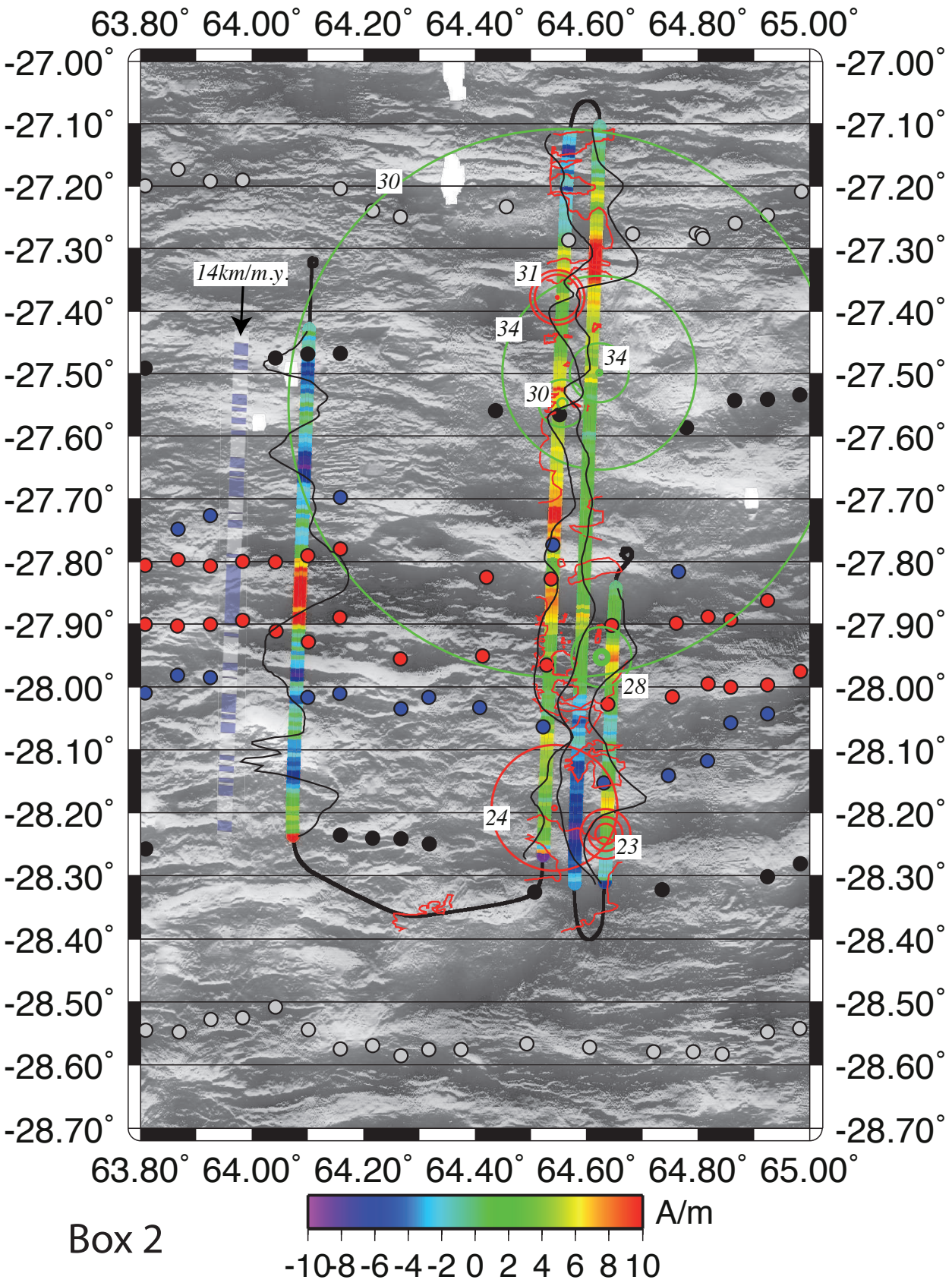

Figure 3 : Box 2, Inverted magnetization represented by colored strips on which the magnetic anomaly profile is superimposed. The multibeam bathymetry is represented as a shaded gray scale background. Red circles represent relative NRM values of dredged basalts whereas green circles represent NRM of dredged peridotites. The red lines representing the edges of the volcanic seafloor, are from Sauter et al. (2013). Picking of magnetic anomalies is the same as Figure 1.

5.2. THE EASTERN CORRIDOR

The eastern corridor (profiles 2-1, 2-2 and 2-3) shows a more complex morphological structure. It is at the transition from an exclusively volcanic seafloor in the west to a wide exhumed mantle domain in the east. It is characterized by a series of broad rounded serpentinized peridotite ridges south of the axial valley, whereas a shallower and flatter topography prevails to the north. The northern end of the survey (near anomaly 5, north of 27.37°S, Figures 2, 3 and 4) shows 2 corrugated surfaces where the recovery of more frequent gabbroic rocks (Sauter et al., 2013) associated with a low RMBA (<20mGal, Sauter et al., 2008) suggest more robust magmatic activity. Apart from this particular area and some thin small volcanic patches less than 300 m thick observed within the axial domain and at the top of some serpentinized peridotite ridges, the eastern corridor is formed almost exclusively of smooth exhumed mantle surfaces associated with very little magmatic supply. Moreover, evidence was found that the ~2400 m high, 25° south dipping northern axial valley wall corresponds to the footwall of a recent large detachment fault cutting the earlier sedimented smooth inner floor and accommodating the plate separation (Sauter et al., 2013).

What has been interpreted as the central magnetic anomaly (Sauter et al., 2008) goes from a very low magnetic anomaly (<100 nT amplitude) above the detachment footwall in the west (profiles 2-3 and 2-2) to a slightly stronger anomaly ~250 nT in the deeper part of the axial valley to the east (profile 2-1; Figures 2 and 3). Similarly, on the south flank, the anomaly picked as C2A on profile 2-1 is shifted 10 km north on profile 2-3 and is almost missing from the profile 2-2. On the conjugate plate to the north, in between the ridge axis and anomaly 5, the magnetic signal is also flat with no clear seafloor spreading anomalies and no lateral continuity; only anomaly C5 seems resolvable and quite continuous.The inverted magnetization profiles (Figure 3) show a similar pattern to those from the eastern corridor: a very flat magnetization associated with smooth magnetic contacts over the exhumed mantle areas. Only anomaly 5 and very local magnetization highs, such as north of the ridge axis on profile 2-3, are observed.

5.3. MAGNETIC STRUCTURE OF THE DIFFERENT TYPES OF SEAFLOOR

At the ridge axis, the magnetization of the exhumed mantle is generally low (< 5A/m), but it can be locally significant (e.g. up to 10 A/m on profile 1-7) and shows ill-defined magnetic contrasts compared to the volcanic areas. No clear wide central block is observed in the western corridor as large magnetized blocks are alternatively observed above the Cannibal Ridge (profile1-7; Figure 4) or in the deeper part of the axial valley (profile1-6; Figure 4). Similarly, the central block is virtually absent within the eastern corridor; a small anomaly with slightly larger magnetizations (up to 8 A/m) is shifting from the southern (profile 2-1; Figure 4) to the northern axial valley wall (profile 2-3; Figure 4). Off-axis, the exhumed mantle surfaces show no evidence for volcanic material (e.g. north

side of the profile 2-2; Figure 4) and are characterized by low magnetizations (mostly < 2 A/m) without any clear continuous magnetic anomaly from one profile to the other.

Apart from profile 2-5 showing large amplitude magnetizations over exclusively volcanic seafloor, the higher magnetization cannot be associeted with volcanic seafloor, either at the axis or on the flanks. The presence of extrusive rocks may, in some places, account for a higher magnetization whereas elsewhere not. For instance, although a lava flow is identified just north of the Cannibal Ridge on both profiles 1-7 and 1-6, larger magnetization values are only observed on the eastern profile (profile1-6; Figure 4). Similarly, although relatively higher magnetizations (up to 10 A/m) may be related to the proximity of the small volcanic patch north of the axial valley wall (profile 2-3), the few volcanic patches observed south of the axis of the western corridor do not produce any significant magnetization (<+/-2 A/m; Figure 4)

The corrugated surfaces observed at the northern end of the profiles 2-2 and 2-3 seem to be associated with stronger magnetizations (up to 10 A/m) and a slightly continuous magnetic anomaly identified as the anomaly C5.

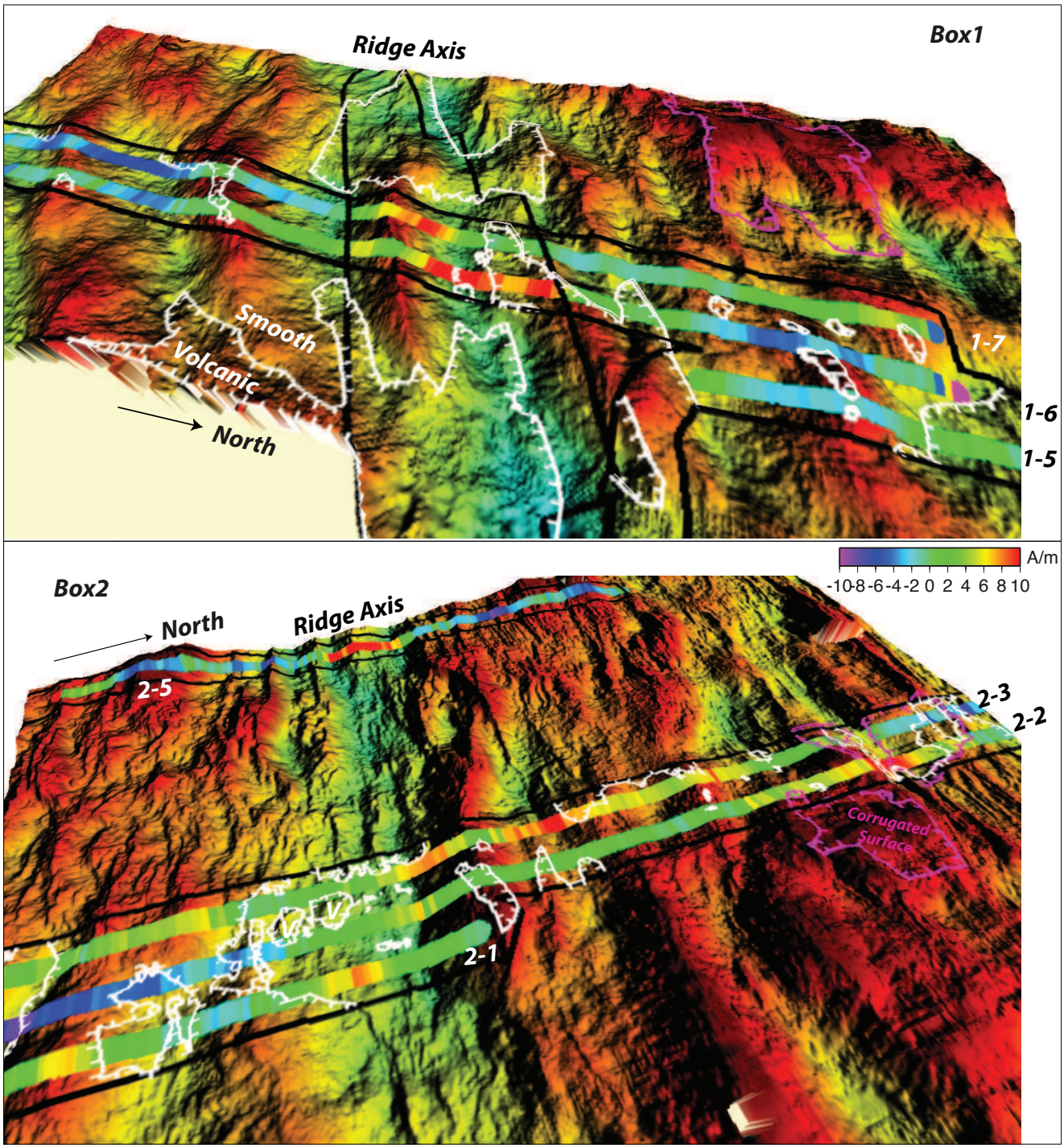

Figure 4 : 3D bathymetric view of the two survey areas. The inverted magnetization (colored strips) and the limits (from Sauter et al. (2013) of both the corrugated surfaces and the volcanic seafloor are draped on the bathymetry. The black lines indicate the edges of the TOBI side-scan swath.

6.MAGNETIC PROPORTIES OF THE DREDGED SAMPLES

Natural remanent magnetization (NRM) and magnetic susceptibility (K) were measured over 13 basalt and 31 peridotite samples dredged in the two survey areas (Figure 1 and Table 1). Susceptibility values for peridotites range from 0.07 to 0.69 SI, whereas NRM values fall between 0 and 23 A/m with a mean value of 1.9 A/m (Figure 5). Some dredged peridotites have a significant NRM, comparable to those from basaltic rocks (up to 8 or 23 A/m), but associated with higher susceptibility (K up to 0.045 SI) and lower Koenigsberger ratio (Q) (mean Q for serpentinized peridotites is ~2 whereas the mean value for basalt is ~40). Moreover, both NRMs and susceptibilities are highly variable even for a set of samples collected within the same dredge. The strongest magnetized peridotite samples were recovered within a short lateral distance of each other in the middle of the north side of profiles 2-2 and 2-3 (Figure 3). Two samples are especially magnetized with a respective NRM of 23 and 8 A/m. However, such a high magnetization is not recorded by the deep-tow magnetic data (Figure 3), suggesting that either the magnetized source layer is thin or that high magnetizations occur only punctually, suggesting that such magnetization are limited to small surfaces that cannot be detected by the deep-tow magnetometer.

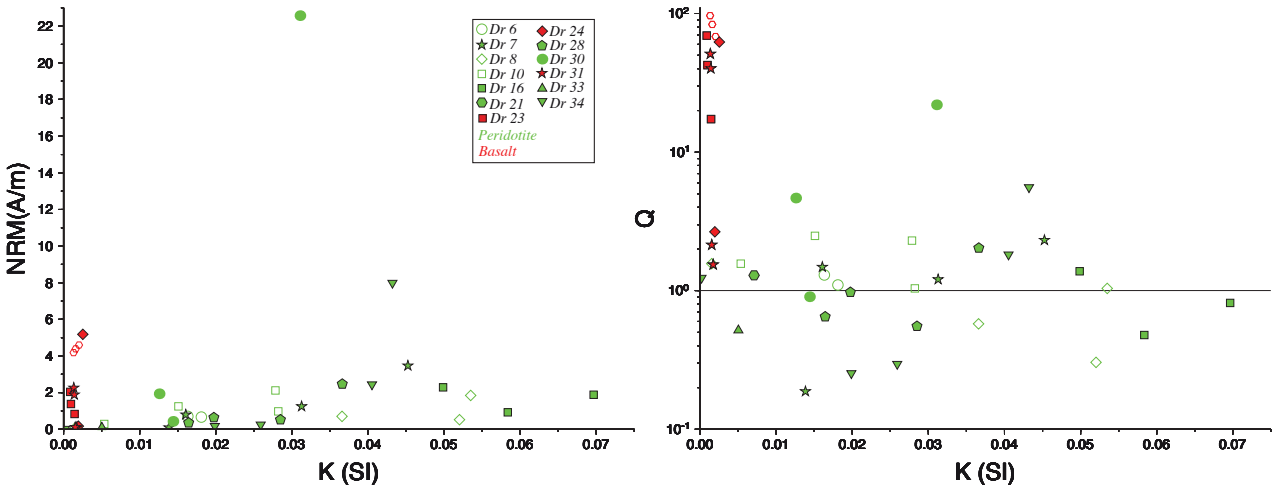

Figure 5 : Natural remanent magnetization (NRM) and Koenigsberger ratio (Q) in samples from dredged peridotites and basalts, as a function of the magnetic susceptibility (K). Note that Q has a logarithmic scale.

Table 1: Magnetic properties of the dredge samples

Dedge #	Type	MagneticSusceptibility (SI)	NRM (A/m)	Koenigsberger ratio	Total Magnetization (A/m)
6	Peridotite	0,016	0,70	1,30	1,24
6	Peridotite	0,018	0,66	1,10	1,26
7	Peridotite	0,016	0,79	1,48	1,32
7	Peridotite	0,045	3,47	2,32	4,97
7	Peridotite	0,031	1,25	1,20	2,28
7	Peridotite	0,014	0,09	0,19	0,54
8	Peridotite	0,002	0,08	1,57	0,13
8	Peridotite	0,052	0,52	0,30	2,25
8	Peridotite	0,037	0,70	0,58	1,91
8	Peridotite	0,054	1,84	1,04	3,61
10	Peridotite	0,028	2,12	2,30	3,04
10	Peridotite	0,005	0,28	1,56	0,45
10	Peridotite	0,028	0,97	1,04	1,90
10	Peridotite	0,015	1,24	2,48	1,74
16	Peridotite	0,058	0,92	0,48	2,86
16	Peridotite	0,050	2,28	1,38	3,93
16	Peridotite	0,070	1,88	0,81	4,18
16	Basalt	0,002	4,60	68,30	4,67
16	Basalt	0,001	4,18	96,77	4,22
16	Basalt	0,002	4,39	83,37	4,44
21	Peridotite	0,007	0,30	1,29	0,54
23	Basalt	0,001	1,38	42,54	1,41
23	Basalt	0,001	2,04	69,40	2,07
23	Basalt	0,001	0,83	17,29	0,87
24	Basalt	0,003	5,18	62,22	5,27
24	Basalt	0,002	0,17	2,66	0,24
25	Nodule	0,002	0,01	0,18	0,07
28	Peridotite	0,020	0,64	0,97	1,29
28	Peridotite	0,016	0,35	0,65	0,90
28	Peridotite	0,028	0,52	0,55	1,46
28	Peridotite	0,037	2,47	2,03	3,68
30	Peridotite	0,013	1,94	4,66	2,35
30	Peridotite	0,031	22,57	21,95	23,60
30	Peridotite	0,014	0,43	0,90	0,91
31	Basalt	0,001	2,26	51,23	2,31
31	Basalt	0,001	1,88	40,17	1,92
31	Basalt	0,002	0,09	1,54	0,14
31	Basalt	0,002	0,11	2,14	0,16
33	Peridotite	0,005	0,09	0,52	0,25
34	Peridotite	0,026	0,25	0,30	1,11
34	Peridotite	0,020	0,17	0,25	0,82
34	Peridotite	0,041	2,44	1,82	3,78
34	Peridotite	0,043	7,98	5,57	9,41
34	Peridotite	0,000	0,01	1,24	0,01

7.FORWARD MODELLING

Magnetic anomalies were interpreted over domains that lack a volcanic upper crustal layer in the easternmost part of the SWIR (Sauter et al., 2008) suggesting that other deeper sources may play a significant role in preserving the Earth magnetic field polarity. Along both the MAR and the SWIR serpentinized peridotites have been suspected to carry a "more positive" induced magnetization in areas of thin crust (Hosford et al., 2003; Tucholke et al., 2008). Indeed, studies of abyssal peridotites from ODP holes have suggested that a degree of serpentinization superior to 75% could be responsible for the formation of a large amount of magnetite leading to a significant, but highly variable, remanent magnetization (Oufi et al., 2002). Moreover, in agreement with results from Oufi et al. (2002), Koenigsberger ratios for SWIR serpentinized peridotites remain significantly lower than those for basaltic rocks. We therefore perform two different forward modelling, one based on a 500 m thick basaltic layer preserving the Earth magnetic field polarity and another based on an induced magnetized layer, in order to test the contribution of volcanic rocks versus serpentinized peridotites. We disregard the contribution of a lower crustal layer made of gabbroic rocks that is volumetrically scarce in the samples dredged within the exhumed mantle domains.

7.1. SEAFLOOR SPREADING MODEL

The model calibrated on the volcanic seafloor (line 2-5) was then compared to the magnetic profiles acquired above the exhumed mantle domains of both eastern and western corridors. In the absence of a high amplitude central anomaly, the axial Brunhes block was centered either at the bathymetric axis or underneath the central magnetic anomaly. Figure 2 shows the predicted magnetic anomaly along each across-axis profile (dashed black line). The parameters derived from profile 2-5 give a poor fit to the observed magnetic field for the two corridors. The picked axial anomaly and anomaly C2A or C3A on sea surface magnetic profiles (Cannat et al., 2006) do not clearly show on the deep-tow profiles over the exhumed mantle domains. Furthermore, the modeled anomaly C5 at the end of both profiles 2-2 and 2-3 appears to be shifted a few kilometers to the north with respect to the previously picked anomaly C5. This offset may be explained by either asymmetrical spreading, changes in spreading rate between C3A and C5 or unconstrained location of the central Brunhes anomaly.

7.2. INDUCED MAGNETIZED MODEL

To account for the unconstrained lateral and vertical variations in both intensity and direction of the remanent component of magnetization, we tested whether a uniform induced magnetized layer could solely account for the observed magnetic anomalies. Seismic velocities in the exhumed mantle domains of the Iberian margin, as well as over slow-spreading ridges, suggest a serpentinization degree greater than 75% in the first 2 km below the seafloor (Minshull et al., 1998; Chian et al., 1999;

Dean et al., 2008). Thus, based on average NRM values measured on our dredge samples but also on serpentinites at ODP Holes 897D, 899B, 1070A and 1277 (Zhao et al., 2001), we use a 1.5 A/m magnetazation and 2 km constant thickness draped on the bathymetry as a source for the magnetic anomalies. Such model is then equivalent to assume that the whole magnetic signal is exclusively related to the seafloor topography.

The results are represented in Figure 2 by the thin black continuous lines. In the western corridor, there is a poor fit between the synthetic and the observed magnetic anomaly along profile 1-5 and especially in the axial valley of profile 1-6. However, the agreement is better on profile 1-7, even within the central domain. The only continuous anomaly between both profile 1-6 and 1-7 (picked as anomaly C2A by Sauter et al. (2008)) is quite well expressed on both profiles. In the eastern corridors, where the areas of flat topography correspond to a flat observed magnetic field, the data are quite comparable to the model except in the axial domain. Over the volcanic seafloor, the synthetic magnetic anomaly fits poorly the observed magnetic anomaly profile 2-5 in both axis and off-axis regions.

8. DEPTH OF THE MAGNETIC SOURCES

Following Bronner et al. (2013), we use the equivalent layer method for the estimation of the depth of the magnetic sources. Indeed, Dampney (1969) has shown that the distance between the surface where the field is measured and the location of the equivalent source dipoles should satisfy a lower and upper bound for avoiding respectively the aliasing effect in the computed field and an ill-conditioned inversion matrix. In our case, because the data spacing (~10 m) is clearly smaller to the altitude of the TOBI above the seafloor, the upper bound can be constrained by the top of the seafloor rather than the aliasing frequency. An equivalent source located too far below the measurement surface makes the matrix representing the distance between the dipoles and the observation plane ill conditioned and the associated solution unreliable (Dampney, 1969). In marine geophysics the sources responsible for the magnetic anomalies are usually considered to be located in the upper part of the oceanic crust and within a layer of constant thickness. Therefore, the lower bound (i.e. depth where the “distance” matrix becomes ill-defined) provides a first guess of the maximum depth of the “true” causative sources. This can be empirically estimated by iteratively increasing the depth of the source until either (1) high frequencies in both computed field and magnetization are lost, or (2) oscillations first appear in the solutions.

Applying this method to our survey, in the case of the “volcanic” profile (line 2-5), the whole frequency content of the measured field was well retrieved for dipoles located around 500 m below the seafloor (Figure 6). Shallower and deeper solutions lead respectively to the appearance

of high frequency oscillations in the computed field and loss of resolution in the computed field and magnetization solution. At the opposite, for the profiles acquired above the exhumed mantle domains (e.g. profile 2-2; Figure 6), the weakness of the signal associated with a quasi absence of short wavelength anomalies allow reasonable solutions for both synthetic field and magnetization within a wider range of depth (up to 2000 m below the seafloor; Figure 6).

As for any methods used to estimate the depth of magnetic sources, these results have to be taken with care. The maximum depth of 500 m obtained above the volcanic seafloor is in agreement with the 500 m thick basaltic layer generally used to account for the marine magnetic anomalies at mid oceanic ridges. This suggests that the 2D hypothesis used here is reliable in the case of a 2D homogeneous crustal accretion but we do not have much constraints on the magnetization structure of the exhumed mantle domains and the 2D assumption may lead to some errors. The deeper solutions found for the sources in exhumed mantle domains mainly suggest that the short wavelength magnetic anomalies recorded above the volcanic areas are missing from the profiles acquired above serpentinized peridotites. This can be explained by deeper sources or by smoother magnetic contacts.

9.DISCUSSION

9.1. SEAFLOOR SPREADING ANOMALIES

Because the shape of the marine magnetic anomalies strongly depends on the distance between two-polarity reversals (i.e. frequency of polarity reversal versus spreading rate), magnetic reversal patterns along ultraslow spreading ridges are not always identifiable. At the SWIR, geomagnetic reversals used for the resolution of spreading rates for the last 24 Ma have often been restricted to long reversals of constant polarity, such as chrons C5 and C6, of about one million years duration (Patriat et al., 2008). Moreover, at the eastern part of the SWIR, three different types of seafloor occur (Cannat et al., 2006): the volcanic seafloor represented by 100% volcanic accretion, the corrugated seafloor associated with about 50% and 70% of mantle exhumation (Buck et al., 2005), and the smooth seafloor formed by nearly 100% of detachment faulting associated with no or very little volcanic activity (Sauter et al., 2013). Large variations in both crustal thickness (inferred from RMBA; Cannat et al., 2006) and lithology (from volcanic basalt to tectonized serpentinised peridotites) associated with these different modes of seafloor generation. Thus, in addition to the ultraslow spreading rate, these are responsible for the complexity of the magnetic signal in this area. As a result, short reversals such as C3 or C2A (~0,5 My) are detectable only above well-established thick volcanic crust associated with minor tectonic activity. Therefore, the identification of magnetic anomalies from sea surface magnetic profiles above smooth seafloor was mainly extrapolated from the surrounding volcanic areas (Sauter et al., 2008). Moreover, mapping of exhumed mantle domains from multibeam

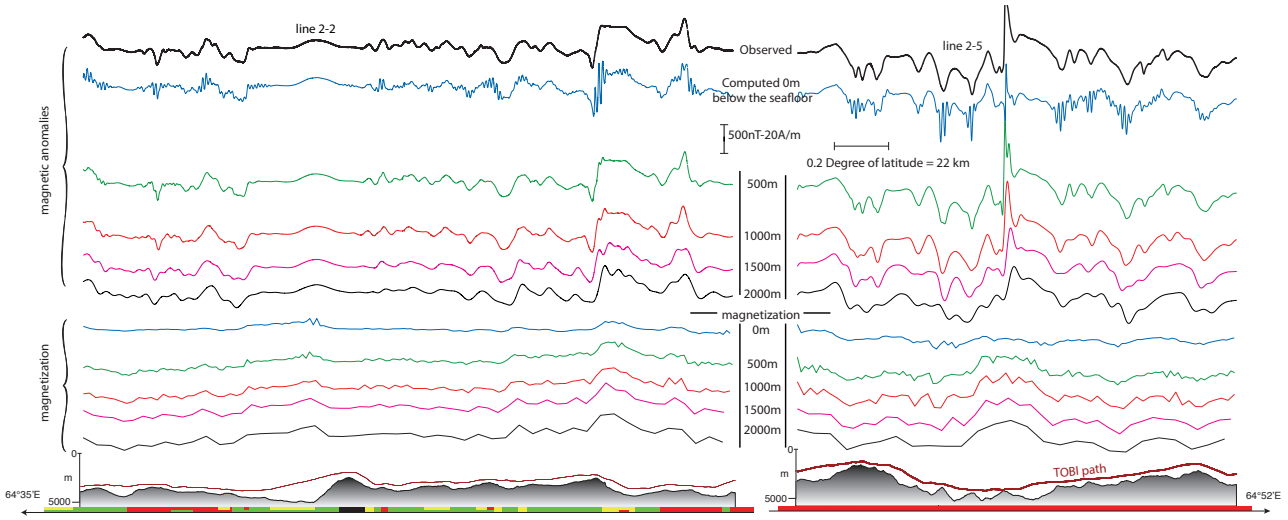

Figure 6 : Comparison between the deep-tow measured field and the computed field along the TOBI path for different depths of inferred magnetized dipoles from 0 to 2000 m below the seafloor. The shallowest and deepest dipoles lead respectively to the appearance of high frequency oscillations in the computed field and loss of resolution in both computed field and magnetization solution. The best compromise is found for dipoles located around 500 m below the seafloor for the profile acquired above the volcanic crust and 1000 m for the profile collected above the exhumed mantle derived rocks. A significant loss in resolution is observed for dipoles located below 1000 m in the case of the volcanic crust whereas both computed field and magnetization are quite well preserved up to 2000 m for the case of exhumed mantle seafloor.

bathymetric data at 150 m resolution and from TOBI images at <10 m resolution reveals that sources of some magnetic anomalies were erroneously attributed to volcanic seafloor by Sauter et al. (2008).

We are now able, with the high-resolution deep-tow data, to provide a precise analysis of the magnetic signal with the respect to the geological nature of the seafloor. We confirm, as observed by Searle and Bralee (2007) in this region, that despite an ultra-slow spreading rate, marine magnetic anomalies are still well identifiable above volcanic seafloor. However, these identifications are more difficult above the exhumed mantle domains where the magnetic patterns is highly variable from one profile to another. This is well illustrated in our studied corridors where closely spaced magnetic profiles show a very heterogeneous magnetic signal. Except for anomaly 5, a simple seafloor-spreading model (calibrated on line 2-5) does not fit the magnetic anomaly pattern, even for the central anomaly (Figure 2). Moreover, although the exhumed mantle domains are expected to be formed by asymmetrical detachment faulting, there is no evidence for lateral discontinuity between exhumed mantle areas and symmetrically accreted volcanic crust for which ages of accretion are quite well constrained (e.g. Chrons younger than C5; Searle and Bralee, 2007). We thus expect both alternating flip-flop exhumation and volcanic accretion to be quite contemporary leading to a reasonable lateral continuity (in terms of age) between both types of seafloor.

9.2. WHICH MAGNETIC SIGNATURE FOR WHICH SEAFLOOR?

9.2.1. CONTRIBUTION OF MANTLE DERIVED ROCKS

The ferromagnetic behavior of serpentinized peridotites has been shown to be directly linked to the serpentinization process (Toft et al., 1990). Magnetite is formed during serpentinization from the interaction between fluids and ferromagnesian minerals such as olivine and pyroxene. A degree of serpentinization larger than 75% is necessary for the acquisition of both significant susceptibility and NRM (Oufi et al., 2002). However, highly variable NRMs are observed from one ODP site to another and also between samples drilled in a single ODP Hole (Oufi et al., 2002). In our study, a similar magnetic behavior is observed for the dredged peridotites. Values of NRM and susceptibility can be significant (up to 23 A/m NRM for one sample) but are highly heterogeneous. The susceptibilities and NRM values in our dredged samples fall in the lower range of values reported for drilled abyssal peridotites (Oufi et al., 2002). However, our samples show similar Koenigsberger ratios to these of drilled peridotites, which rarely exceed 3 and are significantly inferior to those expected for the upper oceanic crust (e.g. ~50 to 300; (Marshall and Cox, 1971). Although peridotite outcroping at the seafloor are subject to low-temperature alteration, we consider that the magnetic properties of the dredged peridotites are representative of a magnetic source layer in the exhumed mantle domains. The high variability in NRM intensity combined with the large range of susceptibility and low Koenigsberger ratio make this layer of serpentinized peridotite magnetically weak and variable.

The presence of such layer is confirmed by the high-resolution deep-tow profiles, which display highly variable magnetic pattern from one profile to another, even where they are closely spaced. Moreover, the magnetic anomalies observed above exhumed mantle are weak (<100 nT), and lack short wavelength anomalies, which suggests deeper magnetic sources than in the volcanic seafloor. It was possible to reproduce some magnetic pattern using a induced magnetic layer but the whole magnetic signal was not retrieved, especially within the axial domain. Similarly, the spreading model does not fit the observed data. It is thus likely that the source combine both induced and remanant magnetization and vary from one local area to another.

Furthermore, in the western and more magmatic part of the SWIR, a significant decrease in magnetization produces the disappearance of the magnetic reversal patterns in the deepest parts of ridge discontinuities (Sauter et al., 2004). This observation was linked to the thinning of the upper part of the oceanic crust due to a decreasing magmatic budget toward the segment ends. It has also been shown, at the MAR (13-15°N), within a highly complex accretion context combining detachment faulting and freshly erupted seafloor, that the magnetic pattern could be significant in amplitude but highly heterogeneous on a scale of ~5 km (Mallows, 2011) leading to difficulties in the identification of the spreading anomalies, even for the large Brunhes central reversal. This further suggests that a sufficiently homogeneous upper crust is required to produce well developed marine magnetic

anomalies, and that in the absence of this main magnetic source made of extrusive (and perhaps intrusive material), exhumed serpentinized peridotites are not sufficiently uniform magnetic sources to produce undisputable seafloor spreading magnetic anomalies.

9.2.2. CORRUGATED SEAFLOOR AND THE MAGNETIC SIGNAL

A corrugated surface is observed below the indetified anomaly C5 toward the north end of profiles 2-2 and 2-3 in the eastern corridor. This area is strongly magnetized (up to 10 A/m; Figure 2 and 3) and displays high amplitude magnetic anomaly up to 450 nT. This corrugated surface is surrounded by lineated volcanic terrains and the conjugate anomaly C5, on the opposite flank, was idetified over well established volcanic crust. This observation, together with a frequent recovery of gabbro in this area (Sauter et al., 2013), suggests that the anomaly C5 was emplaced in a more robust magmatic accretion context, before or just at the onset of continuous mantle exhumation. We thus speculate that in this particular area the magnetization is carried by extrusive or intrusive material rather than peridotites.

9.2.3. VOLCANIC SEAFLOOR AND THE MAGNETIC SIGNAL

Some small volcanic patches have been identified respectively just north of the axial valley of the western corridor and within the axial region of the eastern corridor (Figure 4). It is not clear whether this extrusive material accounts for magnetization higher than over the smooth, exhumed mantle seafloor. The magnetic data rather confirm the interpretation of Sauter et al. (2013) based on deep-tow sonar images that these volcanics are very thin flows, not exceeding a hundred meters of thickness, and thus have insufficient volume to be identified by the deep-tow magnetometer.

9.2.4. MARINE MAGNETIC ANOMALIES AT OCT

“Flip-flop” mantle exhumation is one of the proposed mechanism responsible for the formation of the transitional domains at magma poor rifted continental margins where serpentinized mantle rocks have been drilled (Tucholke and Sibuet, 2007). Sibuet et al. (2007) proposed that a strong magnetization (up to 9 A/m) can be produced by the serpentinization of a 2 to 3 km thick fractured layer, within the root of an active detachment fault exhuming serpeninized peridotites. Based on NRM intensity measured in ODP holes at the Iberia margin, these authors argued that this first serpentinization phase is sufficient to preserve the polarity of the ambient magnetic field. They support that only the upper ten meters below the seafloor is affected by cold-water alteration that produce s incoherent magnetic properties. At the eastern part of the SWIR, a similar “flip-flop” mechanism is suggested to accommodate the plate separation. Detachment faulting flipping from one side of the ridge axis to the other within a time scale of 1 to 2 Ma (Sauter et al., 2013) would provide a mechanism compatible with the recording of a symmetrical magnetic pattern. At least long polarity reversals such as C1 could be identifiable at both ultra slow spreading ridges and OCTs. However, both exhumed mantle domains of the SWIR and the transition zones of the Iberia-Newfoundland

margins are characterized by a weak and ill-defined magnetic signal. At these margins, only the seaward termination of the exhumed mantle domain is associated with a slightly linear and high amplitude (up to 1000 nT) magnetic anomaly ("J anomaly"). This anomaly is interpreted as the end of the M sequence of spreading anomalies and its amplitude was explained by a strongly serpentinized crust (Srivastava et al., 2000).

However, no clear central anomaly is observed over the exhumed mantle areas of the SWIR, neither where active detachment faulting is identified nor on the flanks. This leads to the conclusion that the serpentinization process is not sufficiently homogeneous to produce stable large remanent magnetization as it depends strongly on the fluid-rock interaction, the temperature, the mineral composition and the tectonic context. Therefore, in view of the low magnetization of the freshly serpentinized rock at the SWIR, it is unlikely that strong magnetic anomalies could be related solely to serpentinization; this would be even more true at >100 Ma old OCTs (Sibuet et al., 2007). This instead supports the hypotheses that (1) intrusive or extrusive material is required (Bronner et al., 2011; Russell and Whitmarsh, 2003) to account for a significant magnetic signal in the exhumed mantle domains of OCTs and that (2) the interpretation of this signal as resulting from seafloor spreading is precluded in the absence of a homogeneous and well established upper oceanic crust. Consequently, the kinematic reconstructions of magma poor passive margins using weak anomalies identified over exhumed mantle domains need to be taken with caution.

10. CONCLUSION

We have investigated the magnetic structure of newly discovered large exhumed mantle domains of the SWIR (Sauter et al., 2013) combining high resolution sidescan sonar images, deep-tow magnetic data and results from dredge sampling. We show that the seafloor spreading magnetic pattern disappears from the volcanic seafloor toward the exhumed mantle domains. Forward modelling allows a reasonable fit to the observed magnetic anomalies over the volcanic seafloor. However, the lack of a central magnetic anomaly and the highly heterogeneous and weak magnetic pattern observed above exhumed mantle-derived rocks prevents any identification of polarity reversals. Moreover, analysis of the magnetic proprieties of the dredge samples shows that serpentinized peridotites are highly variable magnetic sources. We conclude that the serpentinization process is not sufficiently homogeneous to produce a significant stable magnetization at the scale of the exhumed mantle domains of the SWIR. We further suggest that a homogenous volcanic crust associated with minor tectonic activity is required to record well-defined seafloor spreading magnetic lineations.

Chapitre 3: Quelle est l'origine du signal magnétique associé à la transition océan-continent des marges Ibérie/Terre-Neuve?

Cette troisième partie s'intéresse à l'étude des marges conjuguées Ibérie/Terre-Neuve. Dans ces deux régions du globe, la récente découverte d'une large zone de transition (>100 km au sud, < 100 km au nord) pose la question de la nature de la limite entre le continent et l'océan. En effet, cette limite est traditionnellement représentée par l'apparition de la première anomalie magnétique d'accrétion océanique. Comme sur la dorsale Sud-Ouest Indienne, cette zone de transition est principalement constituée de roches mantelliques exhumées, associées à un signal magnétique de faible amplitude et de faible continuité spatiale. De plus, les forages ODP montrent qu'une large portion de cette transition résulte d'un magmatisme de type alcalin complexe et polyphasé alors que le magmatisme de type MORB, caractéristique des dorsales océaniques, n'est présent que dans la partie la plus distale de la transition (Jagoutz et al., 2007). La nature des roches et le caractère polyphasé du magmatisme observé à la transition océan-continent des marges Ibérie/Terre-Neuve posent donc la question de la nature des anomalies magnétiques qui y sont observées.

Dans ce chapitre nous mettons en parallèle les données d'anomalies magnétiques et les coupes de sismique réfraction et réflexion disponibles sur ces deux marges. Nous montrons que la première anomalie clairement identifiable, l'anomalie « J » (précédemment interprétée comme la superposition des isochrones M0-M3 (125-128 Ma)) est associée à une structure crustale particulière appelée «outer high» et caractérisée par un haut topographique accompagné d'un épaississement crustal. En s'appuyant ensuite sur les données de forages (ODP site 1277), nous proposons qu'un événement magmatique à la transition Aptien-Albien ~112Ma (pendant la période magnétique calme du Crétacé 125 à 84 Ma) est à l'origine de la création de cette structure. Nous proposons finalement que cet événement magmatique entraîne la mise en place de la première croûte océanique et donc le passage d'un régime d'exhumation vers un régime d'accrétion focalisé à l'axe de la nouvelle dorsale océanique. L'anomalie J n'est donc plus interprétée comme résultante d'une inversion du champ magnétique mais comme une anomalie liée à un événement magmatique responsable de la rupture continentale. La datation de cet événement nous permet finalement de rajeunir l'ouverture de l'Atlantique Nord de 10 Ma par rapport à ce que suggéraient les modèles précédents, ce qui pourrait expliquer certaines inconsistances dans les précédentes reconstructions cinématiques de cette région du globe.

Ce travail a été publié dans la revue « Nature Geoscience » sous la référence suivante :

Bronner, A., Sauter, D., Manatschal, G., Peron-Pinvidic, G., and Munschy, M., 2011, Magmatic breakup as an explanation for magnetic anomalies at magma-poor rifted margins: Nature Geoscience, 4, 549-553.

Dans ce troisième chapitre, nous avons décidé d'inclure cette publication dans sa version antérieure à celle publiée dans le journal ainsi que le commentaire auquel elle a donné lieu. En effet, à la demande de l'un des reviewers, en raison d'une interprétation controversée concernant la nature de la zone de transition le long du profil Screech 1, le modèle associé a dû être retiré. De plus, cette publication a donné lieu à un commentaire (Tucholke and Sibuet, 2012) auquel nous avons répondu (Bronner et al., 2012). Ces deux points de vue sont présentés et discutés en fin de chapitre.

Magmatic break-up as an explanation for magnetic anomalies at magma poor rifted margins

Adrien Bronner[1], Daniel Sauter[1], Gianreto Manatschal1[1], Gwenn Péron-Pinvidic[2] and Marc Munschy[1]

[1]Institut de Physique du Globe de Strasbourg, IPGS - UMR 7516, CNRS - Université de Strasbourg, 1 rue Blessig 67084 Strasbourg cedex,

[2]NGU, Geological Survey of Norway, Leiv Eirikssons vei 39, 7491 Trondheim, Norway,*Contact: a.bronner@unistra.fr

In classical plate tectonic models, continental break-up is abrupt, resulting in a sharp contact between continental and oceanic crusts. The discovery of a wide transitional domain, partly composed of exhumed subcontinental mantle, at magma poor rifted margins radically changed this view. At present, the definition of break-up as well as its timing and location remain debated. The seafloor spreading origin of the magnetic anomalies discovered in the transitional domain is particularly questioned. Here we propose an alternative model based on forward modelling of magnetic anomaly profiles using seismic and drill hole data of the Iberia-Newfoundland margins. We show that the main magnetic anomaly (J anomaly), located at the seaward edge of the transitional domain, is associated with both a basement high and a thick crust and can be explained by excess magma associated with the emplacement of lava flows and underplated bodies on top and below the exhumed mantle, respectively. We therefore suggest that the J anomaly is not a seafloor-spreading anomaly but is the signature of the break-up that triggered oceanic spreading at the Aptian-Albian transition (~112 Ma). As a result, the paleogeographic position of Iberia during early Cretaceous time needs to be revised.

1. HOW ROBUST IS THE IDENTIFICATION OF THE M SEQUENCE OF MAGNETIC ANOMALIES AT THE IBERIA – NEWFOUNDLAND CONJUGATED MARGINS?

At the Iberia – Newfoundland rift system, the seaward edge of the ocean-continent transition (OCT) is characterized by a large amplitude magnetic anomaly (the J anomaly). It is interpreted as the beginning of the M sequence of seafloor spreading magnetic anomalies (M0-M3) which have been identified up to anomaly M20 in the Newfoundland basin (NB) and the Iberia Abyssal Plain (IAP) (Srivastava et al., 2000) (Figure 1). However, the sources for these magnetic anomalies are debated as they were not identified over typical oceanic crust but over exhumed mantle (Russell and Whitmarsh, 2003; Sibuet et al., 2007) and thinned continental crust (Funck et al., 2003). They are thought to be caused either by serpentinized perodotites (Sibuet et al., 2007) or by magmatic intrusions (Russell and Whitmarsh, 2003). While Sibuet et al. (2007) suggested that the M sequence of magnetic anomalies up to M17 results from mantle exhumation at an ultraslow-spreading ridge (Cannat et al., 2009), Russel and Whitmarsh (Russell and Whitmarsh, 2003) found no evidence for anomalies formed by seafloor spreading before M5r.

Figure 1 :

Although the M sequence of magnetic anomalies in the NB and IAP is clearly different from standard seafloor spreading magnetic anomalies, it has been extensively used to constrain the position of Iberia relative to the adjacent plates (Srivastava et al., 2000; Sibuet et al., 2004). The M0 reconstruction (125 Ma) shows a gap between eastern Iberia and Europe in the space now occupied by the Pyrenees (Srivastava et al., 2000; Sibuet et al., 2004). This gap was closed by Albian time as a consequence of a counterclockwise rotation of Iberia (Gong et al., 2008). This implies ~600 km of convergence between eastern Iberia and Europe in the early Cretaceous. Sibuet et al. (2004) therefore suggested that the Pyrenean basins developed above a north-dipping subducting slab. However, this appears to be inconsistent with geophysical observations (Souriau et al., 2008). One possible implication of these observations is that the inferred paleogeographic position of Iberia relative to Newfoundland during early Cretaceous may need revision.

2. THE J ANOMALY: THE MAGNETIC SIGNATURE OF A MAGMATIC EVENT

South of the NB the J anomaly is viewed as an undisputed seafloor spreading magnetic anomaly (Rabinowitz et al., 1979) although it displays unusually high amplitudes (> 800 nT) (Figure 1). It is coincident with a basement ridge (the J-anomaly Ridge) that is characterized by an anomalously thick layer 2B, evidence for subaerial exposure of basalts, and upper Barremian to early Albian shallow-water carbonates (Deep Sea Drilling Project Hole 384 Figure 1) (Tucholke and Ludwig, 1982). North of the Southeast Newfoundland ridge, the J anomaly is less well developed (Rabinowitz et al., 1979) (Figure 1). In the IAP, the J anomaly follows the alignment of seamounts of the Madeira-Tore Rise (Rabinowitz et al., 1979), which has been proposed to be built up by large alkaline magmatic pulses

of late Cretaceous times (103-80.5 Ma) (Merle et al., 2009) and significant underplating of unknown age (Peirce and Barton, 1991). North of the Madeira-Tore Rise, the J anomaly is associated with a topographic high at the seaward edge of the OCT, referred to as an outer high (Péron-Pinvidic et al., 2007). Both the amplitude of the J anomaly and the distance between J and anomaly C34 decreases northward in the NB and IAP (Figure 1).

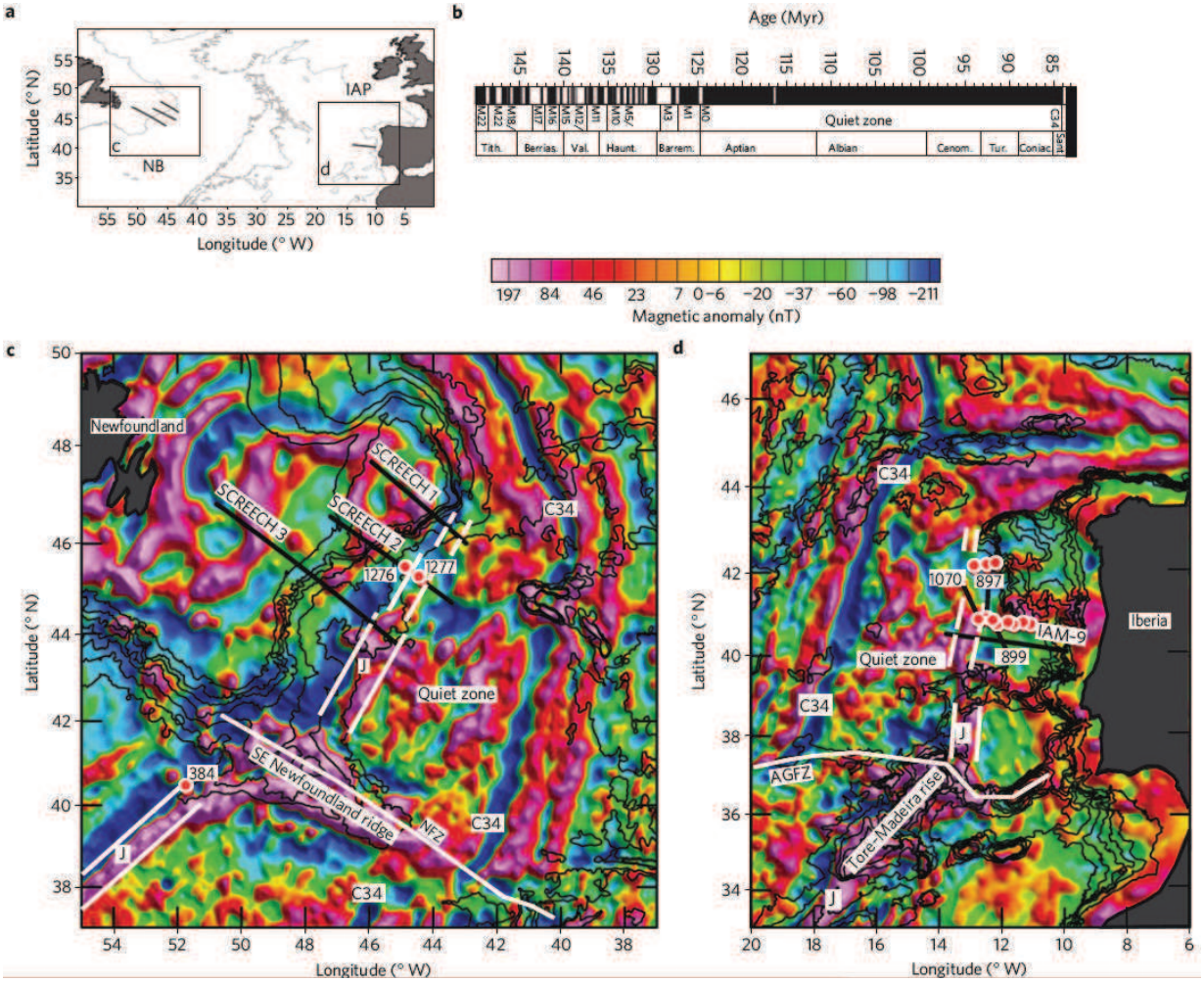

Figure 1 :Magnetic anomaly maps and location of the Iberia-Newfoundland margin system. **a,** location map. Thin black lines indicate the seismic and magnetic anomaly profiles used in this study; red dots indicate ODP sites. **b,** Geomagnetic polarity time scale of Ogg and Smith (2004) used throughout this paper. **c,** Magnetic anomaly map of the Newfoundland margin (Quesnel et al., 2009). **d,** Magnetic anomaly map of the Iberia margin (Quesnel et al., 2009). Thin black lines indicate bathymetric contours. C34 indicate the location of the first undisputed seafloor spreading magnetic anomaly. J and the thin white parallel lines indicate the location of the J anomaly.

Drill holes that sampled this outer-high in the NB and IAP (Ocean Drilling Program (ODP) Sites 1070 and 1277) penetrated exhumed mantle with intrusive and extrusive mafic material indicating that magmatic activity has been persistent from ~128 Ma to ~70 Ma (Jagoutz et al., 2007). This outer-high, and hence the J anomaly, correspond to an area of thicker crust as indicated by wide-angle seismic surveys (Van Avendonk et al., 2006) (Figure 2). Although we cannot exclude that this thickening may be related to serpentinization, we suggest that it is better explained by a major magmatic event that underplated and intruded previously exhumed and serpentinized subcontinental mantle. Such a

hypothesis is further supported by drilling of highly differentiated magmatic veins at ODP Site 1277, indicating that large magma reservoirs exist at depth (Jagoutz et al., 2007). Seismic reflection data show tilted Aptian strata onlapped by Albian sediments on the continent side of the outer-high in the NB (Figure 2) and drilling at the high recovered turbidites and debris flows, including reworked mantle rocks interlayered with basalt flows (Péron-Pinvidic et al., 2007). This argues for a significant tectonic uplift accompanied by a magmatic event at the Aptian-Albian transition (~112 Ma). The widespread distribution of Albian igneous sills, intruded at very shallow levels within the sedimentary cover in the NB (Peron-Pinvidic et al., 2010) together with numerous Cretaceous seamounts (Merle et al., 2009) argue for ongoing magmatism after this event. We therefore speculate that the J anomaly in the NB and IAP can be explained by mafic plutons and/or sills intruded at depth and lava flows at the surface at the Aptian-Albian boundary. This magmatic event may be at the origin of crustal break-up and onset of steady state seafloor spreading.

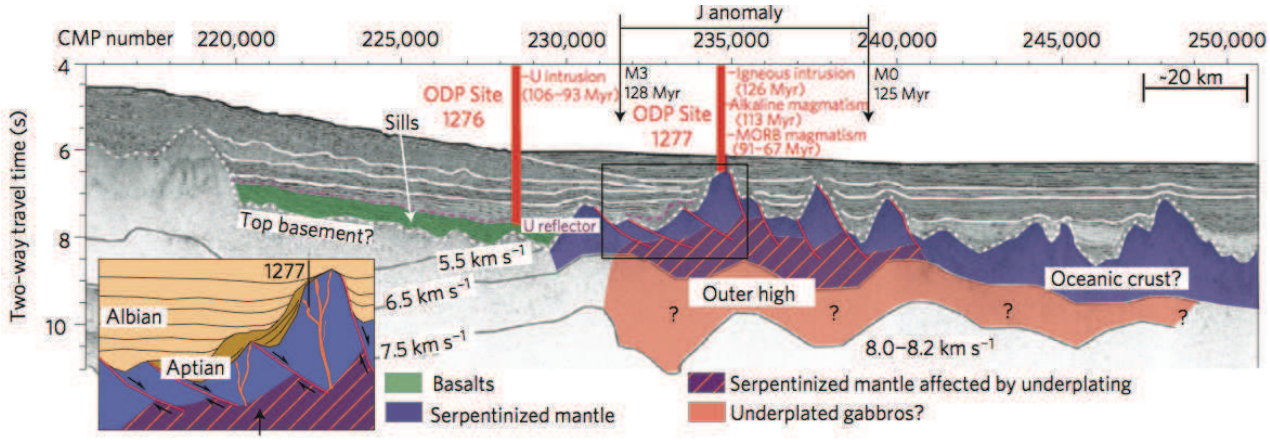

Figure 2 : Interpretation of seismic data along SCREECH line 2 showing the thickening of the crust beneath the outer-high. Seismic data (Shillington et al., 2006; Van Avendonk et al., 2006; Van Avendonk et al., 2009) show that the J anomaly occurs where the crust starts to thicken and the top basement starts to rise. Location of the sills is from Péron-Pinvidic *et al.* (2010). Ages in ODP Sites 1276 and 1277 are from Jagoutz *et al.* (2007) and Tucholke and Sibuet (2007). Magnetic anomalies are from Srivastava *et al.* (2000). The inset shows the over tilted serpentinized bedrock and Aptian strata onlapped by Albian sediments resulting from the tectonic and magmatic event at the Aptian-Albian transition.

3. FORWARD MODELING OF MAGNETIC ANOMALY PROFILES

We use magnetic anomaly forward modelling based on reflection and refraction seismic data to validate this speculation (see the Methods section and Supplementary Methods for details). Among the major seismic profiles crossing the J anomaly, we chose SCREECH line 2 in the NB to illustrate the results of the modelling (Figure 3 and Supplementary Figure 1 for the modelling of SCREECH line 1 and 3). It is the only section across an OCT worldwide where reflection (Shillington et al., 2006) and refraction (Van Avendonk et al., 2006) seismic data and drill hole data (Tucholke and Sibuet, 2007) are available. The low amplitude (~300 nT) J anomaly in this profile can be explained by the contribution of two magnetic sources without recourse to geomagnetic reversals (Figure 3). The magnetization contrast at the landward edge of the gabbroic body accounts for the relatively wide J anomaly whereas the basement topography accounts for the superimposed smaller scale

anomalies. The seaward termination of the sill complex partly generates the weak anomaly previously interpreted as the M4 seafloor spreading anomaly (Srivastava et al., 2000) while the anomaly over the landward termination has been previously interpreted as the M15 anomaly (Srivastava et al., 2000). Although restorations of the position of the Iberia plate before the C34 anomaly are debated, the IAM-9 profile (Dean et al., 2000) in the IAP can be considered as an adequate conjugate profile of SCREECH line 2. Along the IAM-9 profile, the deep gabbroic layer proposed in our model at the eastern side of J can account for the seaward irregular magnetic anomaly increase (Figure 3), which has been previously interpreted as the M3-M4 seafloor spreading anomaly sequence (Sibuet et al., 2007). This is in agreement with depth estimations of magnetic sources (at ~6–8 km depth below the basement) by Euler deconvolution and the inversion of power spectra in the western part of the IAM-9 profile (Russell and Whitmarsh, 2003). As the seaward end of the IAM-9 profile abuts onto a large seamount, we attribute the steep western side and the high amplitude (>500 nT) of the J anomaly to the magnetization contrast between a thick volcanic layer and the exhumed serpentinized peridotites.

4. DISCUSSION

We thus propose that a period of excess magma is responsible for the formation of the J anomaly and suggest that the variable width and amplitude of the J anomaly result from the interplay between the extent of lava flows at the top of the basement and the location of underplated magmatic bodies at depth (Figure 4). The northward amplitude decrease of the J anomaly would then suggest that there was more magma delivered to the south and that the magma budget decreased northward. The northward decreasing distances between anomaly J and the seaward edge of the area of thinned continental crust and the nearest undisputed seafloor isochron (anomaly C34) also suggest a northward propagation. We therefore propose that the period of excess magmatism first began in the south of the NB and IAP and reached the northern part (ODP Sites 1277 and 1070) at the Aptian/Albian transition (~112 Ma). There, we speculate that mafic plutons and/or sills were emplaced beneath the serpentinized exhumed mantle (Figure 4). The introduction of underplated hot material may have resulted in the uplift of a topographic ridge and the tilting of the pre-Albian syn-rift sedimentary sequences (Péron-Pinvidic et al., 2007). Where magmatic pressure was sufficiently high, magma injections were able to break through the domain of previously exhumed serpentinized mantle resulting in both lava flows at the top basement and sill emplacement in the sedimentary sequence (Peron-Pinvidic et al., 2010). At some places, volcanic constructions overprinted the topographic high for as much as several millions of years (Merle et al., 2009) obscuring the original basement structure (Figure 4). Extension, which was spatially distributed before this critical period, eventually focused at the distal margins and may be at the origin of final break-up (Tucholke and Sibuet, 2007).

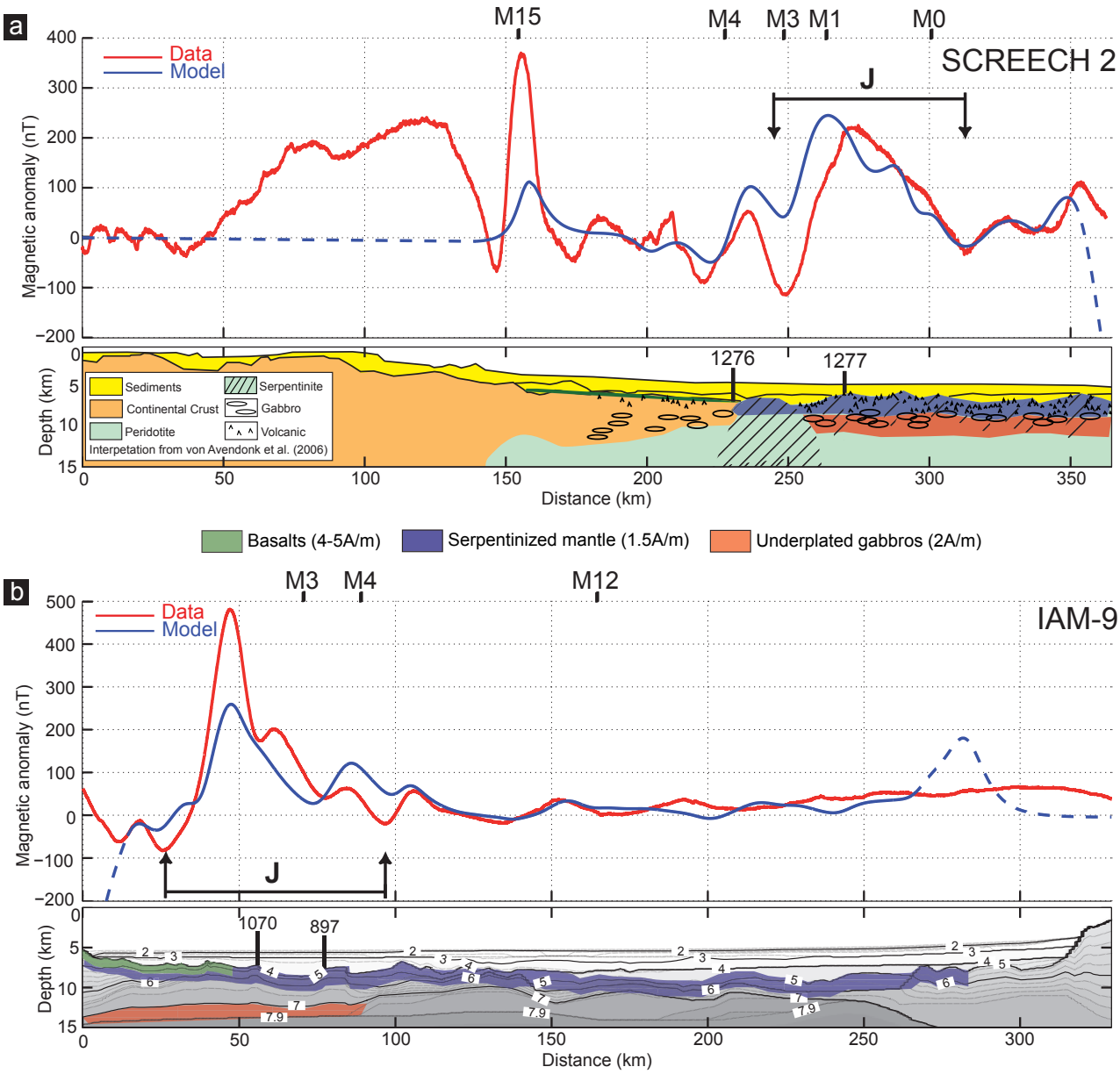

Figure 3 :Forward modelling of the SCREECH line 2 in the Newfoundland basin and the IAM-9 profile in the Iberia Abyssal Plain. The contributions of three magnetized layers (basalts, serpentinized peridotites and gabbroic rocks) explain the magnetic anomaly profiles. The dotted blue lines indicate the parts of the profiles which are not modelled. Magnetic anomalies are from by Srivastava *et al.* (2000) . **a,** Magnetic model of the SCREECH line 2 superimposed on the interpretation of the seismic velocity structure of van Avendonk *et al.* (2006); **b,** Magnetic model of the IAM-9 profile superimposed on the seismic velocity structure of Dean *et al.* (2000). See Supplementary Figure 1 for the forward modelling of SCREECH lines 1 and 3.

The excess magma required to form the J anomaly ridge south of the NB has been attributed to the occurrence of a mantle plume injecting magma along the Mid Atlantic Ridge (MAR) ~10 Myr earlier than in the NB (at about M0-M4 times; Tucholke and Ludwig, 1982). Because large transform faults can inhibit along-axis melt flow (Georgen and Lin, 2003) these ~10 Myr could correspond to the time needed for the hot sub-oceanic asthenosphere to pass through the Newfoundland-Gibraltar transform faults, penetrate laterally beneath the Newfoundland – Iberia rift zone (Reston and Morgan, 2004) and produce magma in excess that finally triggered oceanic spreading. This event of high melt delivery coincides with the opening of the southern MAR and with the 100-110 Ma old change

of plate velocity observed on a global scale (Torsvik et al., 2008). We therefore suggest that there might be a feedback between this major kinematic reorganization and redistribution of asthenospheric masses beneath the nascent plate boundaries.

The processes inducing the production of large volumes of magma beneath an area that includes the Southeast Newfoundland and Gibraltar-Azores ridges (Figure 1) and the propagation of magma both southward and northward remain to be identified. Hot plume influenced asthenosphere invading the NB and IAP rifted area has been previously suggested by Reston and Phipps Morgan (2004). Whether the enriched nature of the alkaline magmatism argues for a hotspot-driven origin of the Tore–Madeira Rise and the J anomaly ridge is controversial (Geldmacher et al., 2006; Merle et al., 2009). Merle et al. (2009) rather suggested that short-lived, small-sized magma pulses were emitted from a wide thermal anomaly located under the Tore–Madeira–Azores–Canary area.

The consequences of our findings are large and numerous. The J anomaly does not correspond to the beginning of the M sequence of seafloor spreading anomalies in the IAP and NB. Consequently, the current kinematic reconstructions of Iberia predating anomaly C34 need to be revised. We suggest that a single mantle exhumation phase occurred between ~140 Ma and ~112 Ma, which is in contradiction with what has been proposed before (Sibuet et al., 2007; Tucholke and Sibuet, 2007). We propose that a magmatic event triggered the continental break-up and onset of seafloor spreading, a process that may have occurred also at other magma-poor rifted margins (e.g. S-Atlantic and S-Australia margins). The recognition of "break-up anomalies" along these rifted margins, such as the J anomaly in the NB and IAP, may help to locate the transition from mantle exhumation to seafloor spreading. A more quantitative approach addressing the nature of the sources of the magnetic anomalies over exhumed mantle domains at the seaward edge of magma-poor rifted margins may validate our conceptual idea.

5.METHODS SUMMARY

We assume that the J anomaly was formed in the late Aptian to early Albian time, about mid-time of the Cretaceous Normal Superchron. We therefore do not use any reversal of the Earth's magnetic field to explain the J anomaly and instead hypothesized that it results from magnetization contrasts between both lava flows at the surface and magmatic bodies emplaced at depth and the surrounding serpentinized mantle. We use the results of the refraction seismic studies (Van Avendonk et al., 2009) along the SCREECH (Study of Continental Rifting and Extension on the Eastern Canadian sHelf) profiles in the NB and the IAM-9 profile in the IAP (Dean et al., 2000) to locate the depth and landward edge of these magmatic bodies and of the serpentinized exhumed mantle in the 2D forward modelling. We also use the seismic mapping of Péron-Pinvidic et al. (2010) to constrain the thickness, depth and edges of basaltic sill complexes. The magnetization of the source layers in

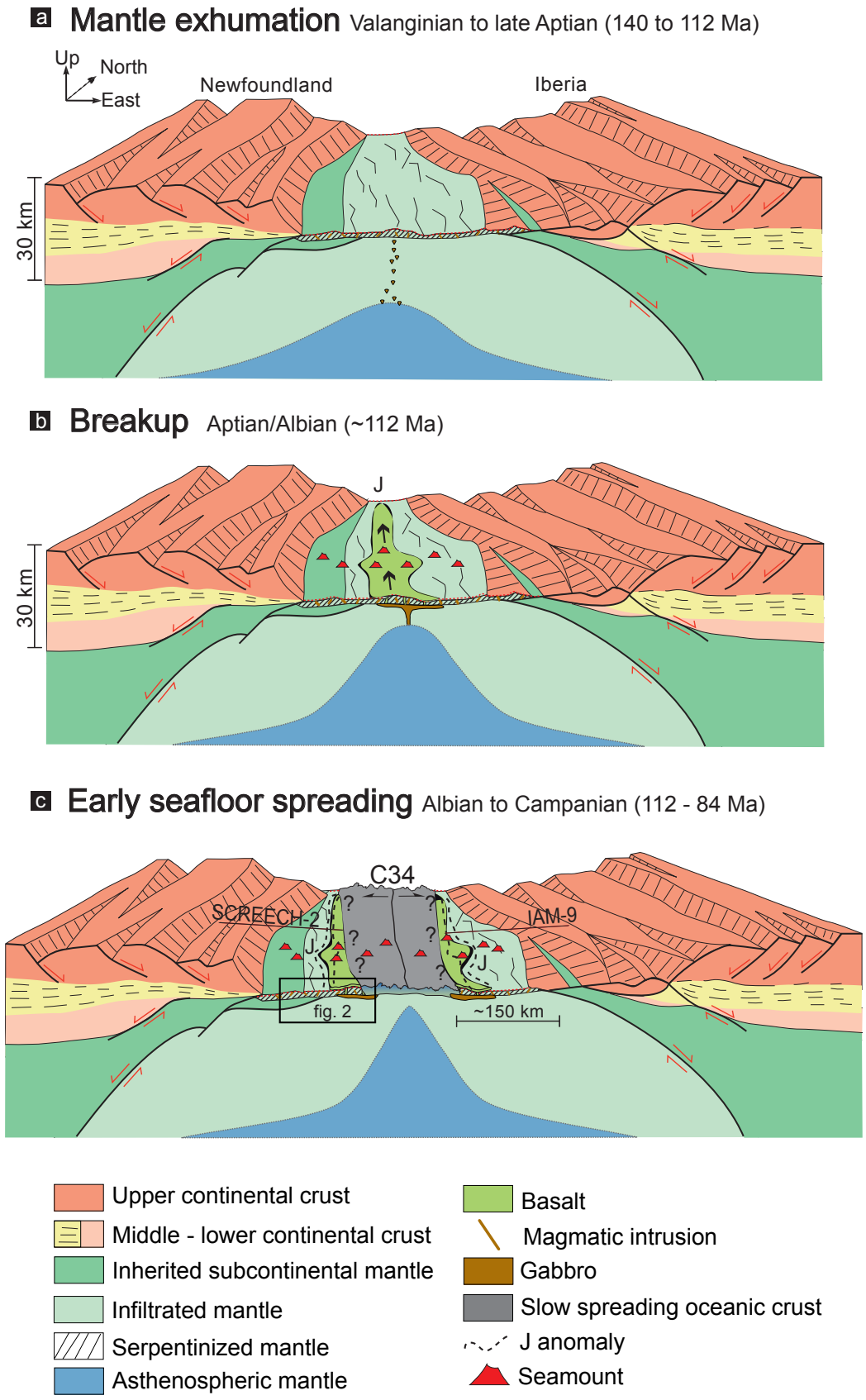

Figure 4 : Conceptual lithosphere-scale model of rifted magma-poor margins showing the role of magmatic processes in the onset of seafloor spreading. a, mantle exhumation occurred between ~140 and ~112 Ma. b, excess magma broke through the domain of exhumed serpentinized mantle in the south of the NB and IAP. It reached the northern part and induced the uplift of the outer-high at the Aptian/Albian transition (~112 Ma). c, alkaline volcanism and oceanic spreading may have been concomitant along the nascent plate boundary. The first seafloor spreading magnetic anomaly (C34) formed 84 Ma ago at the end of the Cretaceous Normal Superchron.

our forward modelling is constrained as much as possible by the results of the ODP drilling sites (e.g. from Tucholke and Sibuet (2007)) located on or in the vicinity of the seismic profiles. We use magnetizations obtained for basaltic sills, basalt flows and serpentinized peridotites at ODP Holes 897D, 899B, and 1070A in the IAP and ODP Sites 1276 and 1277 in the NB (e.g. from Zhao (2001)). As the few samples of gabbroic rocks collected at these sites are strongly altered and show very low magnetization intensities (Zhao et al., 2001) we prefer to rely on estimates obtained in the 1.5 km thick section of gabbroic crust drilled at ODP Hole 735B at the ultra slow spreading Southwest Indian Ridge (Pariso and Johnson, 1993). Although a better fit can be obtained using variable magnetization contrasts, we choose to be as consistent as possible with all data available by using, in all forward models, the same magnetization value for each magnetized layer. See Supplementary Methods for a more detailed description of the forward modelling of the magnetic anomaly profiles.

6.SUPPLEMENTARY INFORMATION

We assume that the J anomaly was formed in the late Aptian to early Albian time, about mid-time of the Cretaceous Normal Superchron. We hypothesized that it results from magnetization contrasts between both lava flows and magmatic bodies emplaced at depth, and the surrounding serpentinized exhumed mantle. We constrained our 2-D forward modelling by the seismic data and drill hole data along the SCREECH (Study of Continental Rifting and Extension on the Eastern Canadian sHelf) profiles in the Newfoundland Basin (NB) and the IAM-9 profile in the Iberia Abyssal Plain (IAP). The seismic and sea-surface magnetic data along these profiles were collected during the R/V Maurice Ewing cruise EW-0007 in 2000 and the RRS Discovery cruise 215 in 1995. Seismic data (Dean et al., 2000; Funck et al., 2003; Hopper et al., 2004; Hopper et al., 2007; Lau et al. 2006; Shillington et al., 2006; Van Avendonk et al., 2006; Van Avendonk et al., 2009; Peron-Pinvidic et al., 2010) were used to locate the depth and edges of the magnetic source layers. The magnetization of the source layers was constrained as much as possible by the results of the ODP drilling sites on top or in the vicinity of the seismic profiles (Zhao et al., 2001; Jagoutz et al., 2007; Tucholke and Sibuet, 2007; Zhao et al., 2007). We show that a mixed contribution of underplated magmatic rocks and lava flows respectively beneath and over exhumed serpentinized mantle can fully explain the observed magnetic anomaly profiles. There is no need to take into account inversions of the Earth's magnetic field as it was previously suggested (Srivastava et al., 2000; Sibuet et al., 2007).

6.1. FORWARD MODELLING OF THE MAGNETIC CONTRIBUTION OF THE UNDERPLATED GABBROIC ROCKS

Thickening of the crust beneath the J anomaly is supported by both geological and geophysical observations. The geological arguments are presented in the main text. Here we present the geophysical arguments for a magnetized source layer of underplatted mafic rocks at depth. We interpret the deepening of seismic velocities between ~6.5 and ~7.9 km/s as indicating a thickening of a lower layer of intruded mafic bodies (e.g. see Dean et al. (2000)). As this velocity gradient does not show strong lateral changes on the seaward edges of the seismic lines in the NB and IAP we extend seaward this lower layer of mafic bodies (e.g. SCREECH line 2 shown in Figure 2). We do not expect a strong magnetization contrast oceanward between a typical oceanic layer 3 and underplated gabbros. Only a few samples of altered gabbroic rocks have been collected during ODP Leg 149/173 and 210 and show very low natural remanent magnetization intensities (~0.2–0.5 A/m) (Zhao et al., 2001; Zhao et al., 2007). As gabbroic rocks are known to carry significant stable remanent magnetization, which is sufficient to account for sea-surface magnetic anomalies (Pariso and Johnson, 1993; Worm, 2001), we prefer to rely on estimates obtained in the 1.5 km thick section of gabbroic crust drilled at ODP Hole 735B at the ultra slow spreading Southwest Indian Ridge (Dick et al., 2000). A mean remanent intensity of ~2.0-2.5 A/m and large Koenigsberger ratios have been measured there (Kikawa and Pariso, 1991; Pariso and Johnson, 1993). We therefore assume a conservative estimate of 2 A/m for the average effective magnetization of gabbroic rocks following Pariso and Johnson (Pariso and Johnson, 1993). We use a source layer with remanent magnetizations, according to the magnetization vector from Van der Voo (1990) (IM = 46°, DM = 0°).

6.2. FORWARD MODELLING OF THE MAGNETIC CONTRIBUTION OF THE SERPENTINIZED MANTLE ROCKS

As serpentinized harzburgites and lherzolites were drilled in the ocean continent transitions (OCTs) in both IAP and NB, we also explore the contribution of a thin magnetized layer of serpentinized peridotites which has been proposed to account for both small magnetic anomalies toward the area of thinned continental crust (Russell and Whitmarsh, 2003) and the J anomaly (Sibuet et al., 2007). Studies of the magnetic properties of variably serpentinized peridotites (Toft et al., 1990; Oufi et al., 2002;) show that their natural remanent magnetization can indeed be significant for high degrees of serpentinization (4-10 A/m on average for degrees of serpentinization greater than 75% (Oufi et al., 2002)). These studies also show, however, that this natural remanent magnetization is highly variable. In particular, it depends on the distribution and size of magnetite grains produced during serpentinization, and on the iron content and abundance of secondary hydrous minerals such as brucite (Oufi et al., 2002; Toft et al., 1990). Serpentinized peridotites are therefore versatile magnetic sources that may or may not produce strong signals depending on fluid-rock interactions and elemental exchanges that prevailed during serpentinization. Serpentinites from ODP Holes 897D, 899B, and

1070A in the IAP yielded mean NRM intensities of 0.35, 1.8, and 1.6 A/m respectively (Zhao et al., 2001). Highly variable magnetizations (1-9 A/m) were found for the serpentinized peridotites at ODP Site 1277 in the NB (Zhao et al., 2007). However the mean value for the whole recovered section at Site 1277 (~1.7 A/m) is similar to the mean estimates obtained for the ODP holes in the IAP. We therefore assume a conservative estimate of 1.5 A/m for the average effective magnetization of a serpentinized peridotite layer. We use a source layer with solely an induced uniform magnetization in order to make no assumption about unconstrained lateral changes of magnetization intensity and polarity. The extend of the serpentinization at depth is constrained by the seismic refraction data (Dean et al., 2000; Funck et al., 2003; Hopper et al., 2004; K. W. Helen Lau, 2006; Van Avendonk et al., 2006; Van Avendonk et al., 2009). We interpret the upper high-velocity-gradient layer in the OCTs with velocities increasing from 4.5 to 6.6 km/s as exposed mantle (e.g. see Minshull (2009)). These velocities for the upper basement are within the bounds predicted for peridodites serpentinized between ~50% and 100% (Miller and Christensen, 1997). We exclude higher velocities of 7.0-7.6 km/s which we interpret as indicating more weakly serpentinized mantle rocks, following a recent review of mid-ocean ridge data which shows that significant serpentinization of exhumed mantle there does not extend to depths greater than 3 to 4 km (Cannat et al., 2009). As the velocity gradient in the upper basement does not show strong lateral changes on the seismic lines in the NB and IAP we extend seaward the domain of exhumed mantle (e.g. SCREECH line 2 shown in Figure 2). This is further supported by the observations of large domains of exhumed mantle rocks at ultra-slow spreading ridges (Cannat et al., 2006).

6.3. FORWARD MODELLING OF THE MAGNETIC CONTRIBUTION OF BASALTIC ROCKS

We also take into account the contributions of basalts as both sills and lava flows have also been imaged by seismic experiments and drilled in the OCT of the NB. Two sills were drilled at ODP Site 1276 and have been dated at ~105 Ma and ~98 Ma, in the Cretaceous Normal Superchron (Hart and Blusztajn, 2006). Péron-Pinvidic *et al.* (2010) use multichannel seismic reflection data to calculated that the thickness of the sill complex ranges from ~50 m to ~1,200 m, with a mean value of ~480 m. We use the seismic mapping of Péron-Pinvidic *et al.* (2010) to locate the depth and edges of one unique 500 m thick sill complex in our 2-D model. We use a 4 A/m positive remanent magnetization for this sill according to the mean magnetization of sill diabases obtained by Zhao et al. (2007) at ODP Site 1276. Lava flows were drilled at ODP Site 1277 but their total thickness do not exceed ~15 m so we dismiss their contribution. Where seismic profiles were collected close to seamounts (e.g. SCREECH 3 (Lau et al. 2006) and IAM-9 (Dean et al., 2000)) we also assume a basaltic layer on top of the basement which is also supported by the occurrence of basalt clasts in Aptian debris flows drilled at Sites 1277, 897, 899 and 1070 (Péron-Pinvidic et al., 2007). As these seamounts were proposed to be built up by a large alkaline magmatic pulse during Cretaceous times (103-80.5 Ma) (Merle et al.,

2009; Sullivan and Keen, 1977), we use a positive standard 5 A/m remanent magnetization for this basaltic layer. Seismic refraction data over such seamount in the Tagus abyssal plain have shown that the crust beneath the seamounts is approximately twice as thick as the oceanic crust (Peirce and Barton, 1991). We have therefore made the assumption that the upper part of the basement consists of a 500-1000 m thick volcanic layer. Such a thick volcanic layer near these seamounts is also supported by their large height (over 3000 m above the sea floor (Merle et al., 2009)). This shallow magnetic layer only partly explains the sharp seaward and landward side of the J anomaly in the IAM-9 and SCREECH 3 profiles respectively. We suggest that a larger magnetic contrast between basalts and highly serpentinized peridotites and/or a thicker volcanic source layer may be responsible for the whole amplitude of the J anomaly there.

Supplementary Informations

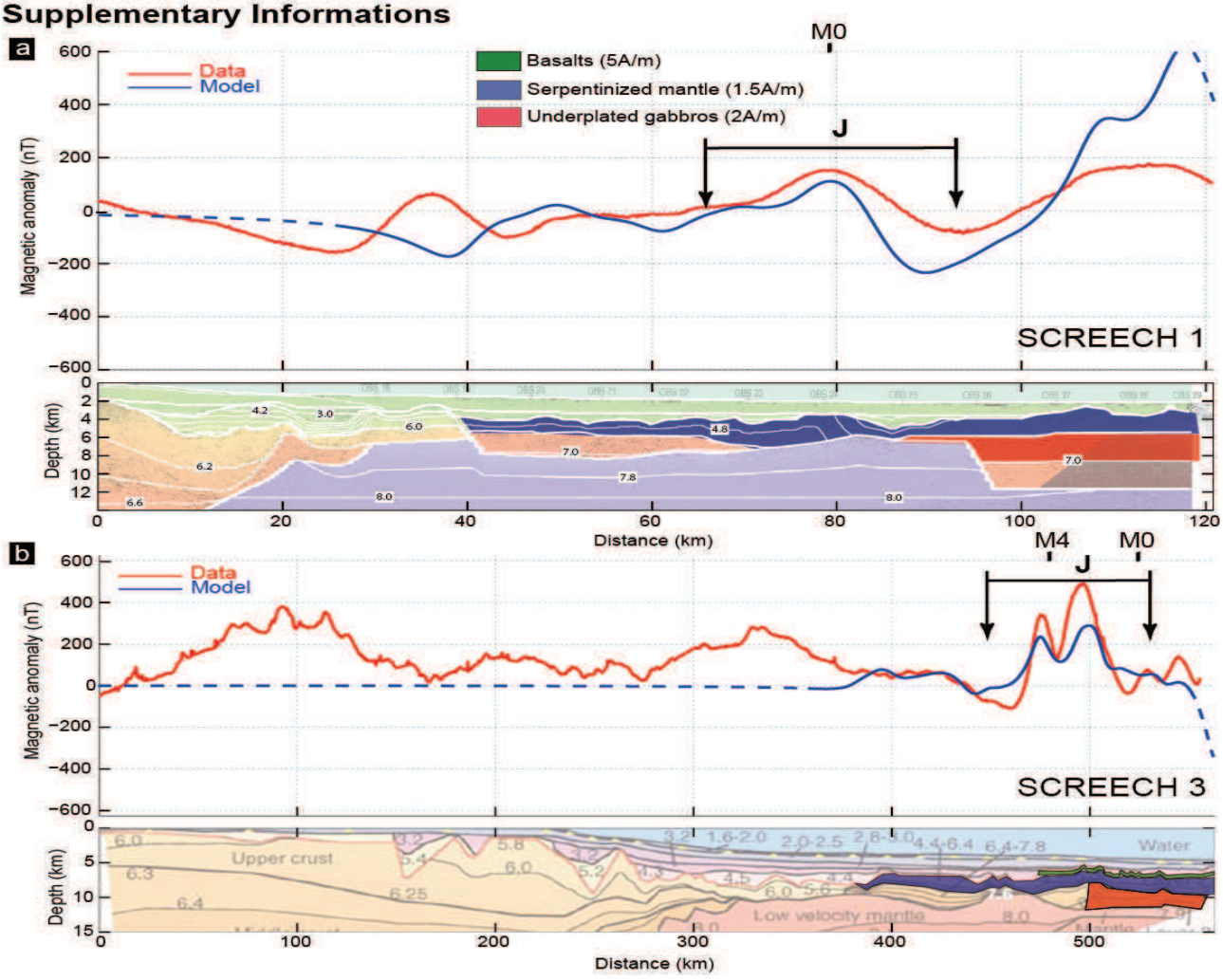

Figure 5 : Forward modelling of the magnetic anomaly profiles along SCREECH line 1 and 3 in the Newfoundland basin. The contributions of three magnetized layers (basalts, serpentinized peridotites and gabbroic rocks) explain the magnetic anomaly profiles. The dotted blue lines indicate the parts of the profiles which are not modelled. The magnetic anomalies are from Srivastava *et al.* (2000) . **a,** Magnetic model of the SCREECH line 1 superimposed on the seismic refraction profile from Hopper et al. (2007). The magnetic anomaly profile over SCREECH line 1 displays a weak J anomaly (<300 nT) at the eastern end of the profile. This J anomaly is best explained by the contribution of both a deep magmatic body and a shallower serpentinized peridotite layer. **b,** Magnetic model of the SCREECH line 3 superimposed on the seismic refraction profile from Lau et al, (2006). Like the IAM-9 profile, SCREECH line 3 displays a high amplitude J anomaly (>500 nT) which we explain by both a thick volcanic layer on top of the exhumed serpentinized mantle and by a deeper magmatic underplated body. However, the edge of the volcanic layer is located further landward than the deep magmatic body by contrast to the IAM-9 profile where we suggest it is the opposite.

7.CONTROVERSIAL ISSUES

The publication presented in this chapter lead to important discussions through the review process. We would like to highlight two main criticisms that have been addressed and that are still under debate.

7.1. INTERPRETATION OF SCEECH LINE 1

The first point concerns the forward model of the Screech line 1 that is presented in the supplementary information above. The manuscript presented here is slightly different from the one published in the Nature Geoscience Journal as it includes a forward modeling of the Screech line 1. Indeed, this line was removed from the published paper because of controversial interpretations regarding the nature of the transitional domain in this area of the Newfoundland margin. Indeed, one of the reviewers argued that the velocity gradient as well as the reflectivity pattern is fully consistent with the presence of an oceanic layer 2 and preclude the presence of a transitional zone formed by exhumed serpentinite. Nevertheless, we would like to underline that we learn from Sauter et al. (2013) that both ~10 m resolution images of the seafloor and dredge samples are required to reasonably distinguish between volcanics and serpentinized peridotites at the SWIR. Moreover, we show in chapter 2 that the presence of volcanic material within the exhumed mantle domains of the SWIR is not necessarily correlated with a magnetic signature. These arguments further support the assumption made above to build the forward model of the Screech line 1 and rather suggest that in the absence of drilling samples neither the velocity gradient nor the reflectivity can provide undisputable arguments regarding the nature of the crust.

7.2. PLATE RECONSTRUCTION

The second point raised concern the implications of our finding regarding kinematic plate reconstructions. This point is discussed in the correspondence below which has been published in Nature Geoscience in 2012:

Tucholke, B. E. & Sibuet, J.-C. Problematic plate reconstruction; Comment on ‘Magmatic breakup as an explanation for magnetic anomalies at magma-poor rifted margins’ by Bronner, et al. (Nature Geoscience, 4, 549-553, 2011). Nature Geosci 5, 676-677 (2012).

Bronner, A., Sauter, D., Manatschal, G., Peron-Pinvidic, G. & Munschy, M. Reply to ‘Problematic plate reconstruction’. Nature Geosci 5, 677-677 (2012).

7.2.1. PROBLEMATIC PLATE RECONSTRUCTION

Brian E. Tucholke[1]* and Jean-Claude Sibuet[2]

[1]Department of Geology and Geophysics, Woods Hole Oceanographic Institution, Woods Hole, Massachusetts 02543, USA, [2]Ifremer Centre de Brest, BP 70, 29280 Plouzané Cedex, France, and 44 rue du Cloître, 29280 Plouzané

As has been previously proposed (Tucholke et al., 2007; Tucholke and Sibuet, 2007), Bronner et al. (2011) suggest that opening of the rift between Newfoundland and Iberia involved exhumation of mantle rocks until 112 million years (Myr) ago, subsequent seafloor spreading, and crustal thickening along the high-amplitude magnetic J anomaly by magma that propagated from the Southeast Newfoundland Ridge area. Conventionally, the anomalous magnetism and basement ridges associated with the J anomaly north of the Newfoundland–Gibraltar Fracture Zone are thought to have formed about 125 Myr ago at chron M0 (Bronner et al., 2011; Tucholke and Sibuet, 2007; Figure 6a), although the crust probably experienced some later magmatic overprinting (Merle et al., 2009). The M0 age would make their formation simultaneous with that of the similar J anomaly and basement ridges (the J Anomaly Ridge and Madeira Tore Rise) along the Mid-Atlantic Ridge to the south (Rabinowitz et al., 1978; Tucholke and Ludwig, 1982) and place them within a zone of exhumed mantle in the Newfoundland–Iberia rift (Tucholke and Sibuet, 2007; Bronner et al., 2011). In contrast, Bronner et al. (2011) propose that the J anomaly and associated basement ridges were formed by later magmatism — about 112 Myr ago — that marked the end of mantle exhumation in the rift. We argue here that constraints from plate tectonic reconstructions render this possibility untenable.

The magnetic model central to the Bronner et al. (2011) paper is plausible (although no more so than models based on M-series geomagnetic reversal data (Srivastava et al., 1990; Srivastava et al., 2000; Russell and Whitmarsh, 2003; Tucholke and Sibuet, 2007), but it is problematic in terms of plate reconstructions. Bronner and colleagues propose that an offset between the axes of the Mid-Atlantic Ridge and Newfoundland–Iberia rift at the Newfoundland–Gibraltar Fracture Zone around 125 Myr ago (M0 offset ~70 km; bold dashed lines, Figure 6b) inhibited northward transport of magma from the Southeast Newfoundland Ridge for about 10 Myr. If true, such a scenario would necessitate rapid propagation of magma through the rift by 112 Myr ago, and thus require the J anomaly there to have formed almost isochronally. During the period between 125 and 112 Myr ago, the conjugate J Anomaly Ridge and Madeira Tore Rise south of the Newfoundland–Gibraltar Fracture Zone became widely separated (Figure 6b). However, by about 84 Myr ago (chron C34, Figure 6d), the Madeira Tore Rise north of the Newfoundland–Gibraltar Fracture Zone was collinear with the Madeira Tore Rise to the south and has remained so to the present (Srivastava et al., 1990). Thus, the scenario proposed by Bronner and colleagues would require that: (1) a left-lateral offset of the Newfoundland–Gibraltar Fracture Zone of more than 100 km that existed about 112 Myr ago (Figure 6b) reversed to become a 100-km right-lateral offset by 84 Myr ago (Figure 6d); (2) the plate separation rate just

north of the Newfoundland–Gibraltar Fracture Zone was at least ~1.5 times faster than to the south for some period after 112 Myr ago, but it dramatically slowed to the African–North American rate by 84 Myr ago; and (3) within the same time frame, separation between the Iberian and North American plates serendipitously aligned the formerly offset segments of the Madeira Tore Rise located north and south of the Newfoundland–Gibraltar Fracture Zone.

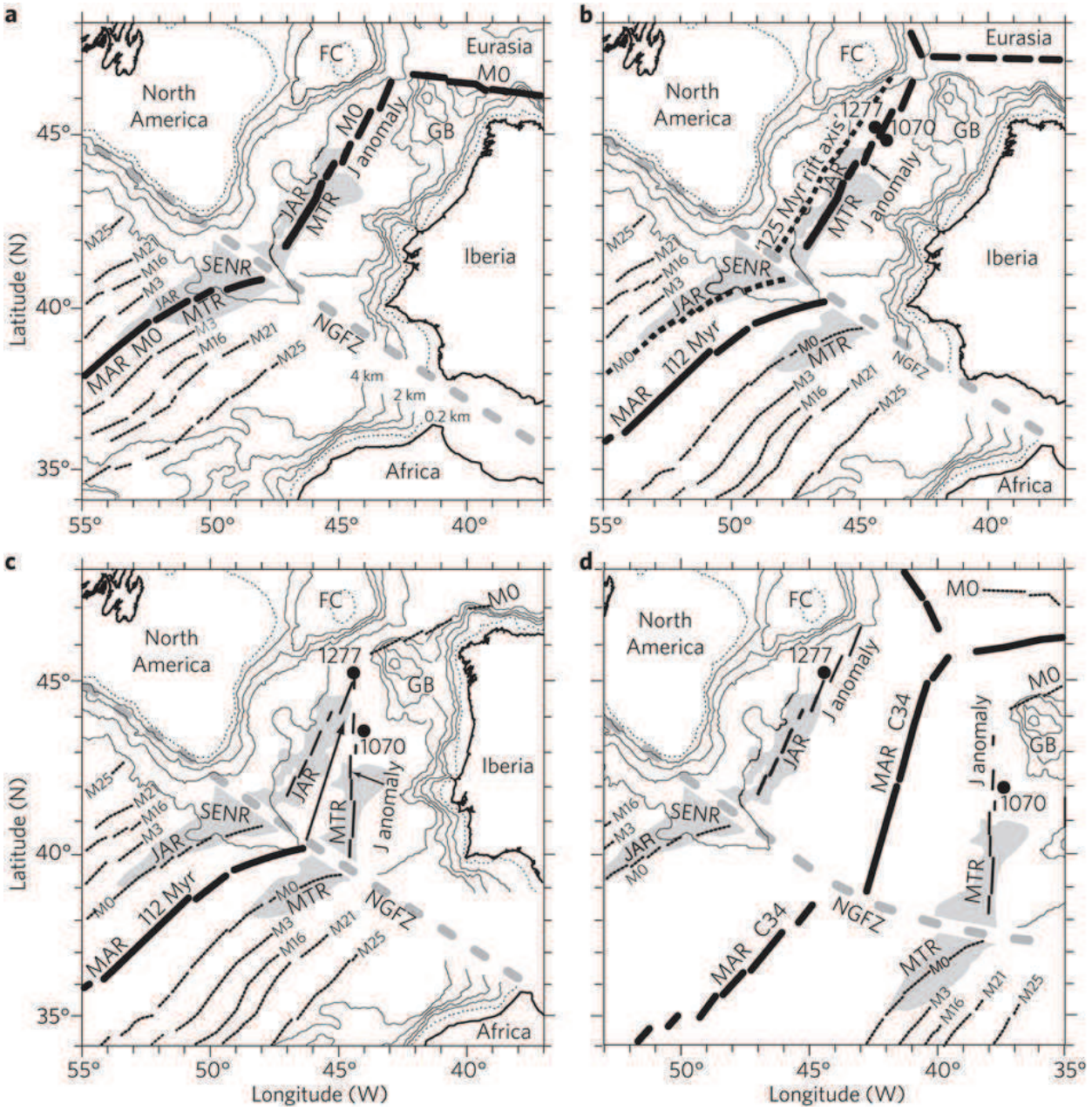

Figure 6 : a, Conventional chron M0 reconstruction of the African–North American (Srivastava et al., 1990) and Iberian–North American (Srivastava et al., 2000) plates, which assumes that the J anomaly both north and south of the Newfoundland–Gibraltar Fracture Zone (NGFZ) formed about 125 Myr ago. J Anomaly Ridge (JAR) and Madeira Tore Rise (MTR) basement ridges are shaded and seafloor isochrons identified. b, Plate reconstruction at 112 Myr ago assuming nearly isochronal formation of the J anomaly by this time in the Newfoundland–Iberia rift. African and North American plate positions interpolated between chron M0 and C34 reconstructions (Dick et al., 2000). Bold dashed lines indicate earlier M0 extension axes on the North American plate (chron M0 south of the NGFZ; assumed extension half rate ~7 mm yr−1 north of NGFZ2). Ocean Drilling Program drill sites 1277 and 1070 indicated. c, Plate reconstruction at 112 Myr ago, assuming JAR–MTR ridges formed by prolonged propagation (arrow) of an isolated magma anomaly northward from the Southeast Newfoundland Ridge (SENR) between about 125 and 112 Myr ago. d, Chron 34 plate reconstruction (Srivastava et al., 1990). MAR, Mid-Atlantic Ridge; FC, Flemish Cap; GB, Galicia Bank.

The presumed reversal of offset of the Newfoundland–Gibraltar Fracture Zone and discrepancy in extension rates occur within the Cretaceous Magnetic Quiet Zone, and thus are unconstrained by geomagnetic age data. However, these presumptions seem highly unlikely. More importantly, the required alignment of the northern and southern Madeira Tore Rise is too coincidental to be believed.

Alternatively, if northward propagation of magma from the Southeast Newfoundland Ridge was prolonged for 10 Myr, rather than delayed, a significantly diachronous J anomaly would result (Figure 6c). This too is problematic. There is no excess magmatism observed in the wake of a supposed propagator, nor was there any mirrored, southward propagation south of the Newfoundland–Gibraltar Fracture Zone. Thus, any melt anomaly that drove propagation from the Southeast Newfoundland Ridge ceased to exist well before 112 Myr ago. Therefore, prolonged propagation would require the unreasonable assumption that an isolated melt anomaly was moving in a northerly direction through the mantle of the Newfoundland–Iberia rift, creating a track in the sea floor nearly opposite in direction to that expected from absolute plate motion (Müller et al., 1993). We conclude from the plate-kinematic constraints that formation of the J-anomaly complex in the Newfoundland–Iberia rift about 112 Myr ago is not a viable proposition and thus that its predicted consequences are not pertinent to the rift evolution.

7.2.2. REPLY TO 'PROBLEMATIC PLATE RECONSTRUCTION'

Adrien Bronner[1], Daniel Sauter[1], Gianreto Manatschal[1], Gwenn Péron-Pinvidic[2] and Marc Munschy[1]

[1]Institut de Physique du Globe de Strasbourg, IPGS - UMR 7516, CNRS - Université de Strasbourg, 1 rue Blessig 67084 Strasbourg cedex,

[2]NGU, Geological Survey of Norway, Leiv Eirikssons vei 39, 7491 Trondheim, Norway,*Contact: a.bronner@unistra.fr

The main criticism by Tucholke and Sibuet on our paper (Bronner et al., 2011) concerns the position, nature and age of the J anomaly that occurs on both sides of the Newfoundland–Gibraltar Fracture Zone. Despite the fact that Tucholke previously proposed a 100 km offset for the J anomaly across the Newfoundland–Gibraltar Fracture Zone (Tucholke and Ludwig, 1982), Tucholke and Sibuet argue that this anomaly is "collinear" and thus formed at the same time (~125 Myr ago; chron M0). However, at that time, the nature of the crust north and south of the Newfoundland–Gibraltar Fracture Zone was different. To the south excess magma resulted in a thickening of the oceanic magnetic layer (Tucholke and Ludwig, 1982) and amplification of its associated magnetic anomaly (M0), whereas the northern domain was formed by exhumed subcontinental mantle and polyphase magmatic activity, as evidenced by rocks from Ocean Drilling Program (ODP) sites 1277 and 1070 (Jagoutz et al., 2007). To account for the drilling and seismic results, we proposed that this excess magmatic event occurring south of Newfoundland–Gibraltar Fracture Zone at around M0 time (Tucholke and Ludwig, 1982) propagated into the Newfoundland–Iberia rift and finally resulted in onset of seafloor spreading in the northern part (ODP sites 1277 and 1070) at about 112 Myr ago. Such a mechanism for break-up

has been previously proposed (Reston and Morgan, 2004), and we suggested that the J anomaly is the signature of this diachronous propagating event (Bronner et al., 2011).

The consequence of our finding is that the J anomaly does not result from a sharp boundary as expected from a reversal of Earth's magnetic field, but rather corresponds to a ~20- to 40-km-wide zone of magma that overprints previously exhumed mantle rocks of unknown age. In contrast to true oceanic crust, the basement underneath the J anomaly is polyphased. This implies that it can neither be viewed as a conventional seafloor-spreading anomaly nor used to constrain plate reconstructions of Iberia and North America. Therefore, our model invalidates the assumptions used to construct Tucholke and Sibuet's Figure 6a, b and their related ensuing arguments.

Tucholke and Sibuet's Figure 6c could potentially provide a first approach to alternative palaeogeographic restorations before about 84 Myr ago (chron C34). Nevertheless, this interpretation is also problematic because it requires a 112 Myr age for the crust at ODP holes 1277 and 1070. Yet, the oldest rocks drilled at those locations are 128 Myr old. Moreover, the offset of the Newfoundland–Gibraltar Fracture Zone used to construct this figure is the same as the one observed at present, but, in the absence of robust magnetic anomalies, this point remains unconstrained for times older than chron C34.

To conclude, we note that the classical interpretation using the J anomaly as a seafloor-spreading anomaly of M0 age, as suggested by Tucholke and Sibuet, requires an up-to-600-km-wide domain between Iberia and Europe to have been subducted during the subsequent convergence that led to the present-day Pyrenees (Sibuet et al., 2004). However, hints for the existence of such a subduction zone can neither be observed in the field (Jammes et al., 2009) nor in the most recent tomographic images (Souriau et al., 2008). Thus, we do believe that our model is a first step to elucidating inconsistencies in the previous plate kinematic reconstructions within the southern North Atlantic, as well as in the Pyrenean domain.

Synthèse et Perspectives

Les anomalies magnétiques observées en domaines océaniques qui ont permis de confirmer la théorie de la dérive des continents, ont été et restent encore un point clef de la compréhension de la tectonique des plaques. Elles sont associées aux inversions de polarité du champ magnétique enregistrées par les roches extrusives et intrusives mises en place lors de la formation, aux limites de plaques divergentes, d'une nouvelle lithosphère océanique. Néanmoins, ces vingt dernières années, de nombreuses campagnes océanographiques ont mis en évidence la présence de roches mantelliques exhumées de type péridotites serpentinisées à l'aplomb des dorsales lentes et ultra-lentes et aux transitions océan-continent des marges passives appauvries en magma. Ces découvertes ont démontré le rôle non négligeable de la tectonique, et plus particulièrement des failles de détachement pour accommoder la divergence des plaques. En raison de la nature des roches qui les composent et des processus complexes qui sont associés à leur formation, les zones de manteau exhumé présentent un signal magnétique dont l'origine reste incertaine et controversée. Le but de ce travail était donc d'étudier le signal magnétique associé à l'exhumation de roches mantelliques au droit d'une dorsale océanique et d'une transition océan-continent. Ceci dans le but d'en déduire (1) si l'exhumation de roches mantelliques aux dorsales océaniques est compatible avec l'enregistrement d'inversions de polarité du champ magnétique terrestre, (2) quels processus sont associés aux anomalies magnétiques observées à l'aplomb des zones de transitions océan-contient et (3) quelles sont les conséquences de ces processus sur les mécanismes de l'océanisation.

1. LES MESURES « DEEP-TOW » TROIS COMPOSANTES DU CHAMP MAGNÉTIQUE TERRESTRE: MÉTHODOLOGIE

Les données magnétiques déjà publiées et acquises à l'aplomb de zones de manteau exhumé des dorsales ultra-lentes (Sauter et al., 2008) et des marges appauvries en magma (Miles et al., 1996; Srivastava et al., 2000; Russell and Whitmarsh, 2003; Sibuet et al., 2007) révèlent un signal complexe de faible amplitude et de faible continuité spatiale. Il était donc primordial, pour l'étude de ces zones, de travailler avec des données de qualité et de résolution maximale. Dans ce but, nous avons tout d'abord cherché à développer des méthodes de traitement et d'interprétation des anomalies magnétiques acquises à l'aide de magnétomètres trois composantes tractés proche du fond. Nous avons testé une méthode de calibration utilisée pour la magnétométrie satellitaire et nous l'avons adaptée aux mesures magnétiques de fond de mer. Nous avons montré que contrairement aux méthodes communément utilisées en géophysique marine, l'interférence magnétique du véhicule tracté pouvait être efficacement corrigée sans connaissance préalable de l'orientation spatiale du magnétomètre. De façon à s'affranchir des effets liés aux variations d'altitude du magnétomètre durant l'acquisition nous avons également développé une méthode d'inversion des profils magnétiques basée sur une couche équivalente. Nous montrons qu'il est possible, en drapant cette couche sur la bathymétrie et par l'intermédiaire d'une unique inversion linéaire, d'estimer l'aimantation crustale et de recalculer le champ d'anomalie et ses composantes en n'importe quel point en dehors des sources.

2. APPLICATION À L'EXPLORATION MAGNÉTIQUE MARINE

Les magnétomètres scalaires communément utilisés en géophysique marine nécessitent d'être tractés à plusieurs centaines de mètres derrière le navire pour s'affranchir de l'interférence magnétique de la structure métallique de celui-ci. Il est donc souvent difficile voir impossible de combiner cet instrument à d'autres types de collecte de données géophysiques (e.g. sismiques) ou géologiques (imagerie, dragage) car les vitesses d'acquisition sont différentes et il y a un risque de perte des instruments de mesure. La méthode de calibration présentée dans ce travail pourrait donc également être testée sur un magnétomètre trois composantes fixé de façon permanente au pont supérieur du navire. Une bonne correction de l'effet du navire (impossible dans le cas d'un magnétomètre scalaire) pourrait ensuite permettre de s'affranchir de la mise à l'eau du magnétomètre scalaire et faciliter la cartographie magnétique marine de façon à étayer à moindre coût les jeux de données existants.

3. LE SIGNAL MAGNÉTIQUE ASSOCIÉ AUX DOMAINES DE MANTEAU EXHUMÉ DE LA DORSALE SUD-OUEST INDIENNE

Nous avons ensuite utilisé ces méthodes pour l'étude et l'interprétation des données magnétiques « deep-tow » acquises lors de la campagne « Smoothseafloor » (Octobre 2010), dans la partie Est de la dorsale Sud-Ouest Indienne. Nous avons mis en parallèle les données de dragages, les images sonar haute-résolution du plancher océanique et les données magnétiques acquises proche du fond. Nous montrons que le plancher océanique de type volcanique, associé à une épaisseur relativement importante de croûte (Residual Mantle Bouguer Anomalies < 20 mGal), permettait de préserver convenablement les inversions du champ magnétique terrestre. A l'inverse, nous montrons que les anomalies magnétiques associées aux changements de polarité ne sont plus clairement identifiables à l'aplomb des zones de manteau exhumé. Nous montrons également, via une modélisation directe des anomalies magnétiques que ni une aimantation induite ni un modèle d'accrétion océanique ne permettent d'expliquer le signal magnétique observé à l'aplomb de ces zones. De plus, à travers l'étude des propriétés magnétiques des échantillons dragués, nous montrons que les péridotites serpentinisées sont des sources magnétiques instables. A l'inverse des basaltes, elles peuvent présenter une forte susceptibilité magnétique et leur aimantation rémanente n'est pas nécessairement dominante. Finalement, l'absence d'anomalie axiale à l'aplomb des zones de manteau exhumé et l'hétérogénéité du signal magnétique sur une échelle de quelques kilomètres nous permet de conclure que les péridotites serpentinisées ne portent pas une aimantation rémanente suffisamment stable pour être associées à la formation de linéations magnétiques marines. De fait, ces résultats suggèrent que la présence de roches extrusives (et ou intrusives) associée à un minimum d'activité tectonique est requise pour préserver les inversions de polarité à l'aplomb des dorsales océaniques.

4.LE SIGNAL MAGNÉTIQUE ASSOCIÉ À LA TRANSITION CONTINENT OCÉAN DES MARGES IBÉRIE/TERRE-NEUVE : UNE ANOMALIE LIÉE À UNE RUPTURE CONTINENTALE MAGMATIQUE ?

Dans une dernière partie, nous nous sommes intéressés au signal magnétique au niveau de la transition océan-continent des marges Ibérie/Terre-Neuve. Ces deux régions présentent également des zones de manteau exhumé s'étendant sur une centaine de kilomètres. Toutefois, contrairement à ce que l'on observe sur la dorsale Sud-Ouest Indienne, les forages montrent qu'une large portion de ces zones de transition subit un magmatisme de type alcalin complexe et polyphasé alors que le magmatisme de type MORB (Mid Oceanic Ridge Basalt), caractéristique des dorsales océaniques, n'apparaît que dans la partie la plus distale des deux marges. Toutes ces roches magmatiques peuvent présenter une aimantation significative et sont donc des sources potentielles d'anomalies magnétiques. De plus, l'échantillonnage par forage montre qu'elles correspondent à des événements géologiques distincts dont certains sont indépendants d'un processus d'accrétion océanique. Tous ces éléments amènent à questionner l'origine des anomalies magnétiques dans cette région du globe. Dans ce travail nous avons mis en parallèle les données de forages et de sismique avec les données d'anomalies magnétiques. Nous avons montré que l'anomalie J, précédemment interprétée comme la fin de la séquence « M » d'inversions de polarité du Crétacé inférieur était associée à un haut topographique et un épaississement crustal. En s'appuyant ensuite sur les données de forages (ODP site 1277), nous proposons qu'un évènement magmatique à la transition Aptien-Albien ~112Ma (pendant la période magnétique calme du Crétacé 125 à 84 Ma) est à l'origine de la création de cette structure. Lors de cet évènement, la partie distale de la transition est affectée par des sous-plaquages de gabbros. Nous proposons que ces corps sous-plaqués se placent sous le front de serpentinisation et produisent les premiers dikes qui vont traverser le manteau serpentinisé pour s'épancher en surface sous forme de laves. Finalement, grâce à un modèle direct, nous montrons qu'il est possible d'expliquer l'anomalie J sans recourir à des inversions de polarité du champ magnétique mais simplement par un contraste d'aimantation lié à la signature magnétique de ces roches intrusives et extrusives placées dans la partie distale de la marge. Nous proposons finalement que cet évènement magmatique est le déclencheur de la mise en place de la première croûte océanique et donc du passage d'un régime d'exhumation vers un régime d'accrétion focalisé à la dorsale océanique. L'anomalie J n'est donc plus interprétée comme une isochrone mais comme une anomalie liée à un évènement magmatique responsable de la rupture continentale. La datation de cet évènement nous permet finalement de rajeunir l'ouverture de l'Atlantique Nord de 10 Ma par rapport à ce que suggéraient les modèles précédents ce qui pourrait expliquer certaines incohérences dans les précédentes reconstructions cinématiques associées à cette région du globe.

5.IMPLICATIONS SUR L'INTERPRÉTATION DES ANOMALIES MAGNÉTIQUES

Ce travail illustre donc les limites de l'interprétation des anomalies magnétiques en domaine océanique. Le succès du modèle classique d'accrétion océanique et des anomalies magnétiques associées repose essentiellement sur sa validité et son applicabilité à l'échelle du plus grand système volcanique présent sur Terre que sont les dorsales océaniques. Néanmoins, l'écartement des plaques se fait, pour environ 35% de ces dorsales à des vitesses inférieures à 20 cm/a (Dick et al., 2003). Nous montrons que de la même façon que le modèle classique d'accrétion océanique se complexifie pour des vitesses de divergence lentes et ultra-lentes, la lisibilité des anomalies magnétiques associées en est affectée. Les dorsales à taux lents et ultra-lents subissent des déficits locaux de magmatisme caractérisés par de larges portions a-magmatiques (e.g. partie Est de la dorsale Sud-Ouest Indienne, au-delà de 60°E) ou par la focalisation du magmatisme (e.g. dorsale Sud-Ouest Indienne vers 55°E ; Sauter et al., 2004). Dans les deux cas, il en résulte une couche de roches extrusives et intrusives d'épaisseur faible voir inexistante dans certaines zones (e.g. les discontinuités axiales) par rapport aux dorsales à taux d'accrétion plus rapides. L'absence d'anomalies magnétiques d'accrétion océanique associées à l'exhumation de roches mantelliques que nous illustrons dans ce travail se retrouve également en extrémité de segment, vers 55°E de la dorsale Sud-Ouest Indienne (Figure 1 ; Sauter et al., 2004). Dans cette région, l'épaisseur de croûte (déduite de la RMBA) se corrèle relativement bien avec les valeurs d'aimantation. L'activité magmatique est maximale au centre de segment, elle est caractérisée par une forte épaisseur de croûte, une forte aimantation et des linéations magnétiques bien marquées. A l'inverse, les extrémités de segments présentent une faible épaisseur de croûte associée à une aimantation de faible amplitude et de faible continuité spatiale (Figure 1).

Un signal magnétique aussi hétérogène est observé dans la partie centrale de la dorsale médio-atlantique (15°N ; 2,5 cm/a ; Mallows, 2011). Ce signal est associé à un mode d'accrétion complexe combinant failles de détachement et volcanisme (Figure 2). A cet endroit, l'hétérogénéité lithologique crustale se traduit par une hétérogénéité du signal magnétique. De fait, l'hypothèse d'une accrétion crustale deux dimensions proposée dans le modèle classique d'accrétion océanique ne semble plus vérifiée.

Comme les données que nous présentons dans ce travail, ces deux exemples suggèrent qu'une accrétion crustale caractérisée par la mise en place de roches intrusives et extrusives et associée à un une activité tectonique limitée est requise pour préserver l'enregistrement de la polarité du champ magnétique à travers la croûte océanique.

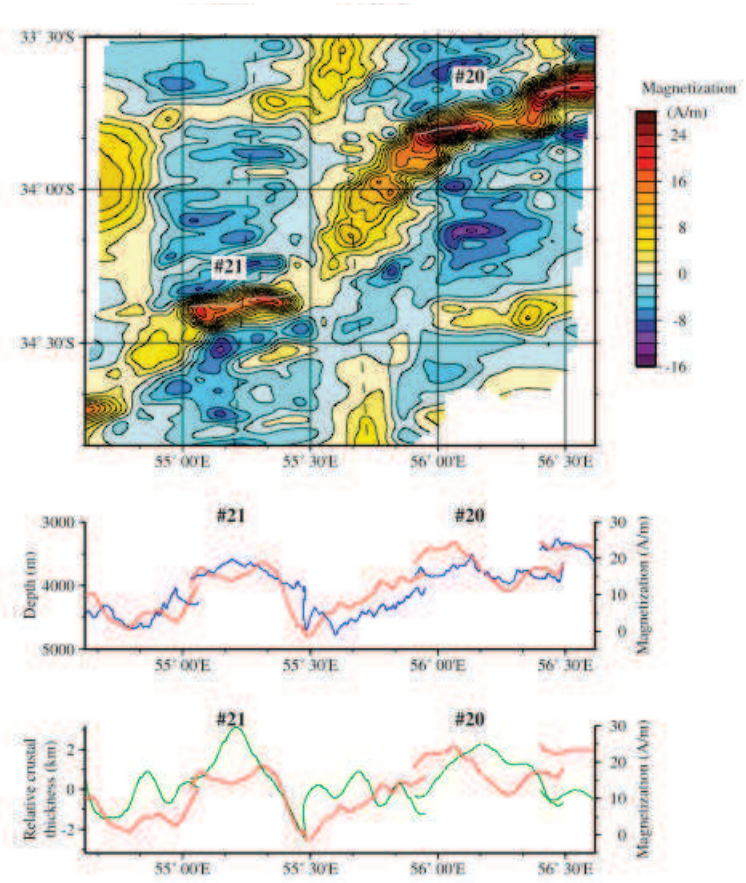

Figure 1 : Carte d'aimantation déduite de données magnétiques acquises au niveau de la mer à l'aplomb des segments 20 et 21 de la dorsale Sud-Ouest Indienne (54°40'E à 56°30'E). Les profils représentent la variation d'aimantation (rouge) en fonction de la bathymétrie et de l'épaisseur relative de la croûte (déduite de la RMBA) le long de l'axe d'accrétion. D'après Sauter et al. (2004).

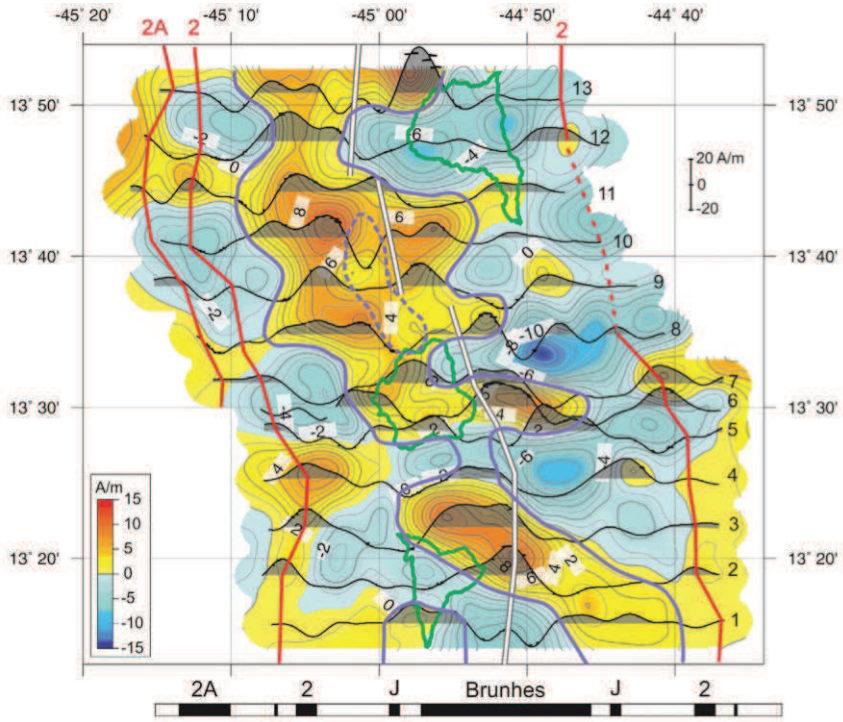

Figure 2 : Aimantation de la croûte océanique déduite d'une inversion 2D et 3D de données acquises proche du fond, à la dorsale médio-atlantique (13°N). La ligne blanche représente l'axe de la dorsale médio-atlantique, les lignes rouges représentent les pointés de l'anomalie 2 et les lignes vertes délimitent les surfaces de détachement. L'échelle d'inversion de polarité est associée à un taux d'ouverture symétrique de 2,6 cm/a. D'après Mallows and Searle (2012).

Dans le cas des marges appauvries en magma, nous avons vu que l'interprétation du signal magnétique à l'aplomb des zones de manteau exhumé est d'autant plus complexe qu'il peut être associé à des événements magmatiques polyphasés. Nous proposons une explication alternative à la présence d'anomalies magnétiques en ces endroits du globe. Notre modèle suggère qu'un évènement magmatique soit à l'origine de la rupture continentale et qu'une signature magnétique observée à l'extrémité de la TOC lui est associée. Or, les anomalies magnétiques associées aux nombreuses transitions océan-continent formées de roches mantelliques exhumées ont souvent été interprétées comme des isochrones et utilisées pour contraindre les reconstruction cinématiques. Il a par exemple été proposé d'étendre l'interprétation des anomalies magnétiques jusqu'à l'anomalie M41n à l'aplomb de la zone de transition de la marge centrale du Mozambique (Leinweber et al., 2013). De la même façon l'origine des anomalies magnétiques antérieures à l'anomalie 31 et identifiées à l'aplomb des domaines de transition des marges conjuguées Sud australienne et antarctique reste controversée. Certains attribuent ces anomalies à des inversions de polarité et les utilisent à des fins de reconstruction cinématiques (Whittaker et al., 2007, 2008) alors que d'autres excluent la présence d'une croûte océanique et soutiennent que ces anomalies ne sont pas des isochrones (Tikku and Cande, 1999; Tikku and Direen, 2008). Ces anomalies sont un cas particulièrement intéressant car certains travaux en cours nous montrent, par exemple, que l'anomalie 34 semble être identifiée à l'aplomb de corps magmatiques associés à l'exhumation de roches mantelliques alors que l'anomalie 33 se situe dans la partie la plus distale de la marge, dans ce qui semble être une zone transitionnelle entre le domaine de manteau exhumé et le domaine océanique (Figure 3 ; Gillard et al., 2013). Comme pour les marges Ibérie/Terre-Neuve, ces anomalies pourraient donc être associées à des processus magmatiques et tectoniques complexes et polyphasés.

Au-delà de la problématique des zones de manteau exhumé, on retrouve également des linéations magnétiques difficiles à associer à des inversions de polarité et dont l'origine reste à confirmer. Par exemple, dans certains bassins de l'Atlantique Sud, des anomalies magnétiques sont observées pendant la période calme du Crétacé (e.g. Bassin de Santos ; Stanton et al., 2013). De la même façon, des linéations magnétiques sont observées sur le rift d'Afar, avant l'ouverture océanique (Bridges et al., 2012).

On retrouve également la même problématique dans le cas de marges plus « magmatiques ». Dans l'Atlantique Sud, la première linéation magnétique dite « LMA » (Large Marginal Anomaly) est identifiée dans les parties distales des marges conjuguées associées au segment austral de la dorsale médio-atlantique. Contrairement à une isochrone, cette anomalie présente une forte amplitude et une longueur d'onde très variable (Moulin et al., 2010 ;Figure 4). Certains auteurs l'ont d'abord interprétée comme un effet de bord entre le socle océanique et continental (Rabinowitz, 1976). Puis d'autres ont pu l'associer à la présence de SDRs (Sea Dipping Reflectors ; Franke et al., 2006; Hinz et al., 1999). Par la suite cette anomalie a été utilisée à des fin de reconstructions cinématiques

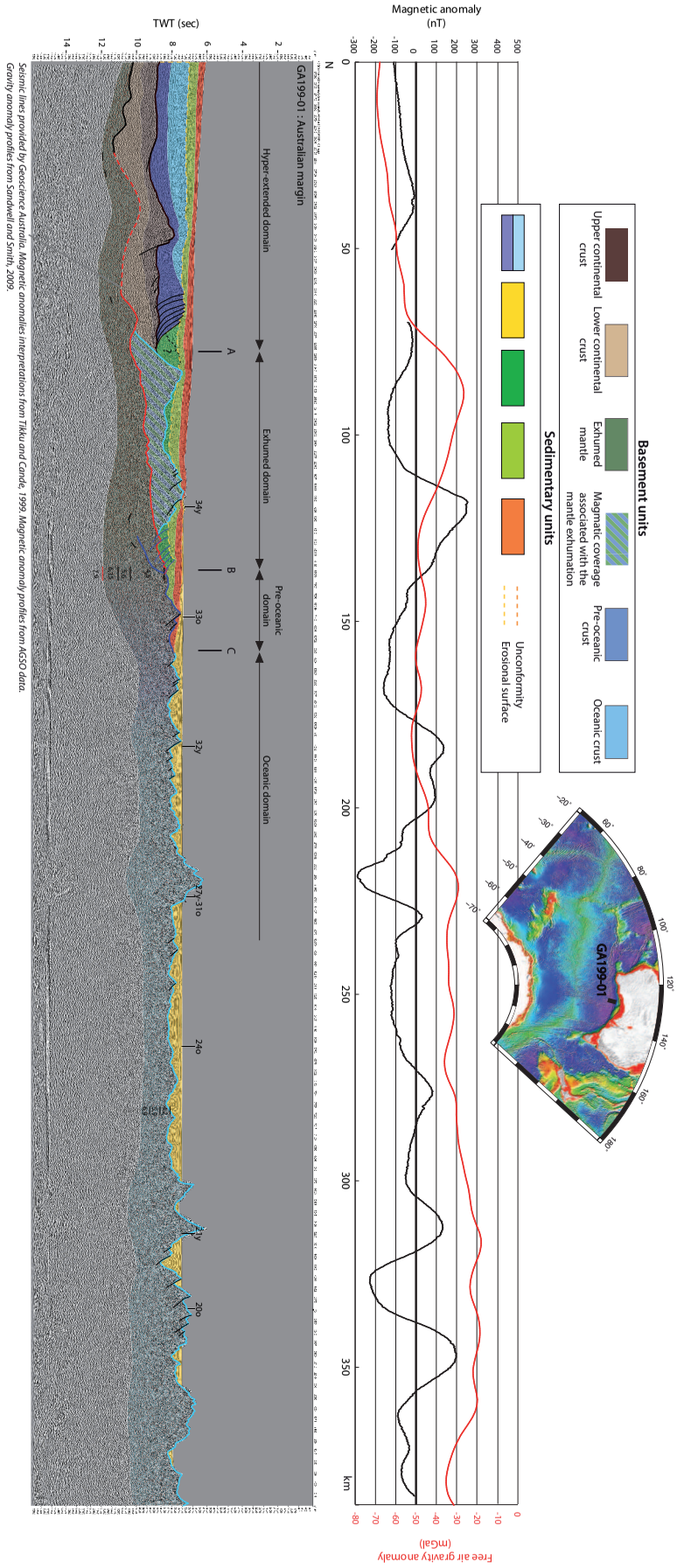

Figure 3 : Interprétation du profil de sismique réflexion GA199-01 de la marge Sud australienne et profils magnétique et gravimétrique associés. Le pointé des anomalies magnétiques est d'après Tikku and Cande (1999). Figure et interprétations d'après Gillard et al. (2013).

(Moulin et al., 2010), reconstructions dont la validité reste débattue (Aslanian and Moulin, 2010; Moulin et al., 2010; Torsvik et al., 2009; Torsvik et al., 2010). Ainsi, comme pour les marges Ibérie/Terre-Neuve, on peut pas exclure que cette anomalie soit la signature d'un évènement magmatique responsable de l'ouverture de l'Atlantique Sud (Franke, 2013).

Notre travail a donc des implications à la fois sur les reconstructions cinématiques fines aux dorsales lentes et ultra-lentes et sur l'interprétation des linéations magnétiques observées dans les zones de rifting. S'il suggère d'aborder avec prudence l'interprétation des anomalies magnétiques associées aux marges passives, il pourrait également permettre de mieux comprendre le mécanisme de rupture continentale, tant du point de vue de son timing que des processus qui lui sont associés. Il n'existe pas actuellement de données permettant de confirmer ou d'infirmer clairement la présence de sous plaquages de gabbros sous la croûte de serpentine formant les parties distales des marges Ibérie/Terre-Neuve. L'idée d'une anomalie magnétique résultante d'un processus magmatique précurseur de l'océanisation doit donc être testée à d'autres endroits du globe.

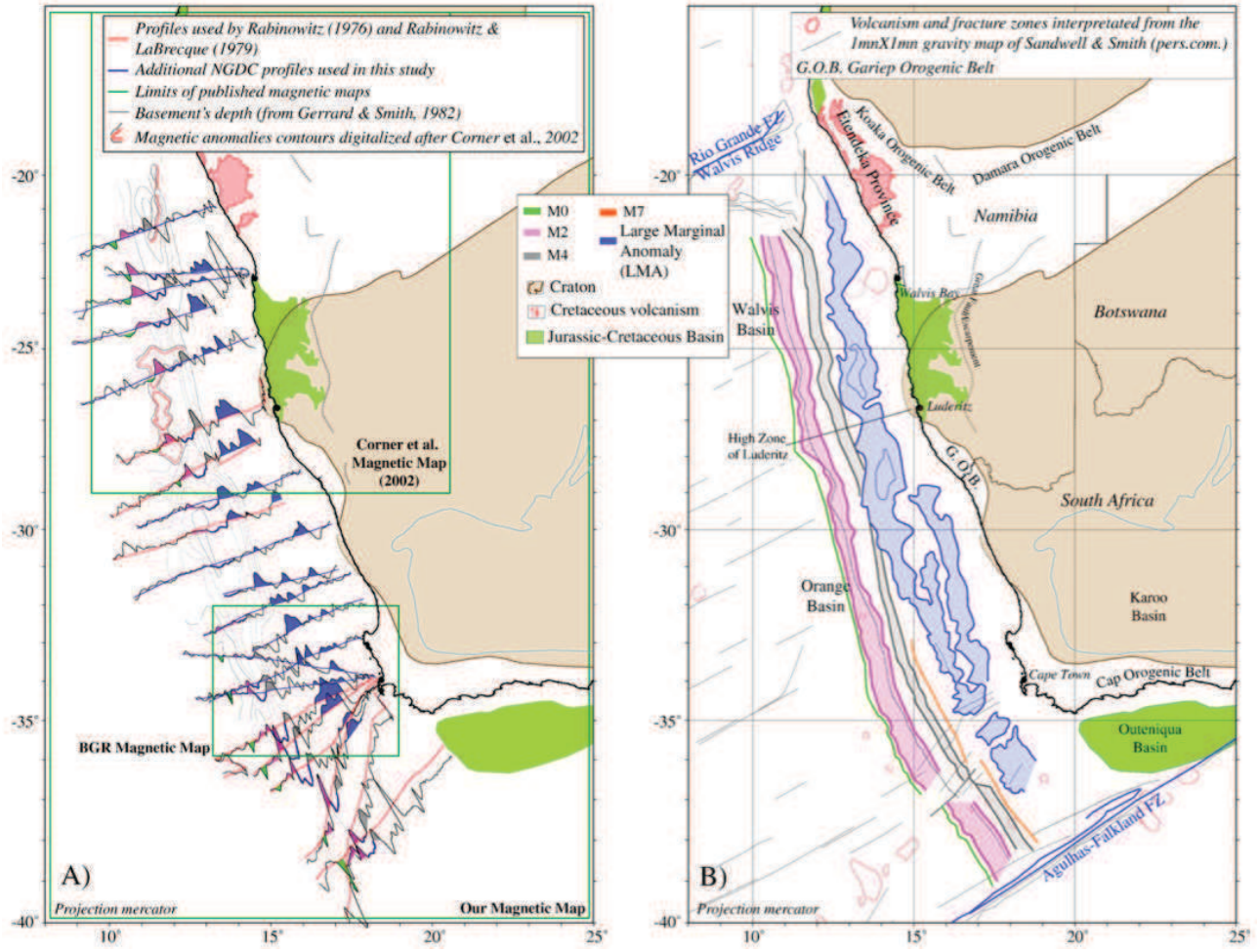

Figure 4 : Large Marginal Anomaly (LMA) observée au large de l'Afrique du Sud. Contrairement aux autres isochrones observées dans cette région, cette anomalie est de forte amplitude et de longueur d'onde variable. D'après Moulin et al. (2010)

A l'heure actuelle, la problématique liée à l'interprétation des anomalies magnétiques de « bordure » de marge est principalement mise en lumière par certaines incohérences liées aux reconstructions cinématiques. En effet, la première linéation observée dans la partie distale des marges est souvent associées au début de l'accrétion océanique et utilisée pour contraindre les reconstructions cinématiques. Peu de travaux tentent d'associer le signal magnétique à la nature des roches qui forment la croûte sous-jacente, faute d'arguments géologiques. Il s'avère donc intéressant de mettre en parallèle les interprétations géologiques des données de sismique avec les profils d'anomalies magnétiques disponibles. Par exemple Blaich et al. (2011) mettent ainsi clairement en évidence, la correspondance entre la LMA et la présence de SDR.

Nous proposons la démarche suivante pour l'étude des anomalies magnétiques de bordure de marge dont l'origine est controversée :

(1) Sélectionner les données de sismique disponibles et les profils et carte d'anomalie magnétique associés.

(2) Tester la présence de structures potentiellement porteuses d'une aimantation significative telles que les « SDRs » ou le « outer high » (sismique réflexion) ou encore un épaississement crustal (sismique réfraction).

(3) Vérifier si ces structures sont associées à une ou plusieurs anomalies magnétiques.

(4) Tester la contribution de ces structures à l'aide d'un modèle direct ou d'autre méthodes magnétiques (inversions, signal analytique etc.).

BIBLIOGRAPHIE

Anderson, R. N., Honnorez, J., Becker, K., Adamson, A. C., Alt, J. C., Emmermann, R., Kempton, P. D., Kinoshita, H., Laverne, C., Mottl, M. J., and Newmark, R. L., 1982, DSDP Hole 504B, the first reference section over 1 km through Layer 2 of the oceanic crust: Nature, 300, 589-594.

Anonymous, 1972, Penrose field conference on ophiolites: Geotimes, 17, 24-25.

Aslanian, D., and Moulin, M., 2010, Comment on 'A new scheme for the opening of the South Atlantic Ocean and the dissection of an Aptian salt basin'by Trond H. Torsvik, Sonia Rousse, Cinthia Labails and Mark A. Smethurst: Geophysical Journal International, 183, 20-28.

Bell, R. E., and Buck, W. R., 1992, Crustal control of ridge segmentation inferred from observations of the Reykjanes Ridge: Nature, 357, 583-586.

Blaich, O. A., Faleide, J. I., and Tsikalas, F., 2011, Crustal breakup and continent-ocean transition at South Atlantic conjugate margins: Journal of Geophysical Research: Solid Earth, 116, B01402.

Boillot, G., Grimaud, S., Mauffret, A., Mougenot, D., Kornprobst, J., Mergoil-Daniel, J., and Torrent, G., 1980, Ocean-continent boundary off the Iberian margin: a serpentinite diapir west of the Galicia Bank: Earth and Planetary Science letters, 48, 23-34.

Bown, J. W., and White, R. S., 1994, Variation with spreading rate of oceanic crustal thickness and geochemistry: Earth and Planetary Science letters, 121, 435-449.

Bridges, D. L., Mickus, K., Gao, S. S., Abdelsalam, M. G., and Alemu, A., 2012, Magnetic stripes of a transitional continental rift in Afar: Geology, 40, 203-206.

Bronner, A., Sauter, D., Manatschal, G., Peron-Pinvidic, G., and Munschy, M., 2011, Magmatic breakup as an explanation for magnetic anomalies at magma-poor rifted margins: Nature Geosci, 4, 549-553.

Bronner, A., Sauter, D., Manatschal, G., Peron-Pinvidic, G., and Munschy, M., 2012, Reply to 'Problematic plate reconstruction': Nature Geoscience, 5, 677-677.

Bronner, A., Munschy, M., Sauter, D., Carlut, J., Searle, R., and Maineult, A., 2013, Deep-tow 3C magnetic measurement: Solutions for calibration and interpretation: Geophysics, 78, J15-J23.

Buck, W. R., Lavier, L. L., and Poliakov, A. N. B., 2005, Modes of faulting at mid-ocean ridges: Nature, 434, 719-723.

Bullard, E., and Manson, R., 1963, The magnetic field over the ocean: The Sea, 3, 175-217.

Cande, S. C., and Kent, D. V., 1992, A new geomagnetic polarity time scale for the Late Cretaceous and Cenozoic: Journal of Geophysical Research. Res., 97, 13917-13951.

Cande, S. C., and Kent, D. V., 1995, Revised calibration of the geomagnetic polarity timescale for the Late Cretaceous and Cenozoic: Journal of Geophysical Research, 100, 6093-6095.

Cann, J. R., 1979, Metamorphism in the ocean crust, Deep Drilling Results in the Atlantic Ocean: Ocean Crust, Volume 2: Washington, DC, AGU, p. 230-238.

Cann, J. R., Blackman, D. K., Smith, D. K., McAllister, E., Janssen, B., Mello, S., Avgerinos, E., Pascoe, A. R., and Escartin, J., 1997, Corrugated slip surfaces formed at ridge-transform intersections on the Mid-Atlantic Ridge: Nature, 385, 329-332.

Cannat, M., Bideau, D., and Bougault, H., 1992, Serpentinized peridotites and gabbros in the Mid-Atlantic Ridge axial valley at 15°37'N and 16°52'N: Earth and Planetary Science Letters, 109, 87-106.

Cannat, M., Mevel, C., Maia, M., Deplus, C., Durand, C., Gente, P., Agrinier, P., Belarouchi, A., Dubuisson, G., Humler, E., and Reynolds, J., 1995, Thin crust, ultramafic exposures, and rugged faulting patterns at the Mid-Atlantic Ridge (22°–24°N): Geology, 23, 49-52.

Cannat, M., Lagabrielle, Y., Bougault, H., Casey, J., de Coutures, N., Dmitriev, L., and Fouquet, Y., 1997, Ultramafic and gabbroic exposures at the Mid-Atlantic Ridge: geological mapping in the 15°N region: Tectonophysics, 279, 193-213.

Cannat, M., Rommevaux-Jestin, C., Sauter, D., Deplus, C., and Mendel, V., 1999, Formation of the axial relief at the very slow spreading Southwest Indian Ridge (49°-69°E): Journal of Geophysical Research, 104, 22825-22843.

Cannat, M., Sauter, D., Mendel, V., Ruellan, E., Okino, K., Escartin, J., Combier, V., and Baala, M., 2006, Modes of seafloor generation at a melt-poor ultraslow-spreading ridge: Geology, 34, 605-608.

Cannat, M., Sauter, D., Bezos, A., Meyzen, C., Humler, E., and Le Rigoleur, M., 2008, Spreading rate, spreading obliquity, and melt supply at the ultraslow spreading Southwest Indian Ridge: Geochemistry, Geophysics, Geosystems, 9, Q04002, Doi 10.1029/2007gc001676.

Cannat, M., Manatschal, G., Sauter, D., and Peron-Pinvidic, G., 2009, Assessing the conditions of continental breakup at magma-poor rifted margins: What can we learn from slow spreading mid-ocean ridges?: Comptes Rendus Geosciences, 341, 394-405

Chian, D., Louden, K. E., Minshull, T. A., and Whitmarsh, R. B., 1999, Deep structure of the ocean-continent transition in the southern Iberia Abyssal Plain from seismic refraction profiles:Ocean Drillng Program (Legs 149 and 173) transect: Journal of Geophysical Research, 104, 7443-7462.

Dampney, C., 1969, The equivalent source technique: Geophysics, 34, 39.

Dean, S. M., Minshull, T. A., Whitmarsh, R. B., and Louden, K. E., 2000, Deep structure of the ocean-continent transition in the southern Iberia Abyssal Plain from seismic refraction profiles: The IAM-9 transect at 40°20'N: Journal of Geophysical Research, 105, 5859-5885.

Dean, S. M., Minshull, T. A., and Whitmarsh, R. B., 2008, Seismic constraints on the three-dimensional geometry of low-angle intracrustal reflectors in the Southern Iberia Abyssal Plain: Geophysical Journal International, 175, 571-586.

Dick, H. J. B., Natland, J. H., Alt, J. C., Bach, W., Bideau, D., Gee, J. S., Haggas, S., Hertogen, J. G. H., Hirth, G., Holm, P. M., Ildefonse, B., Iturrino, G. J., John, B. E., Kelley, D. S., Kikawa, E., Kindom, A., LeRoux, P. J., Maeda, J., Meyer, P. S., Miller, D. J., Naslund, H. R., Niu, Y.-L., Robinson, P. T., Snow, J., Stephen, R. A., Trimby, P. W., Worm, H.-U., and Yoshinobu, A. S., 2000, A long in situ section of the lower oceanic crust: results of ODP leg 176 drilling at the Southwest Indian Ridge: Earth and Planetary Science Letters, 179, 31-51.

Dick, H. J. B., Lin, J., and Schouten, H., 2003, An ultraslow-spreading class of ocean ridge: Nature, 426, 405-412.

Dietz, R. S., 1962, Ocean-basin evolution by sea-floor spreading, The Crust of the Pacific Basin, Volume 6: Washington, DC, AGU, p. 11-12.

Engels, M., Barckhausen, U., and Gee, J. S., 2008, A new towed marine vector magnetometer: methods and results from a Central Pacific cruise: Geophysical Journal International, 172, 115-129.

Flewellen, C., Millard, N., and Rouse, I., 1993, TOBI, a vehicle for deep ocean survey: Electronics & communication engineering journal, 5, 85-93.

Franke, D., Neben, S., Schreckenberger, B., Schulze, A., Stiller, M., and Krawczyk, C. M., 2006, Crustal structure across the Colorado Basin, offshore Argentina: Geophysical Journal International, 165, 850-864.

Franke, D., 2013, Rifting, lithosphere breakup and volcanism: Comparison of magma-poor and volcanic rifted margins: Marine and Petroleum Geology, 43, 63-87.

Funck, T., Hopper, J. R., Larsen, H. C., Louden, K. E., Tucholke, B. E., and Holbrook, W. S., 2003, Crustal structure of the ocean-continent transition at Flemish Cap: Seismic refraction results: Journal of Geophysical Research, 108, 2531.

Gee, J. S., and Cande, S. C., 2002, A surface-towed vector magnetometer: Geophys. Res. Lett., 29, 1670.

Gee, J. S., and Kent, D. V., 2007, Source of Oceanic Magnetic Anomalies and the Geomagnetic Polarity Timescale, in Schubert, G., ed., Treatise on Geophysics, Volume 5, Elsevier, 455-507.

Geldmacher, J., Hoernle, K., Klügel, A., Bogaard, P. v. d., Wombacher, F., and Berning, B., 2006, Origin and geochemical evolution of the Madeira-Tore Rise (eastern North Atlantic): Journal of Geophysical Research, 111, B09206.

Georgen, J., and Lin, J., 2003, Plume-transform interations at ultra-slow spreading ridges: implications for the Southwest Indian Ridge: Geochemistry, Geophysics, Geosystems, 4, 9106, doi:9110.1029/2003GC000542.

Georgen, J. E., Lin, J., and Dick, H. J. B., 2001, Evidence from gravity anomalies for interactions of the Marion and Bouvet hotspots with the Southwest Indian Ridge: effects of transform offsets: Earth and Planetary Science Letters, 187, 283-300.

Gillard, M., Autin, J., Karpoff, A. M., Manatschal, G., Munschy, M., Sauter, D., and Schaming, M., Unravelling the process of continental breakup: a case study of the Australia-Antarctica conjugate margins, in Proceedings EGU, Vienna, 2013.

Gong, Z., Langereis, C. G., and Mullender, T. A. T., 2008, The rotation of Iberia during the Aptian and the opening of the Bay of Biscay: Earth and Planetary Science Letters, 273, 80-93.

Guspi, F., 1987, Frequency-domain reduction of potential field measurements to a horizontal plane* 1: Geoexploration, 24, 87-98.

Harrison, C., 1987, Marine magnetic anomalies-The origin of the stripes: Annual Review of Earth and Planetary Sciences, 15, 505-543.

Hart, S. R., and Blusztajn, J., 2006, Age and geochemistry of the mafic sills, ODP site 1276, Newfoundland margin: Chemical Geology, 235, 222-237.

Heirtzler, J. R., Dickson, G. O., Herron, E. M., Pitman, W. C., and Le Pichon, X., 1968, Marine magnetic anomalies, geomagnetic field reversals, and motions of the ocean floor and continents: Journal of Geophysical Research, 73, 2119-2136.

Hinz, K., Neben, S., Schreckenberger, B., Roeser, H. A., Block, M., Souza, K. G. d., and Meyer, H., 1999, The Argentine continental margin north of 48°S: sedimentary successions, volcanic activity during breakup: Marine and Petroleum Geology, 16, 1-25.

Hopper, J. R., Funck, T., Tucholke, B. E., Larsen, H. C., Louden, K. E., Shilington, D., and Lau, H., 2004, Continental breakup and the onset of ultraslow seafloor spreading off Flemish Cap on the Newfoundland rifted margin: Geology, 32, 93–96.

Hopper, J. R., Funck, T., and Tucholke, B. E., 2007, Structure of the Flemish Cap margin, Newfoundland: insights into mantle and crustal processes during continental breakup: Geological Society, London, Special Publications, 282, 47-61.

Hosford, A., Tivey, M., Matsumoto, T., Dick, H., Schouten, H., and Kinoshita, H., 2003, Crustal magnetization and accretion at the Southwest Indian Ridge near the Atlantis II fracture zone, 0–25 Ma: Journal of Geophysical Research: Solid Earth, 108, 2169.

Hussenoeder, S. A., Tivey, M. A., and Schouten, H., 1995, Direct inversion of potential fields from an uneven track with application to the Mid-Atlantic Ridge: Geophys. Res. Lett., 22, 3131-3134.

Isezaki, N., 1986, A new shipboard three-component magnetometer: Geophysics, 51, 1992-1998.

Jagoutz, O., Muntener, O., Manatschal, G., Rubatto, D., Peron-Pinvidic, G., Turrin, B. D., and Villa, I. M., 2007, The rift-to-drift transition in the North Atlantic: A stuttering start of the MORB machine?: Geology, 35, 1087-1090.

Jammes, S., Manatschal, G., Lavier, L., and Masini, E., 2009, Tectonosedimentary evolution related to extreme crustal thinning ahead of a propagating ocean: Example of the western Pyrenees: Tectonics, 28, doi: 10.1029/2008tc002406.

Karson, J. A., Thompson, G., Humphris, S. E., Edmon, J. M., Bryan, W. B., Brown, J. B., Winters, A. T., Pockalny, R. A., Casey, J. F., Campbell, A. C., Klinkhammer, G. P., Palmer, M. R., Kinzler, R. J., and Sulanowska, M. M., 1987, Along-axis variations in seafloor spreading in the MARK Area: Nature, 328, 681-685.

Kato, H., Isezaki, N., Park, C. H., Kim, C. H., and Nakanishi, M., 2007, Characteristics of crustal magnetic structures in the Tsushima (Ulleung) and Japan Basins from vector magnetic anomalies: Earth Planets and Space, 59, 887-895.

Kikawa, E., and Pariso, J. E., 1991, Magnetic properties of gabbros from hole 735B, Southwest Indian Ridge, in Herzen, R. P. V., and Robinson, P. T., eds., Proceedings of the Ocean Drilling Program, Scientific Results, Volume 118: College Station, TX, Ocean Drilling Program, p. 285-307.

Korenaga, J., 1995, Comprehensive analysis of marine magnetic vector anomalies: J. Geophys. Res., 100, 365-378.

Lau, K. W. H., Louden, K. E., Funck, T., Tucholke, B. E., Holbrook, W. S., Hopper, J. R., and Larsen, H. C., 2006, Crustal structure across the Grand Banks-Newfoundland Basin Continental Margin- I. Results from a seismic refraction profile: Geophysical Journal International, 167, 127-156.

Leinweber, V. T., Klingelhoefer, F., Neben, S., Reichert, C., Aslanian, D., Matias, L., Heyde, I., Schreckenberger, B., and Jokat, W., 2013, The crustal structure of the Central Mozambique continental margin – wide-angle seismic, gravity and magnetic study in the Mozambique Channel, Eastern Africa: Tectonophysics, 599, 170-196.

Leliak, P., 1961, Identification and Evaluation of Magnetic-Field Sources of Magnetic Airborne Detector Equipped Aircraft: Aerospace and Navigational Electronics, 95-105.

Lin, J., Purdy, G. M., Schouten, H., Sempere, J. C., and Zervas, C., 1990, Evidence from gravity data for focused magmatic accretion along the Mid-Atlantic Ridge: Nature, 344, 627-632.

Macdonald, K. C., 1989, Anatomy of the magma reservoir: Nature, 339, 178-179.

Mallows, 2011, Geophysical Studies of Oceanic Core Complexes: The Mid-Atlantic Ridge, 13 - 14°N Doctoral thesis]: Durham University.

Mallows, C., and Searle, R. C., 2012, A geophysical study of oceanic core complexes and surrounding terrain, Mid-Atlantic Ridge 13°N–14°N: Geochemistry, Geophysics, Geosystems, 13, Q0AG08, doi: 10.1029/2012gc004075.

Marshall, M., and Cox, A., 1971, Magnetism of Pillow Basalts and Their Petrology: Geological Society of America Bulletin, 82, 537-552.

McKenzie, D., 1978, Some remarks on the development of sedimentary basins: Earth and Planetary Science letters, 40, 25-32.

Mendel, V., Munschy, M., and Sauter, D., 2005, MODMAG, a MATLAB program to model marine magnetic anomalies: Computers & Geosciences, 31, 589-597.

Merayo, J. M. G., Brauer, P., Primdahl, F., Petersen, J. R., and Nielsen, O. V., 2000, Scalar calibration of vector magnetometers: Measurement Science and Technology, 11, 120-132.

Merle, R., Jourdan, F., Marzoli, A., Renne, P. R., Grange, M., and Girardeau, J., 2009, Evidence of multi-phase Cretaceous to Quaternary alkaline magmatism on Tore-Madeira Rise and neighbouring seamounts from 40Ar/39Ar ages: Journal of the Geological Society, 166, 879-994.

Meyzen, C. M., Toplis, M. J., Humler, E., Ludden, J. N., and Mevel, C., 2003, A discontinuity in mantle composition beneath the southwest Indian ridge: Nature, 421, 731-733.

Miles, P. R., Verhoef, J., and Macnab, R., 1996, Compilation of magnetic anomaly chart west of Iberia: Proceedings of the Ocean Drilling Program, Scientific Results, 149, 659-663.

Miller, D. J., and Christensen, N. I., 1997, Seismic velocities of lower crustal and upper mantle rocks from the slow-spreading mid-Atlantic ridge, south of the Kane Transform zone (MARK): Proceedings of the Ocean Drilling Program, Scientific Results, 153, 437-454.

Minshull, T. A., Muller, M. R., Robinson, C. J., White, R. S., and Bickle, M. J., 1998, Is the oceanic Moho a serpentinization front?: Geological Society, London, Special Publications, 148, 71-80.

Minshull, T. A., Muller, M. R., and White, R. S., 2006, Crustal structure of the Southwest Indian Ridge at 66°E: Seismic constraints: Geophysical Journal International, 166, 135-147.

Minshull, T. A., 2009, Geophysical characterisation of the ocean-continent transition at magma-poor rifted margins: Comptes Rendus Geosciences, 341, 382-393

Moulin, M., Aslanian, D., and Unternehr, P., 2010, A new starting point for the South and Equatorial Atlantic Ocean: Earth-Science Reviews, 98, 1-37.

Müller, R. D., Royer, J.-Y., and Lawver, L. A., 1993, Revised plate motions relative to the hotspots from combined Atlantic and Indian Ocean hotspot tracks: Geology, 21, 275-278.

Müller, R. D., Sdrolias, M., Gaina, C., and Roest, W. R., 2008, Age, spreading rates, and spreading asymmetry of the world's ocean crust: Geochemistry, Geophysics, Geosystems, 9, Q04006, doi: 10.1029/2007gc001743.

Munschy, M., Boulanger, D., Ulrich, P., and Bouiflane, M., 2007, Magnetic mapping for the detection and characterization of UXO: Use of multi-sensor fluxgate 3-axis magnetometers and methods of interpretation: Journal of Applied Geophysics, 61, 168-183.

Müntener, O., and Manatschal, G., 2006, High degrees of melt extraction recorded by spinel harzburgite of the Newfoundland margin: The role of inheritance and consequences for the evolution of the southern North Atlantic: Earth and Planetary Science letters, 252, 437-452.

Ogg, J. G., and Smith, A. G., 2004, The geomagnetic polarity time scale in Gradstein, F. M., Ogg, J. G., and Smith, A. G., eds., A Geological Time Scale 2004, Cambridge University Press, p. 63-86.

Olive, J.-A., Behn, M. D., and Tucholke, B. E., 2010, The structure of oceanic core complexes controlled by the depth distribution of magma emplacement: Nature Geosci, 3, 491-495.

Olsen, N., Risbo, T., Brauer, P., Merayo, J., Primdahl, F., and Sabaka, T., 2001, In-flight calibration methods used for the Ø rsted mission: ESA SP on Space Magnetometer Calibration, ESA SP-490

Oufi, O., Cannat, M., and Horen, H., 2002, Magnetic properties of variably serpentinized abyssal peridotites: Journal of Geophysical Research, 107.

Pariso, J. E., and Johnson, H. P., 1991, Alteration processes at Deep Sea Drilling Project/Ocean Drilling Program Hole 504B at the Costa Rica Rift: Implications for magnetization of oceanic crust: Journal of Geophysical Research: Solid Earth, 96, 11703-11722.

Pariso, J. E., and Johnson, H. P., 1993, Do layer 3 rocks make a significant contribution to marine magnetic anomalies? In situ magnetization of gabbros at Ocean Drilling Program hole 735 B: Journal of Geophysical Research, 98, 16033-16052.

Pariso, J. E., Stokking, L., and Allerton, S., Rock magnetism and magnetic mineralogy of a 1-km section of sheeted dikes, Hole 504B1, in Proceedings Proceedings of the Ocean Drilling Program, Scientific Results1995, Volume 137, 253-262

Patriat, P., Sauter, D., Munschy, M., and Parson, L., 1997, A Survey of the Southwest Indian Ridge Axis Between Atlantis II Fracture Zone and the Indian Ocean Triple Junction: Regional Setting and Large Scale Segmentation: Marine Geophysical Researches, 19, 457-480.

Patriat, P., Sloan, H., and Sauter, D., 2008, From slow to ultraslow: a previously undetected event at the Southwest Indian Ridge at ca. 24 Ma: Geology, 36, 207-210.

Peirce, C., and Barton, P. J., 1991, Crustal structure of the Madeira-Tore Rise, eastern North Atlantic - results of a DOBS wide-angle and normal incidence seismic experiment in the Josephine Seamount region: Geophysical Journal International, 106, 357-378.

Péron-Pinvidic, G., Manatschal, G., Minshull, T. A., and Sawyer, D. S., 2007, Tectonosedimentary evolution of the deep Iberia-Newfoundland margins: Evidence for a complex breakup history: Tectonics, 26, TC2011.

Péron-Pinvidic, G., and Manatschal, G., 2008, The final rifting evolution at deep magma-poor passive margins from Iberia-Newfoundland: a new point of view: International Journal of Earth Sciences, 98, 1581-1597

Peron-Pinvidic, G., Shillington, D. J., and Tucholke, B. E., 2010, Characterization of sills associated with the U reflection on the Newfoundland margin: evidence for widespread early post-rift magmatism on a magma-poor rifted margin: Geophysical Journal International, 182, 113-136.

Phipps Morgan, J., and Chen, Y. J., 1993, Dependence of ridge-axis morphology on magma supply and spreading rate: Nature, 364, 706-708.

Pilkington, M., and Urquhart, W., 1990, Reduction of potential field data to a horizontal plane: Geophysics, 55, 549-555.

Quesnel, Y., Catalan, M., and Ishihara, T., 2009, A new global marine magnetic anomaly data set: Journal of Geophysical Research, 114.

Rabinowitz, P. D., 1976, Geophysical study of the continental margin of southern Africa: Geological Society of America Bulletin, 87, 1643-1653.

Rabinowitz, P. D., Cande, S. C., and Hayes, D. E., 1978, Grand Banks and J-Anomaly ridge: Science, 202, 71-73.

Rabinowitz, P. D., Cande, S. C., and Hayes, D. E., 1979, The J-Anomaly in the Central North Atlantic Ocean, in Tucholke, B. E., and Vogt, P. R., eds., Initial report of the Deep Sea Drilling Project, Volume 43: Washington, U.S. Government Printing Office, p. 879-885.

Raitt, R. W., 1963, The crustal rocks: The Sea, 3, 85-102.

Reid, I., and Jackson, H. R., 1981, Oceanic spreading rate and crustal thickness: Marine Geophysical Researches, 5, 165-172.

Reston, T. J., and Morgan, J. P., 2004, Continental geotherm and the evolution of rifted margins: Geology, 32, 133-136.

Reston, T. J., and McDermott, K. G., 2011, Successive detachment faults and mantle unroofing at magma-poor rifted margins: Geology, 39, 1071-1074.

Russell, S. M., and Whitmarsh, R. B., 2003, Magmatism at the west Iberia non-volcanic rifted continental margin: evidence from analyses of magnetic anomalies: Geophysical Journal International, 154, 706-730.

Sato, T., Okino, K., and Kumagai, H., 2009, Magnetic structure of an oceanic core complex at the southernmost Central Indian Ridge: Analysis of shipboard and deep-sea three-component magnetometer data: Geochemistry, Geophysics, Geosystems, 10, Q06003, doi: 10.1029/2008GC002267.

Sauter, D., Carton, H., Mendel, V., Munschy, M., Rommevaux-Jestin, C., Schott, J.-J., and Whitechurch, H., 2004, Ridge segmentation and the magnetic structure of the Southwest Indian Ridge (at 55°30’E, 55°30’E and 66°20’E): implications for magmatic processes at ultraslow-spreading centers: Geochemistry, Geophysics, Geosystems, 5, Q05K08, doi:10.1029/2003GC000581.

Sauter, D., Cannat, M., and Mendel, V., 2008, Magnetization of 0-26.5 Ma seafloor at the ultraslow spreading Southwest Indian Ridge 61-67°E: Geochemistry, Geophysics, Geosystems, 9, Q04023, doi:10.1029/2007GC001764.

Sauter, D., Cannat, M., Roumejon, S., Andreani, M., Birot, D., Bronner, A., Brunelli, D., Carlut, J., Delacour, A., Guyader, V., MacLeod, C. J., Manatschal, G., Mendel, V., Menez, B., Pasini, V., Ruellan, E., and Searle, R., 2013, Continuous exhumation of mantle-derived rocks at the Southwest Indian Ridge for 11 million years: Nature Geoscience, 6, 314-320.

Sauter, D., Sloan, H., Cannat, M., Goff, J., Patriat, P., Schaming, M., and Roest, W. R., 2011, From slow to ultra-slow: How does spreading rate affect seafloor roughness and crustal thickness?: Geology, 39, 911-914.

Seama, N., Nogi, Y., and Isezaki, N., 1993, A New Method For Precise Determination of the Position and Strike of Magnetic Boundaries Using Vector Data of the Geomagnetic Anomaly Field: Geophysical Journal International, 113, 155-164.

Searle, R. C., and Bralee, A., 2007, Asymmetric generation of oceanic crust at the ultra-slow spreading Southwest Indian Ridge, 64°E: Geochemistry, Geophysics, Geosystems, 8, Q05015, doi:10.1029/2006GC001529.

Searle, R. C., Murton, B. J., Achenbach, K., LeBas, T., Tivey, M., Yeo, I., Cormier, M. H., Carlut, J., Ferreira, P., Mallows, C., Morris, K., Schroth, N., van Calsteren, P., and Waters, C., 2010, Structure and development of an axial volcanic ridge: Mid-Atlantic Ridge, 45°N: Earth and Planetary Science letters, 299, 228-241.

Seyler, M., Cannat, M., and Mevel, C., 2003, Evidence for major-element heterogeneity in the mantle source of abyssal peridotites from the Southwest Indian Ridge (52 degrees to 68 degrees E): Geochemistry Geophysics Geosystems, 4, 9101, doi; 10.1029/2002gc000305.

Shillington, D. J., Holbrook, W. S., Avendonk, H. J. A. V., Tucholke, B. E., Hopper, J. R., Louden, K. E., Larsen, H. C., and Nunes, G. T., 2006, Evidence for asymmetric nonvolcanic rifting and slow incipient oceanic accretion from seismic reflection data on the Newfoundland margin: Journal of Geophysical Research, 111, B09402.

Sibuet, J. C., Srivastava, S. P., and Spakman, W., 2004, Pyrenean orogeny and plate kinematics: J. geophys. Res, 109, B08104.

Sibuet, J. C., Srivastava, S., and Manatschal, G., 2007, Exhumed mantle-forming transitional crust in the Newfoundland-Iberia rift and associated magnetic anomalies: Journal of Geophysical Research: Solid Earth, 112, B06105, 1-23.

Smith, D., 2013, Tectonics: Mantle spread across the sea floor: Nature Geoscience, 6, 247-248.

Souriau, A., Chevrot, S., and Olivera, C., 2008, A new tomographic image of the Pyrenean lithosphere from teleseismic data: Tectonophysics, 460, 206-214.

Srivastava, S. P., Roest, W. R., Kovacs, L. C., Oakey, G., Levesque, S., Verhoef, J., and Macnab, R., 1990, Motion of Iberia since the Late Jurassic - Results from Detailed Aeromagnetic Measurements in the Newfoundland Basin: Tectonophysics, 184, 229-260.

Srivastava, S. P., Sibuet, J. C., Cande, S., Roest, W. R., and Reid, I. D., 2000, Magnetic evidence for slow seafloor spreading during the formation of the Newfoundland and Iberian margins: Earth and Planetary Science letters, 182, 61-76.

Stanton, N., Ponte-Neto, C., Masini, E., Bijani, R., Fontes, S., and Flextro, J.-M., 2013, A Geophysical View of the Southeastern Brazilian Margin at Santos Basin: Insights into Rifting Evolution: Sublmitted.

Sullivan, K. D., and Keen, C. E., 1977, Newfoundland seamounts: Petrology and geochemistry, in Baragar, W. R. A., Coleman, L. C., and Hall, J. M., eds., Volcanic Regimes in Canada, Volume 16, Geological Association of Canada Special Paper, p. 462-476.

Tikku, A. A., and Cande, S. C., 1999, The oldest magnetic anomalies in the Australian-Antarctic Basin: Are they isochrons?: Journal of Geophysical Research: Solid Earth, 104, 661-677.

Tikku, A. A., and Direen, N. G., 2008, Comment on "Major Australian-Antarctic Plate Reorganization at Hawaiian-Emperor Bend Time": Science, 321, 490-491.

Tisseau, J., and Patriat, P., 1981, Identification des anomalies magnétiques sur les dorsales à faible taux d'expansion: Méthode des taux fictifs: Earth and Planetary Science letters, 52, 381-396.

Tivey, M. A., Schouten, H., and Kleinrock, M. C., 2003, A near-bottom magnetic survey of the Mid-Atlantic Ridge axis at 26 degrees N: Implications for the tectonic evolution of the TAG segment: Journal of Geophysical Research:Solid Earth, 108, doi: 10.1029/2002jb001967.

Toft, P. B., Arkani-Hamed, J., and Haggerty, S. E., 1990, The effects of serpentinization on density and magnetic susceptibility: a petrophysical model: Physics of the Earth and Planetary Interiors, 65, 137-157.

Torsvik, T. H., Muller, R. D., Van der Voo, R., Steinberger, B., and Gaina, C., 2008, Global plate motion frames: Toward a unified model: Reviews of Geophysics, 46, RG3004, 1-44.

Torsvik, T. H., Rousse, S., Labails, C., and Smethurst, M. A., 2009, A new scheme for the opening of the South Atlantic Ocean and the dissection of an Aptian salt basin: Geophysical Journal International, 177, 1315-1333.

Torsvik, T. H., Rousse, S., and Smethurst, M. A., 2010, Reply to comment by D. Aslanian and M. Moulin on 'A new scheme for the opening of the South Atlantic Ocean and the dissection of an Aptian salt basin': Geophysical Journal International, 183, 29-34.

Tucholke, B. E., and Ludwig, W. J., 1982, Structure and origin of the J anomaly Ridge, western North Atlantic Ocean: Journal of Geophysical Research, 87, 9389-9407.

Tucholke, B. E., Lin, J., and Kleinrock, M. C., 1998, Megamullions and mullion structure defining oceanic metamorphic core complexes on the Mid-Atlantic Ridge: Journal of Geophysical Research B: Solid Earth, 103, 9857-9866.

Tucholke, B. E., Sawyer, D. S., and Sibuet, J.-C., 2007, Breakup of the Newfoundland–Iberia rift: Geological Society, London, Special Publications, 282, 9-46.

Tucholke, B. E., and Sibuet, J.-C., 2007, Leg 210 synthesis: tectonic, magmatic, and sedimentary evolution of the Newfoundland-Iberia rift, in Tucholke, B. E., Sibuet, J.-C., and Klaus, A., eds., Proceedings of the Ocean Drilling Program, Scientific Results, Volume 210: College Station, TX, Ocean Drilling Program, p. 1-56.

Tucholke, B. E., Behn, M. D., Buck, W. R., and Lin, J., 2008, Role of melt supply in oceanic detachment faulting and formation of megamullions: Geology, 36, 455-458.

Tucholke, B. E., and Sibuet, J.-C., 2012, Problematic plate reconstruction: Nature Geosci, 5, 676-677.

Van Avendonk, H. J. A., Holbrook, W. S., Nunes, G. T., Shillington, D. J., Tucholke, B. E., Louden, K. E., Larsen, H. C., and Hopper, J. R., 2006, Seismic velocity structure of the rifted margin of the eastern Grand Banks of Newfoundland, Canada: Journal of Geophysical Research, 111, B11404.

Van Avendonk, H. J. A., Lavier, L. L., Shillington, D. J., and Manatschal, G., 2009, Extension of continental crust at the margin of the eastern Grand Banks, Newfoundland: Tectonophysics, 468, 131-148.

Van der Voo, R., 1990, Phanerozoic paleomagnetic poles from Europe and North America and comparisons with continental reconstructions: Reviews of Geophysics, 28, 167-206.

Vine, F. J., and Matthews, D. H., 1963, Magnetic Anomalies Over Oceanic Ridges: Nature, 199, 947-949.

Whitmarsh, R. B., and Miles, P. R., 1995, Models of the development of the West Iberia rifted continental margin at 40°30'N deduced from surface and deep-tow magnetic anomalies: J. Geophys. Res., 100, 3789-3806.

Whitmarsh, R., Manatschal, G., and Minshull, T., 2001, Evolution of magma-poor continental margins from rifting to seafloor spreading: Nature, 413, 150-154.

Whittaker, J. M., Müller, R. D., Leitchenkov, G., Stagg, H., Sdrolias, M., Gaina, C., and Goncharov, A., 2007, Major Australian-Antarctic Plate Reorganization at Hawaiian-Emperor Bend Time: Science, 318, 83-86.

Whittaker, J. M., Müller, R. D., Leitchenkov, G., Stagg, H., Sdrolias, M., Gaina, C., and Goncharov, A., 2008, Response to Comment on "Major Australian-Antarctic Plate Reorganization at Hawaiian-Emperor Bend Time": Science, 321, 490.

Worm, H.-U., 2001, Magnetic stability of oceanic gabbros from ODP Hole 735B: Earth and Planetary Science Letters, 193, 287-302.

Yamamoto, M., Seaman, N., and Isezaki, N., 2005, Geomagnetic paleointensity over 1. 2 Ma from deep-tow vector magnetic data across the East Pacific Rise: Earth, Planets, and Space, 57, 465-470.

Zhao, X., Turrin, B. D., Jackson, M., and Solheid, P., 2001, Data report: Paleomagnetic and rock magnetic characterization of rocks recovered from Leg 173 sites. , in Beslier, M.-O., Whitmarsh, R. B., Wallace, P. J., and Girardeau, J., eds., Proc. ODP, Sci. Results,, Volume 173: College Station, TX (Ocean Drilling Program), p. 1-34.

Zhao, X., Galbrun, B., Delius, H., and Liu, Q., 2007, Paleolatitude inferred from Cretaceous sedimentary and igneous cores recovered from Leg 210, Newfoundland margin, in Tucholke, B. E., Sibuet, J.-C., and Klaus, A., eds., Proc. ODP, Sci. Results,, Volume 210: College Station, TX (Ocean Drilling Program), p. 1-37.

Adrien BRONNER

Les anomalies magnétiques dans les domaines de manteau exhumé

Résumé

L'objectif de cette thèse est de comprendre (1) si l'exhumation des roches mantelliques aux dorsales océaniques est compatible avec l'enregistrement des inversions de polarité du champ magnétique terrestre, (2) quels sont les processus associés aux anomalies magnétiques observées à l'aplomb des transitions océan-continent et (3) quelles sont les conséquences de ces processus sur les mécanismes de l'océanisation. Afin de travailler avec des données de résolution maximum, une méthode de calibration et d'interprétation des données magnétiques acquises proches du fond est développée dans le premier chapitre. Dans le deuxième chapitre, cette méthode est appliquée aux données magnétiques acquises à l'aplomb des domaines de manteau exhumé de la dorsale Sud-Ouest Indienne (SWIR). Il est ensuite montré que l'exhumation des roches mantelliques est associée à un signal magnétique de faible amplitude et de faible continuité spatiale rendant impossible l'identification des anomalies magnétiques d'accrétion océanique. De fait, il est proposé que contrairement aux basaltes, les roches mantelliques exhumées de la SWIR ne portent pas une aimantation rémanente suffisamment stable pour fossiliser la direction du champ magnétique terrestre. Dans le dernier chapitre, il est démontré que l'anomalie « J », antérieurement interprétée comme la première isochrone associée à la partie distale des marges Ibérie/Terre-Neuve, est en fait identifiée à l'aplomb d'une structure crustale particulière caractérisée par un haut topographique et un épaississement crustal. Par conséquent, il est proposé qu'un évènement magmatique majeur est à l'origine de la création de cette structure crustale et que cet événement est le déclencheur de la mise en place de la première dorsale océanique.

Mots clés : anomalie magnétique, péridotite serpentinisée, dorsale océanique, marge passive

Abstract

The aim of this work is to constrain (1) whether exhumation of mantle rocks at mid oceanic ridges is compatible with the record of polarity reversals of the Earth magnetic field, (2) what is the origin and the processes responsible for the magnetic anomalies observed at magma-poor rifted margins and (3) what are the consequences of these processes on continental breakup. In a first part, in order to work with high-resolution data, we develop a method for calibration and interpretation of deep-tow three component magnetic data. In a second part, we apply these methods to the data acquired above the large exhumed mantle domains of the ultraslow-spreading Southwest Indian Ridge. We show that, in these areas, neither the magnetic properties of the dredge samples nor the deep-tow magnetic data are consistent with the seafloor-spreading magnetic pattern commonly observed at mid oceanic ridges. We further suggest that in contrast to mid oceanic ridges basalts the exhumed serpentinized mantle rocks do not carry a sufficiently stable remanant magnetization to produce marine magnetic anomalies. In the last part, we show that the "J" anomaly, previously interpreted as the first seafloor-spreading anomaly of the Iberia and Newfoundland passive margins, is associated with locally high topography and thickened crust. We propose that this peculiar crustal structure results from voluminous magma both erupted at the surface and added beneath the exhumed mantle domain. We therefore propose that the J anomaly did not form during seafloor spreading but instead represents a pulse of magmatism that have triggered continental breakup.

Keywords: magnetic anomaly, serpentinized peridotite, mid-oceanic ridge, rifted margin